

# Infinite-Length Limit of Spectral Curves and Inverse Scattering

NIKLAS BEISERT<sup>1</sup>, KUNAL GUPTA<sup>2</sup>

<sup>1</sup> *Institut für Theoretische Physik,  
Eidgenössische Technische Hochschule Zürich,  
Wolfgang-Pauli-Strasse 27, 8093 Zürich, Switzerland*  
nbeisert@itp.phys.ethz.ch

<sup>2</sup> *Department of Physics and Astronomy,  
Uppsala University,  
Box 516, 751 20 Uppsala, Sweden*  
kunal.gupta@physics.uu.se

## Abstract

Integrability equips models of theoretical physics with efficient methods for the exact construction of useful states and their evolution. Relevant tools for classical integrable field models in one spatial dimensional are spectral curves in the case of periodic fields and inverse scattering for asymptotic boundary conditions. Even though the two methods are quite different in many ways, they ought to be related by taking the periodicity length of closed boundary conditions to infinity.

Using the Korteweg-de Vries equation and the continuous Heisenberg magnet as prototypical classical integrable field models, we discuss and illustrate how data for spectral curves transforms into asymptotic scattering data. In order to gain intuition and also for concreteness, we review how the elliptic states of these models degenerate into solitons at infinite length.

# Contents

<b>Contents</b>	<b>2</b>
<b>1 Introduction and Overview</b>	<b>3</b>
<b>2 KdV Elliptic States</b>	<b>5</b>
2.1 Travelling Wave Solution . . . . .	5
2.2 Auxiliary Linear Problem . . . . .	6
2.3 Spectral Curve . . . . .	7
2.4 Local Charges . . . . .	9
2.5 Dynamical Divisor . . . . .	10
2.6 Infinite-Length Limit . . . . .	11
2.7 Small-Amplitude Limit . . . . .	13
<b>3 KdV Finite-Length Extrapolation</b>	<b>14</b>
3.1 Extrapolation . . . . .	15
3.2 Continuum Cuts . . . . .	17
3.3 Continuum Divisor . . . . .	18
3.4 Soliton Intervals . . . . .	19
3.5 Soliton Divisor . . . . .	20
3.6 Local Charges . . . . .	23
3.7 Asymptotic Limit . . . . .	25
<b>4 Continuous Heisenberg Magnet</b>	<b>27</b>
4.1 Scattering Data . . . . .	28
4.2 Spectral Curve and Divisor . . . . .	30
4.3 Simple States . . . . .	32
4.4 Finite-Length Extrapolation . . . . .	36
4.5 Continuum Cuts . . . . .	36
4.6 Soliton Cuts . . . . .	38
4.7 Asymptotic Limit . . . . .	41
<b>5 Conclusions and Outlook</b>	<b>43</b>
<b>A Elliptic Solution in CHM</b>	<b>44</b>
A.1 Equation of Motion . . . . .	44
A.2 Travelling Wave Ansatz . . . . .	45
A.3 Conjugate Field . . . . .	47
A.4 Auxiliary Linear Problem . . . . .	49
A.5 Periodicity and Moduli . . . . .	50
A.6 Dynamical Divisor . . . . .	52
A.7 Charges . . . . .	54
A.8 Soliton Limit . . . . .	56
<b>B Scattering Unitarity on the Double Space</b>	<b>60</b>
<b>References</b>	<b>61</b>

# 1 Introduction and Overview

The classical inverse scattering method and the method of classical spectral curves (also known as finite-gap method or inverse spectral problem) are two well-known and established techniques to analyse and construct general solutions of the equations of motions for classical integrable chain and field models.

The inverse scattering method addresses classical integrable models in one spatial dimension with asymptotic boundary conditions. This method was devised by Gardner, Greene, Kruskal and Miura in [1] to exactly construct soliton solutions in the Korteweg de Vries (KdV) equation. Subsequently, Lax developed the framework of Lax pairs in [2] which established an algebraic foundation for multi-soliton states. Integrability of the KdV model was established in [3]. Since then, the inverse scattering framework has been applied to many other systems like the nonlinear Schrödinger equation (NLS) [4] and the continuous Heisenberg magnet (CHM) [5]. It is based on a scattering problem for an auxiliary linear problem which transforms the physical phase space into a set of abstract scattering data. These scattering data consist of kinematical parameters for discrete solitonic excitations as well as for a continuum of wave-like excitations. Importantly, this map is bijective: it is inverted by solving the Gel'fand–Levitan–Marchenko integral equation [6]. Consideration of the scattering data bears two advantages: First, even though the scattering data is constructed by an abstract procedure, it rather immediately represents physical parameters such as amplitudes and wave numbers for a set of excitations. Such a description of states is preferable in many situations (especially when it comes to quantisation). Second, the time evolution of the scattering data is linear and thus readily solved. In that sense, the map is analogous to a Fourier transformation in many regards albeit it takes the non-linearity of the model properly and exactly into account. The inverse scattering method for solving the equations of motion thus consists in transforming a physical state into abstract scattering data, performing a trivial time evolution in this space, and then mapping back to the time-evolved physical state. It is equally useful to skip the first step by defining the initial state based on its scattering data. The main practical difficulty of the inverse scattering method is that the forward and inverse transforms require solving either differential or integral equations.

The method of spectral curves addresses classical integrable models with a periodic spatial dimension and thus with closed boundary conditions. It was devised for the KdV equation by Novikov, Dubrovin, Its, Matveev [7, 8] as well as Lax and Marchenko [9] based on techniques by Akhiezer [10], see also [11]. The spectral curve method was extended to the integrable NLS model by Kotlyarov and Its [12] and the equivalence of the model and its integrable structure to CHM was shown by Lakshmanan, Zakharov and Takhtajan [13]. Here, the same auxiliary linear problem as mentioned above gives rise to a characteristic matrix, the so-called monodromy, which encodes all the relevant data contained in the state. In particular, the spectrum of eigenvalues is conserved while the direction of eigenvectors evolves with time. Therefore the monodromy naturally provides a splitting of the degrees of freedom into conserved and dynamical variables. Moreover, these physical variables are naturally encoded by a Riemann surface, the so-called spectral curve, and certain meromorphic functions on it. In this form, the investigation of the physical system is enhanced by the powerful tools of complex analysis. In particular, the moduli of such spectral curves again qualitatively translate to the amplitudes of excitations with well-defined wave numbers which in this case are quantised due to the periodicity of space. Time evolution is again simplified and stream-lined in this picture,

and a solution along the lines of the inverse scattering method applies to the periodic case as well. Analogously, the transformation between phase space and the abstract spectral curve data remains difficult, making use of differential and integral equations or special functions which encode these.

Without going into details, the above two constructive methods are qualitatively similar, but they are formulated in terms of rather different sets of abstract data as well as different flavours of mathematical concepts and equations. Nonetheless, they ought to be related for the following reason: Models on the infinite line can be understood as limiting cases of models on a spatial domain of finite extent. The matching between the closed boundary on the periodic interval and asymptotic boundaries on the infinite line may of course introduce some minor adjustments between the two models, but the bulk degrees of freedom should directly transform into each other. In that sense, the inverse scattering method should arise as a limiting case of the method of spectral curves. Consequently, the data and structures of the two methods should transform into each other.

Aspects of this issue have been addressed in several works in the past. The original work [7] on the spectral curve method for KdV points out how a soliton is embedded into the genus-one spectral curve for the wave train. In [14] the spectral curve solution is explicitly degenerated into multi-soliton solutions, and similar results for the nonlinear Schrödinger equation have been presented in [15]. The works [16, 17] address the relationship for small amplitudes and analyse it for piecewise-constant approximations using numerical methods. Features of the distribution of branch cuts for spectral curves in the sine-Gordon model at large periodicity length have been presented in [18].

The purpose of the present investigation is to work out the relationship between the two integrability methods in detail and how their corresponding sets of data transform into each other. In particular, we observe how to meet the asymptotic boundary conditions in the infinite-length limit (sometimes also called decompactification limit as the compact closed circle turns into the non-compact infinite line) and how this turns the states on the periodic domain into a combination of discrete solitons and a continuum of wave-like solutions.

We shall perform the detailed analysis for the sample model of the KdV equation. In order to gather experience in taking the infinite-length limit, we shall consider the spectral curve representation of the elliptic wave train solution of the KdV model. This class of states is particularly suited for this purpose because it can be written explicitly in terms of elliptic functions and it has several parameters that are either used to perform the infinite-length limit or that remain as tuneable parameters in the limit.

We shall then proceed to the general case. Starting from a generic state on the infinite line as described through its scattering data, we introduce a one-parameter family of periodic states with varying periodicity length. We then approximate their spectral curve representations using the scattering data. This provides a clear picture of how to set up a sequence of spectral curves such that their corresponding states have a well-defined infinite-length limit.

Finally, we shall redo the analysis for the CHM model which is another prototypical integrable model of a one-dimensional field. As such it shares many properties with the KdV model including the applicability of an inverse scattering method and a spectral curve method, and one may expect the infinite-length limit to work along the same lines. While this will turn out to be true, some features of the abstract data in these two models are qualitatively different because a different signature applies to the underlying structures of integrability. This implies several adjustments to the precise formulation of

the infinite-length limit of the spectral curve method.

The present article is organised as follows: In Sec. 2 we use the example of elliptic travelling wave solutions of the KdV model to introduce and explore the infinite-length limit for a well-tractable class of states. In the subsequent Sec. 3 we discuss a scheme for extracting and relating data in the infinite-length limit for generic states of the inverse scattering and spectral curve methods for the KdV model. We then apply the scheme to the CHM model in Sec. 4 in order to understand its universality and the corresponding adjustments. In Sec. 5 we conclude and provide an outlook. Finally, we point out that a qualitative summary and illustration of our results is provided in Sec. 3.7 and Sec. 4.7.

## 2 KdV Elliptic States

We start by gaining some experience on the infinite-length limit for the KdV equation. To that end, we consider the well-known class of fixed-profile states which contains periodic as well as infinite-length solutions and which is solved by elliptic functions.

### 2.1 Travelling Wave Solution

We will use the KdV equation for the field  $\phi(x, t)$  in the standard normalisation:

$$\dot{\phi} = 6\phi\phi' - \phi'''. \quad (2.1)$$

The class of elliptic solutions to this equation is well-known. It can be obtained by an ansatz describing a fixed profile  $\phi(x)$  moving at constant velocity  $v$ :

$$\phi(x, t) = \phi(x - vt). \quad (2.2)$$

It reduces the KdV equation to the ordinary differential equation

$$3\phi^2 - \phi'' + v\phi - \gamma_1 = 0. \quad (2.3)$$

Every solution to this equation also solves the KdV equation at all  $x$  and  $t$ . This special feature is due to the system being homogeneous in both time and space.<sup>1</sup>

The reduced KdV equation integrates straight-forwardly to

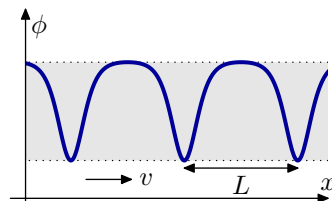
$$3\phi^2 - \phi'' + v\phi - \gamma_1 = 0. \quad (2.4)$$

Another exact integration is enabled upon multiplication by  $\phi'$ :

$$\phi^3 - \frac{1}{2}\phi'^2 + \frac{1}{2}v\phi^2 - \gamma_1\phi - \gamma_2 = 0. \quad (2.5)$$

The two coefficients  $\gamma_1$  and  $\gamma_2$  are integration constants. Equation (2.5) is further integrated by separation of variables, and upon inversion of an elliptic integral one finds the full solution

$$\phi = -\frac{1}{6}v - \frac{2}{3}\alpha^2(1 - 2m) - 2\alpha^2m \operatorname{cn}(\alpha x + \beta, m)^2. \quad (2.6)$$



This is the well-known wave train or cnoidal wave solution which was described in [19] and then analysed in [20]. Here,  $\operatorname{cn}(z, m)$  denotes the Jacobi elliptic cosine function.<sup>2</sup> Next

<sup>1</sup>A combined spatial and temporal translation with speed  $v$  maps the coordinates  $(x, t)$  to  $(x - vt, 0)$ , and it therefore suffices that  $\phi(x - vt)$  solves the equation at every  $x - vt$ .

<sup>2</sup>We shall omit the elliptic modulus  $m$  in most occurrences of elliptic functions, e.g.  $\operatorname{cn}(z) := \operatorname{cn}(z, m)$ .

to the velocity  $v$ , the solution has three degrees of freedom as expected for a differential equation of third order: These are the elliptic modulus  $m$ , the inverse width parameter  $\alpha$  as well as the offset  $\beta$ . All these parameters are real, while the elliptic modulus belongs to the principal interval  $0 \leq m \leq 1$ , and we will assume  $\alpha > 0$ .

## 2.2 Auxiliary Linear Problem

In order to formulate the above state in terms of spectral curves or inverse scattering data, let us construct the corresponding solution of the auxiliary linear problem

$$\Psi' = A\Psi \quad \text{with} \quad A = \begin{pmatrix} 0 & 1 \\ \phi - u & 0 \end{pmatrix} \quad \text{and} \quad \Psi = \begin{pmatrix} \psi \\ \psi' \end{pmatrix}, \quad (2.7)$$

where  $u$  is called the spectral parameter. Here, the first row of  $A$  implies that the second component of the vector  $\Psi$  can be expressed universally as the spatial derivative of the first component which we denote as  $\psi$ . By substituting this relationship in the auxiliary linear problem above, we obtain a second-order linear differential equation for the function  $\psi$ :

$$\psi'' = (\phi - u)\psi. \quad (2.8)$$

Note that it takes the form of a Schrödinger equation for a non-relativistic particle of mass  $m = \hbar^2/2$ , potential  $\phi$  and energy  $u$ .

For the class of elliptic states  $\phi(x)$  introduced in Sec. 2.1, the above differential equation takes the separated form

$$\frac{\psi''}{\psi} = \phi - u = -\frac{1}{6}v - \frac{2}{3}\alpha^2(1 - 2m) - u - 2\alpha^2 m \operatorname{cn}(\alpha x + \beta)^2. \quad (2.9)$$

In order to solve it, we first collect some relevant features of the function on the right-hand side whose features must be matched by the left-hand side  $\psi''/\psi$  with a proper  $\psi(x)$ .

First, the function  $\phi(x)$  is elliptic of minimal degree two. It is periodic with the length

$$L = \frac{2K}{\alpha}, \quad K := K(m). \quad (2.10)$$

In addition, it has an imaginary periodicity in the complexified spatial coordinate  $x$  with length

$$L' = \frac{2iK'}{\alpha}, \quad K' := K(1 - m). \quad (2.11)$$

Furthermore, there is a double pole at  $\tilde{x} = iK'/\alpha$  with coefficient 2, around which we expand (2.9) to get

$$\frac{\psi''}{\psi} = \frac{2}{(x - \tilde{x})^2} + \frac{0}{x - \tilde{x}} + \dots \quad (2.12)$$

Apart from this pole, the function has no further singularities. The double pole on the right-hand side determines the critical behaviour of the function  $\psi$  according to

$$\psi \sim (x - \tilde{x})^\kappa (1 + 0(x - \tilde{x}) + \dots) \quad \implies \quad \frac{\psi''}{\psi} = \frac{\kappa(\kappa - 1)}{(x - \tilde{x})^2} + \frac{0}{x - \tilde{x}} + \dots \quad (2.13)$$

Matching of coefficients implies that  $\psi$  must have a simple pole ( $\kappa = -1$ ) or a double zero ( $\kappa = 2$ ) at  $x = \tilde{x}$ . The former dominates over the latter, and thus a pole is the rule whereas

a double zero merely serves as an exception.<sup>3</sup> The periodicities of the differential equation imply that a shifted solution must again be a solution. We point out that the solutions to the linear differential equation span a two-dimensional space, and so the shifted solution can be a different linear combination of the two basis solutions. Periodicity is thus specified by  $2 \times 2$  matrices, and we can choose solutions such that they are eigenfunctions of periodicity<sup>4</sup>

$$\begin{aligned}\psi(x + L) &= \exp(iq) \psi(x), \\ \psi(x + L') &= \exp(i\tilde{q}) \psi(x).\end{aligned}\tag{2.14}$$

Altogether, the solutions  $\psi$  must be quasi-periodic functions in the sense of the above equation, and they need to have double poles at  $x = \tilde{x}$  with no further poles or multiple zeros. Such functions are typically provided by balanced ratios of elliptic theta functions. A suitable ansatz in terms of the Neville theta function  $\vartheta_n(z, m)$  is as follows:

$$\psi = \exp(i(\alpha x + \beta)q/2K) \frac{\vartheta_n(\alpha x + \beta + z)}{\vartheta_n(\alpha x + \beta) \vartheta_n(z)}.\tag{2.15}$$

Here,  $q$  and  $z$  are parameters that need to be adjusted to solve the above auxiliary linear differential equation. Using the Jacobi zeta function  $\text{zn}(z, m) = (\partial/\partial z) \log \vartheta_n(z, m)$ , we find

$$\begin{aligned}u = u(z) &:= -\frac{1}{6}v + \frac{1}{3}\alpha^2(m - 2) - \alpha^2 \text{cs}(z)^2, \\ q = q(z) &:= 2i(\text{zn}(z) + \text{cs}(z) \text{dn}(z))K, \\ \tilde{q} = \tilde{q}(z) &:= -2(\text{zn}(z) + \text{cs}(z) \text{dn}(z))K' - \frac{\pi}{K}z.\end{aligned}\tag{2.16}$$

Note that the first equation has two solutions  $\pm z$  for each value of the spectral parameter  $u$  corresponding to the two distinct eigenfunctions. It therefore makes sense to replace the spectral parameter  $u = u(z)$  by the uniformising parameter  $z$  on the universal cover of the elliptic surface which is defined up to shifts by  $2K$  and  $2iK'$ . Such shifts leave the expressions invariant up to some shift by integer multiples of  $2\pi$ :

$$\begin{aligned}\psi(z + 2Kn + 2iK'n') &= \psi(z), \\ q(z + 2Kn + 2iK'n') &= q(z) + 2\pi n', \\ \tilde{q}(z + 2Kn + 2iK'n') &= \tilde{q}(z) - 2\pi n.\end{aligned}\tag{2.17}$$

Note that these relations render  $\psi$  as well as the eigenvalues  $\exp(iq)$  and  $\exp(i\tilde{q})$  properly periodic.

## 2.3 Spectral Curve

Let us discuss the function  $dq/du$  describing the spectral curve corresponding to the state  $\phi$ . Its form is in line with the expectation for a genus-one spectral curve of the KdV model:

$$\frac{dq}{du} = \frac{K}{\alpha} \frac{u - u_*}{\sqrt{u - \hat{u}_1} \sqrt{u - \hat{u}_2} \sqrt{u - \hat{u}_3}}.\tag{2.18}$$

<sup>3</sup>In a linear combination of both solutions, the residues of the pole may cancel leaving behind a double zero at this place. In particular, periodic recurrences of a double zero will typically be poles rather than further double zeros.

<sup>4</sup>The genus-one surface has the fundamental group  $\mathbb{Z} \times \mathbb{Z}$ , consequently the two periodicity matrices for shifts by  $L$  and  $L'$  commute and are diagonalised simultaneously.

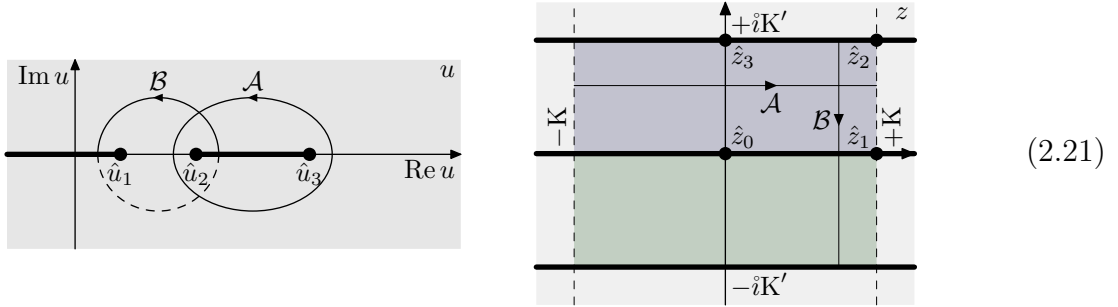
The square-root branch points  $\hat{u}_k$  are the critical points of the map between  $u$  and  $z$ :

$$\begin{aligned} \hat{z}_0 &= 0, & \hat{u}_0 &= \infty, \\ \hat{z}_1 &= K, & \hat{u}_1 &= -\frac{1}{6}v + \frac{1}{3}\alpha^2(m-2), \\ \hat{z}_2 &= K + iK', & \hat{u}_2 &= -\frac{1}{6}v + \frac{1}{3}\alpha^2(1-2m), \\ \hat{z}_3 &= iK', & \hat{u}_3 &= -\frac{1}{6}v + \frac{1}{3}\alpha^2(m+1). \end{aligned} \quad (2.19)$$

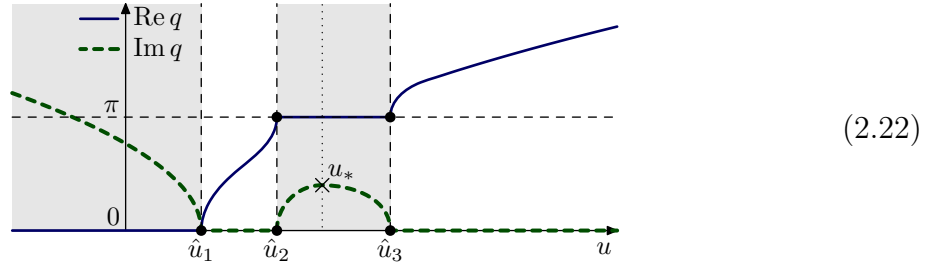
We have ordered them such that  $\hat{u}_1 < \hat{u}_2 < \hat{u}_3$ . Furthermore, the zero  $u_*$  of  $dq/du$  resides in the interval  $\hat{u}_2 < u_* < \hat{u}_3$ , and it is given by

$$u_* = -\frac{1}{6}v + \frac{1}{3}\alpha^2(m-2) + \frac{E}{K}\alpha^2, \quad E := E(m). \quad (2.20)$$

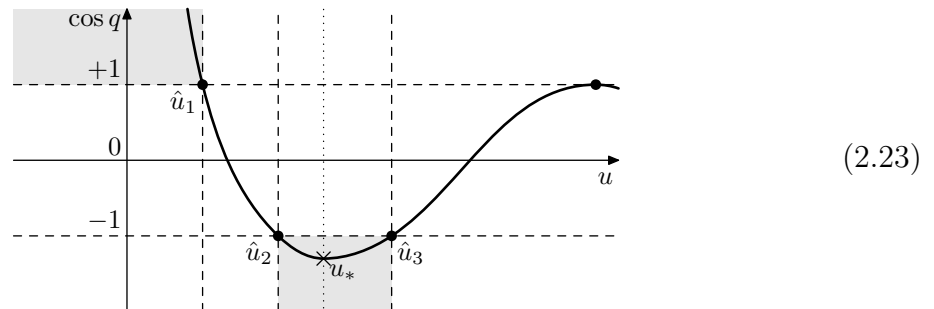
We arrange the branch cuts to connect pairs of consecutive branch points along the real axis starting with  $\hat{u}_0 = -\infty$ . Namely there is a semi-infinite interval from  $\hat{u}_0 = -\infty$  to  $\hat{u}_1$  and a finite interval extending from  $\hat{u}_2$  to  $\hat{u}_3$ :



The shape of the complex function  $q(u)$  just above the real axis is sketched as follows:



Just below the real axis, the function takes the complex conjugate value. Note that the real part resides at 0 and  $\pi$  on the two branch cuts and monotonically increases otherwise. The imaginary part vanishes away from the branch cuts and takes a deformed semi-circle form on them. The positions of the branch cuts are most clearly identified in the continuous function  $\cos q(u)$ :





This function is real for real  $u$ , but it is not restricted to values between  $-1$  and  $+1$ : absolute values bounded by 1 imply a real argument  $q$  of the cosine function while absolute values greater than 1 require the argument  $q$  to be complex and thus indicate a branch cut. As  $u$  increases starting from  $-\infty$ , the function  $\cos q(u)$  decreases exponentially from  $+\infty$ . At some point  $\hat{u}_1$  the function passes through the critical value  $+1$ , later at  $\hat{u}_2$  it undershoots the critical value  $-1$  until the point  $\hat{u}_3$ . Eventually, the function oscillates between the limiting values  $+1$  and  $-1$ . The branch cuts from  $-\infty$  to  $\hat{u}_1$  as well as from  $\hat{u}_2$  to  $\hat{u}_3$  coincide with the two forbidden zones where  $|\cos q(u)| > 1$ .

## 2.4 Local Charges

The KdV equation has an infinite tower of conserved local charges. These represent useful physical information and they provide means for cross checks. Let us therefore introduce and discuss them briefly.

The first few conserved local charges are the potential shift  $Q$ , the momentum  $P$  and the energy  $E$  defined by

$$Q = \int dx \frac{1}{2}\phi, \quad P = \int dx \frac{1}{2}\phi^2, \quad E = \int dx \left[ \frac{1}{2}\phi^2 + \phi^3 \right]. \quad (2.24)$$

We can conveniently read off the values of these charges for the elliptic state from the expansion of  $q(u)$  for large  $u$ :

$$q(u) = L\sqrt{u} - \frac{Q}{u^{1/2}} - \frac{P}{4u^{3/2}} - \frac{E}{16u^{5/2}} + \dots \quad (2.25)$$

One finds their explicit expressions in terms of complete elliptic integrals  $K$  and  $E$ :

$$\begin{aligned} Q &= \left[ -\frac{1}{6}v + \frac{2}{3}(2-m)\alpha^2 \right] \frac{K}{\alpha} - 2\alpha E, \\ P &= \left[ \frac{1}{36}v^2 - \frac{2}{9}(2-m)v\alpha^2 + \frac{4}{9}(1-m+m^2)\alpha^4 \right] \frac{K}{\alpha} + \frac{2}{3}v\alpha E, \\ E &= \left[ \frac{1}{108}v^3 - \frac{1}{9}(2-m)v^2\alpha^2 + \frac{4}{9}(1-m+m^2)v\alpha^4 - \frac{16}{135}(4-6m+12m^2-5m^3)\alpha^6 \right] \frac{K}{\alpha} \\ &\quad + \left[ -\frac{1}{3}v^2 - \frac{16}{15}(1-m+m^2)\alpha^4 \right] \alpha E. \end{aligned} \quad (2.26)$$

Furthermore, the states can be characterised in terms of action variables. The main action variable is given by a period integral on the curve:

$$I = \frac{1}{i\pi} \oint_{\mathcal{A}} u dq = \frac{4\alpha^2}{\pi} \left[ -E^2 + \frac{2}{3}(2-m)KE - \frac{1}{3}(1-m)K^2 \right]. \quad (2.27)$$

An additional action variable corresponding to the average field value is given by the potential shift  $Q$ . The momentum and energy variables expressed in terms of the action variables (assuming a constant length  $L$ ) satisfy two differential equations:

$$dP = \frac{4Q}{L} dQ + \frac{2\pi}{L} dI, \quad dE = \frac{12P}{L} dQ - \frac{2\pi v}{L} dI. \quad (2.28)$$

Note that the coefficients of  $dI$  express the wave number and angular velocity for the periodicities in space and time, respectively.

Unfortunately, the additional degree of freedom corresponding to the average field value complicates our further treatment: In principle, we should fix it to some specific

value, but there is no universally suitable way to do so. Useful choices might be fixing the potential shift  $Q = 0$ , fixing the asymptotic field value  $\phi_0$  for infinite-length states, or fixing one of the branch points  $\hat{u} = 0$ . These conditions are all different, and they all have an impact on the dependencies of the charges on the action variables. To resolve the issue, we can use a Galilean boost transformation

$$\tilde{\phi}(x, t) = \phi(x + \tilde{v}t, t) + \frac{1}{6}\tilde{v}. \quad (2.29)$$

This transforms the charges infinitesimally according to  $\delta Q = \delta\tilde{v}L/12$ ,  $\delta P = \delta\tilde{v}Q/3$ ,  $\delta E = \delta\tilde{v}P$ , and it allows us to construct Galilei-invariant combinations of the charges as

$$\tilde{P} := P - \frac{2Q^2}{L}, \quad \tilde{E} := E - \frac{12PQ}{L} + \frac{16Q^3}{L^2}. \quad (2.30)$$

Essentially, these yield the values of the charges in the inertial frame defined by  $\tilde{Q} = 0$  with the relative velocity  $\tilde{v} = -12Q/L$ . The above relations then simplify to

$$d\tilde{P} = \frac{2\pi}{L} dI, \quad d\tilde{E} = -\frac{2\pi}{L} \left( v + \frac{12Q}{L} \right) dI. \quad (2.31)$$

## 2.5 Dynamical Divisor

The above spectral curve encodes the time-independent data of the state, in particular the momentum  $P$  and the energy  $E$ , or equivalently the potential shift  $Q$  and the action variable  $I$ . However, the state is further specified by one time-dependent variable  $\beta(t)$ . The time-dependent data is typically encoded into the dynamical divisor related to the solution  $\psi$ . For the KdV model, the divisor consists of the points  $\hat{z}_j$  where the logarithmic derivative  $\varpi := \psi'/\psi$  equals a reference value.<sup>5</sup> For the curve at hand, the function  $\varpi$  is an elliptic function of minimal degree in  $z$ ,

$$\varpi := \frac{\psi'}{\psi} = -\alpha [\text{cs}(z) \text{dn}(z) + m \text{sn}(\alpha x + \beta + z) \text{sn}(\alpha x + \beta) \text{sn}(z)], \quad (2.32)$$

and therefore every value is attained precisely twice. It makes sense to choose the reference value for  $\varpi$  to be  $\infty$  in which case the divisor consists of the poles of  $\varpi$ , and one of the two poles is fixed at  $z = 0$  corresponding to  $u = \infty$ . The other pole resides at<sup>6</sup>

$$\hat{z}(x, t) = iK' - \alpha x - \beta(t), \quad (2.33)$$

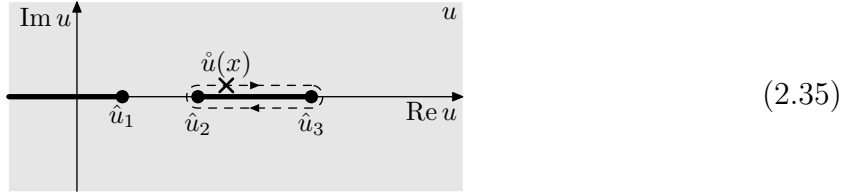
which clearly contains the desired information on the value of  $\beta(t)$ . In terms of the spectral parameter  $u$ , the pole is given by

$$\hat{u}(x) = -\frac{1}{6}v + \frac{1}{3}\alpha^2(1 - 2m) + \alpha^2 m \text{cn}(\alpha x + \beta)^2. \quad (2.34)$$

<sup>5</sup>Note that the logarithmic derivative  $\varpi = \psi'/\psi$  describes the direction of the vector  $\Psi$  in the vector-valued auxiliary linear problem (2.7).

<sup>6</sup>The dependence of the pole  $\hat{z}$  on  $x$  and  $t$  is linear because  $z$  is a uniformising variable. For more general variables, the evolution equations in space and time are first-order differential equations. Therefore, the value of the pole at some point in space and time is sufficient to specify the complete state. In the following we shall disregard the dependence on  $t$  as we are only interested in states on a given time slice. However, we will keep the full dependence on  $x$  because it allows us investigate and reconstruct the states without further ado.

As  $x$  or  $\beta$  changes, the pole oscillates between the real values  $\hat{u}_2$  and  $\hat{u}_3$  which are the endpoints of one of the two branch cuts. Formally, the pole is placed either just above or just below the finite branch cut depending on its direction of motion. In other words, the divisor pole moves around the branch cut along the real axis precisely at its perimeter:



Let us finally comment on the construction of states in terms of the data of the spectral curve and divisor. The properties of a suitable solution  $\psi$  with a given pole at  $\hat{u}$  determine it uniquely as a function of  $x$  and  $u$ . Given such a function, the original state  $\phi$  is then conveniently obtained from the expansion of the logarithmic derivative  $\varpi$  at  $u = \infty$ :

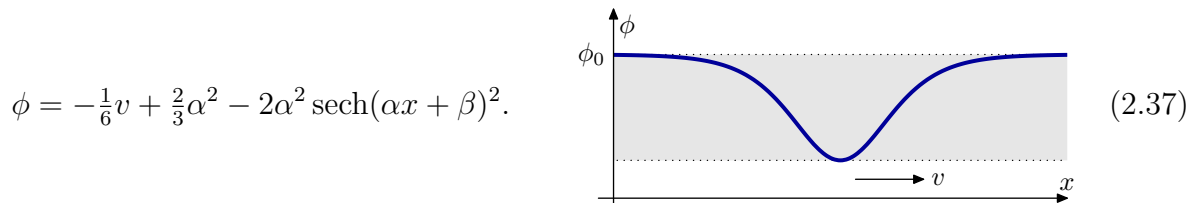
$$\varpi = i\sqrt{u} - \frac{i\phi}{2\sqrt{u}} + \mathcal{O}(u^{-1}). \quad (2.36)$$

This follows from analysis of the auxiliary linear problem  $\varpi' + \varpi^2 = \phi - u$  at the singular value  $u = \infty$ .

## 2.6 Infinite-Length Limit

The class of states described above has an adjustable spatial periodicity of length  $L = 2K/\alpha$ . There are two ways to tune the parameters such that  $L$  becomes infinite. One is to set  $\alpha = 0$ , but this trivialises the state to a constant  $\phi = -v/6$ . The other is to let the modulus assume the upper critical value  $m = 1$  which leads to a non-trivial state.

For  $m = 1$  the state turns into a single exponentially localised excitation:



$$\phi = -\frac{1}{6}v + \frac{2}{3}\alpha^2 - 2\alpha^2 \operatorname{sech}(\alpha x + \beta)^2. \quad (2.37)$$

This is the well-known soliton state but with a non-zero constant background of height

$$\phi_0 = -\frac{1}{6}v + \frac{2}{3}\alpha^2. \quad (2.38)$$

On the infinite line one typically demands the field to have a zero asymptotic value in order to achieve a vanishing asymptotic energy density and moreover a finite overall energy. For this, the width parameter  $\alpha$  should be linked to the velocity  $v$  as  $\alpha = \sqrt{v}/2$ , but here we shall keep it arbitrary.

In the infinite-length limit, the solution of the auxiliary linear problem reduces directly to

$$\psi = \exp(-(\alpha x + \beta) \coth(z)) \left[ 1 + \frac{\tanh(\alpha x + \beta)}{\coth(z)} \right], \quad u = -\frac{1}{6}v + \frac{2}{3}\alpha^2 - \alpha^2 \coth(z)^2. \quad (2.39)$$

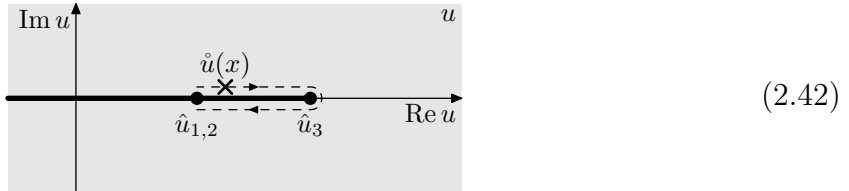
The special points of the elliptic spectral curve reduce to

$$\hat{u}_0 = -\infty, \quad \hat{u}_1 = \hat{u}_2 = u_* = -\frac{1}{6}v - \frac{1}{3}\alpha^2, \quad \hat{u}_3 = -\frac{1}{6}v + \frac{2}{3}\alpha^2 = \phi_0. \quad (2.40)$$

Here, one observes that the branch points  $\hat{u}_1$  and  $\hat{u}_2$  as well as the critical point  $u_*$  coincide [7] and the genus of the spectral curve is reduced by one unit. The points  $\hat{u}_0 = -\infty$  and  $\hat{u}_3 = \phi_0$  serve as branch points of the map between  $u$  and  $\coth(z)$ . The divisor pole reduces to

$$\hat{u}(x) = -\frac{1}{6}v - \frac{1}{3}\alpha^2 + \alpha^2 \operatorname{sech}(\alpha x + \beta)^2. \quad (2.41)$$

For almost all values of  $x$  including the asymptotic regions at  $x \rightarrow \mp\infty$  the divisor pole  $\hat{u}$  remains near the singular point  $\hat{u}_1 = \hat{u}_2 = u_*$ . Conversely, in the region of the soliton where  $\alpha x + \beta$  is small,  $\hat{u}$  moves towards  $\hat{u}_3$  which is reached at the peak of the soliton function:



The above solution to the auxiliary linear problem evidently takes the form of Jost solutions of a scattering problem:

$$\psi_{L/R} = \exp(-ikx) \frac{k - i\alpha \tanh(\alpha x + \beta)}{k \pm i\alpha}, \quad (2.43)$$

where we have adjusted the normalisation such that the solutions approach  $\exp(-ikx)$  in their respective asymptotic regions. To this end, we have introduced the momentum parameter  $k$  as

$$k := -i\alpha \coth(z) = \sqrt{u + \frac{1}{6}v - \frac{2}{3}\alpha^2} = \sqrt{u - \phi_0}. \quad (2.44)$$

The two Jost solutions are related by the scattering relation

$$\psi_L(-k) = \tau(k)\psi_R(-k) + \rho(k)\psi_L(k) \quad (2.45)$$

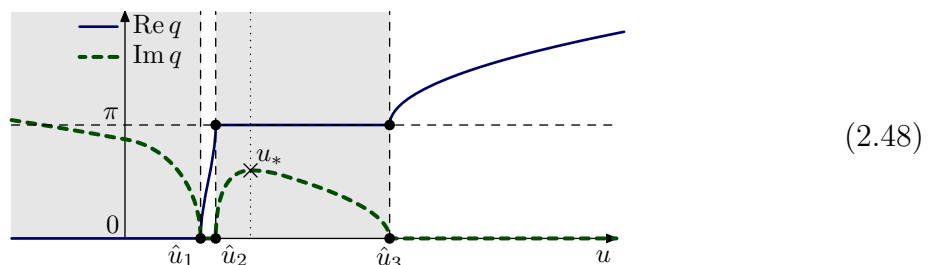
with the transmission and reflection coefficients

$$\tau(k) = \frac{k + \check{k}}{k - \check{k}}, \quad \rho(k) = 0 \quad \text{where} \quad \check{k} := i\alpha. \quad (2.46)$$

Note that the zero and pole  $k = \mp\check{k}$  of the transmission coefficient map precisely to the singular point  $u = \hat{u}_1 = \hat{u}_2 = u_*$  in the  $u$ -plane. The values of the conserved charges take on particularly simple expressions:

$$Q = \frac{1}{2}L\phi_0 - 2\alpha, \quad \tilde{P} = \frac{8}{3}\alpha^3, \quad \tilde{E} = -\frac{32}{5}\alpha^5. \quad (2.47)$$

Later on, we will be interested in a generalisation of this limit to other periodic solutions. We observe that the present limit is well-defined and non-singular, so it bears no trace of the length parameter  $L$ . Let us therefore discuss in more detail, how the relevant quantities attain the limit  $L \rightarrow \infty$ . We start by presenting a sketch of the quasi-momentum function  $q(u)$ :



In the limit, a relevant auxiliary variable is the momentum parameter  $k$ . This variable expresses the spectral parameter  $u$ , but their functional relationship may depend on  $L$ , and this dependency may introduce some arbitrariness in taking the limit. It therefore makes sense to introduce this momentum parameter  $k$  even at finite  $L$  as a replacement for the parameter  $u$  or  $z$ . A plausible choice is

$$k := \frac{i\alpha}{\operatorname{sn}(z)} = \sqrt{u + \frac{1}{6}v - \frac{1}{3}\alpha^2(m+1)}, \quad (2.49)$$

which fixes the isolated branch point  $\hat{k}_3 = 0$  to precisely zero where it should be. The other two branch points are mapped to  $\hat{k}_1 = i\alpha$  and  $\hat{k}_2 = i\alpha\sqrt{m}$ . Now the relationship  $L = 2K/\alpha$  and the logarithmic divergence of the elliptic integral  $K$  at  $m = 1$  leads to  $m$  being exponentially close to 1:

$$m = 1 - 16e^{-\alpha L} + \dots \quad (2.50)$$

Consequently, the two branch points are separated by exponentially small amounts:

$$\begin{aligned} \hat{k}_2 - \hat{k}_1 &= -i\alpha(1 - \sqrt{m}) = -8i\alpha e^{-\alpha L} + \dots, \\ \hat{u}_2 - \hat{u}_1 &= \alpha^2(1 - m) = 16\alpha^2 e^{-\alpha L} + \dots \end{aligned} \quad (2.51)$$

Two further quantities of interest for a spectral curve and its associated divisor are the quasi-momentum  $q$  and the logarithmic derivative  $\varpi$ . By careful expansion we find

$$\begin{aligned} q &= kL + i \log \frac{k - i\alpha}{k + i\alpha} + \dots, \\ \varpi &= \frac{ik(k^2 + \alpha^2) + \alpha^3 \tanh(\alpha x + \beta) \operatorname{sech}(\alpha x + \beta)^2}{k^2 + \alpha^2 \tanh(\alpha x + \beta)^2} + \dots, \end{aligned} \quad (2.52)$$

where further terms are exponentially suppressed. It also makes sense to state the spectral curve equation (2.18) for large  $L$ :

$$\frac{dq}{du} = \frac{L}{2\sqrt{u - \phi_0}} - \frac{\alpha}{\sqrt{u - \phi_0}(u - \phi_0 + \alpha^2)} + \dots \quad (2.53)$$

Note that the leading term describes the asymptotic background while the next-to-leading term combines two square roots into one pole describing the soliton shape. Finally, it will be useful to extract the action variable because it serves as a modulus of the spectral curve. It turns out to scale with the length

$$I = \frac{4\alpha^3 L}{3\pi} + \dots, \quad (2.54)$$

and it does satisfy the wave number and angular velocity relations  $d\tilde{P} = (2\pi/L)dI$  and  $d\tilde{E} = (-8\pi\alpha^2/L)dI$ .

## 2.7 Small-Amplitude Limit

It also makes sense to discuss the solution when the modulus  $m$  approaches the lower critical value 0. Here, the solution approaches a constant at  $m = 0$ , and we should discuss the leading perturbation around this constant solution. As we move  $m$  slightly away from

0, also the other degrees of freedom may receive explicit or implicit contributions from this shift making the resulting perturbative expressions somewhat arbitrary. In order to avoid such arbitrariness, we will fix the action variables  $Q$  and  $I$  as well as the length  $L$ :

$$v = -\frac{6\kappa Q}{\pi} - \kappa^2 + \frac{3I}{\pi} + \mathcal{O}(I^{3/2}), \quad \alpha = \frac{\kappa}{2} + \sqrt{\frac{I}{2\pi}} + \frac{9I}{4\pi\kappa} + \mathcal{O}(I^{3/2}). \quad (2.55)$$

The action variable  $I$  is small for  $m \rightarrow 0$  and it will be used as the perturbative parameter. Furthermore, we have introduced the wave number  $\kappa$  to match the periodicity:

$$m = \frac{8}{\kappa} \sqrt{\frac{I}{2\pi}} + \mathcal{O}(I), \quad \kappa := \frac{2\pi}{L}. \quad (2.56)$$

The state then reads

$$\phi = \frac{\kappa Q}{\pi} - 2\kappa \sqrt{\frac{I}{2\pi}} \cos(\kappa x + 2\beta) - \frac{I}{\pi} \cos(2\kappa x + 4\beta) + \dots \quad (2.57)$$

This state represents a plane wave with wave number  $\kappa$  and a small amplitude.

Let us discuss some key parameters of the curve as well as conserved charges. The distinguished points of the curve are given by

$$\hat{u}_1 = \frac{\kappa Q}{\pi} + \mathcal{O}(I), \quad u_* = \frac{\kappa Q}{\pi} + \frac{\kappa^2}{4} + \mathcal{O}(I), \quad \hat{u}_{2,3} = u_* \mp \kappa \sqrt{\frac{I}{2\pi}} + \mathcal{O}(I), \quad (2.58)$$

We see that the infinite branch cut extends up to  $\hat{u}_1$  which equals the mean value of the field  $\phi$ . The other branch cut is separated by  $\kappa^2/4$  and has a small width proportional to  $\sqrt{I}$ . In fact, the function  $q$  is approximated by a semi-circle on the cut:

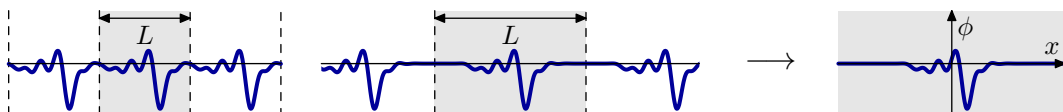
$$q = \pi + \frac{2\pi i}{\kappa^2} \sqrt{\frac{I}{2\pi} \kappa^2 - (u - u_*)^2} + \dots \quad (2.59)$$

As such the resulting action variable equals half the width times the height which amounts to  $I$  as it should. Finally, one finds for the Galilei-invariant conserved charges

$$\tilde{P} = \kappa I, \quad \tilde{E} = \kappa^3 I + \mathcal{O}(I^2). \quad (2.60)$$

### 3 KdV Finite-Length Extrapolation

In the following we shall approximate a generic state on the infinite line  $\phi(x)$  with asymptotic boundary conditions by a family  $\phi_L(x)$  of periodic states on an interval of length  $L$ :



$$(3.1)$$

We do so by constructing the family such that the function  $\phi_L$  periodically repeats a window of interest of  $\phi$  with given length  $L$ . The periodic states are thus defined by

$$\phi_L(x + LZ) := \phi(x) \quad \text{with} \quad x_{-,L} < x < x_{+,L} = x_{-,L} + L, \quad (3.2)$$

where the window of interest in  $\phi(x)$  increases to the whole real line:

$$x_{-,L}, x_{+,L} \rightarrow \mp\infty \quad \text{as} \quad L \rightarrow \infty. \quad (3.3)$$

By considering the spectral curves corresponding to  $\phi_L$  as  $L \rightarrow \infty$ , we will see how the scattering data of  $\phi$  are approximated by spectral curves.

The procedure described above is reminiscent of the truncation of a periodic function onto its fundamental domain on an infinite line which was used in [16, 17] to relate monodromy and scattering matrix. However, in order to properly define the infinite-length limit, we take a fixed infinite-line profile as the starting point and derive a sequence of periodic functions from it.

### 3.1 Extrapolation

We start by assuming a state  $\phi$  on the infinite line with the asymptotic boundary condition

$$\lim_{x \rightarrow \pm\infty} \phi(x) = \phi_0. \quad (3.4)$$

For the inverse scattering method, it is convenient to set up a Lax connection which becomes diagonal in the asymptotic regions. Based on the Lax connection  $A$  introduced in (2.7), this is achieved by the transformation

$$A \rightarrow MAM^{-1} \quad \text{with} \quad M = \begin{pmatrix} -ik & 1 \\ +ik & 1 \end{pmatrix}, \quad k := \sqrt{u - \phi_0}. \quad (3.5)$$

The transformed Lax connection clearly becomes diagonal in the asymptotic regions where  $\phi \rightarrow \phi_0$ :

$$A = \begin{pmatrix} -ik & 0 \\ 0 & ik \end{pmatrix} + \frac{i(\phi - \phi_0)}{2k} \begin{pmatrix} 1 & -1 \\ 1 & -1 \end{pmatrix}. \quad (3.6)$$

The scattering matrix for the inverse scattering method is given by

$$S = \lim_{x_-, x_+ \rightarrow \mp\infty} \text{diag}(e^{ikx_+}, e^{-ikx_+}) W(x_+, x_-) \text{diag}(e^{-ikx_-}, e^{ikx_-}), \quad (3.7)$$

where the parallel transport  $W(x_+, x_-)$  of the Lax connection is defined via the path-ordered exponential integral

$$W(x_+, x_-) := \overleftarrow{\text{P}} \left[ \exp \int_{x_-}^{x_+} dx A(x) \right]. \quad (3.8)$$

The exponential factors in the above definition of the scattering matrix are precisely what it takes to remove the expected oscillatory behaviour in the asymptotic regions. We can thus invert their effect to obtain an approximation for the parallel transport:

$$W(x_+, x_-) \sim \text{diag}(e^{-ikx_+}, e^{ikx_+}) S \text{diag}(e^{ikx_-}, e^{-ikx_-}). \quad (3.9)$$

It is common to express the auxiliary scattering matrix  $S(k)$  in terms of transmission and reflection coefficients  $\tau(k)$  and  $\rho(k)$  for the complementary scattering problem as

$$S(k) = \begin{pmatrix} 1/\tau(k) & \rho(k)/\tau(k) \\ \rho(-k)/\tau(-k) & 1/\tau(-k) \end{pmatrix}. \quad (3.10)$$

We thus find for the asymptotic behaviour of the parallel transport

$$W(x_+, x_-) \sim \begin{pmatrix} e^{-ik(x_+ - x_-)}/\tau(k) & e^{-ik(x_+ + x_-)}\rho(k)/\tau(k) \\ e^{ik(x_+ + x_-)}\rho(-k)/\tau(-k) & e^{ik(x_+ - x_-)}/\tau(-k) \end{pmatrix}. \quad (3.11)$$

This matrix can be used as an approximation to the monodromy of a periodically identified state  $\phi_L$  with the following two approximations: First, the above parallel transport is valid only asymptotically and as far as all the relevant dynamics takes place on the interval  $x_- < x < x_+$ . Second, the construction of the monodromy assumes a periodic state  $\phi_L$  whereas  $W(x_+, x_-)$  is based on a non-periodic interval from the state  $\phi$  on the infinite line. Closing the period on the interval generically introduces some discontinuity or disruption of smoothness which would be represented by distributional terms in the parallel transport for  $\phi_L$ . Therefore, there will be a mismatch between  $W(x_+, x_-)$  and the corresponding monodromy for the periodic identification of the interval. We assume both approximations to be asymptotically small, and thus we will use  $W(x_+, x_-)$  as an approximation for the monodromy.

We can now extract the quasi-momentum function  $q$  via the monodromy trace:

$$\cos q = \frac{1}{2} \text{tr} W(x + L, x) \approx \frac{e^{-ikL}}{2\tau(k)} + \frac{e^{ikL}}{2\tau(-k)}. \quad (3.12)$$

We observe that  $q$  is given in terms of the transmission coefficient  $\tau$ . However, the scattering data for the inverse scattering method is typically specified in terms of reflection coefficient  $\rho$  together with  $N$  soliton momenta  $\check{k}_n \in i\mathbb{R}^+$  and corresponding dynamical coefficients  $\mu_n \in \mathbb{R}^+$ . Now the function  $\tau(k)$  can be reconstructed from these data on the upper half complex plane including the real axis,  $\text{Im } k \geq 0$ , by the dispersion relation [21]

$$\tau(k) = \left[ \prod_{n=1}^N \frac{k + \check{k}_n}{k - \check{k}_n} \right] \exp \left[ \frac{1}{2\pi i} \int \frac{dk'}{k' - k - i0} \log(1 - |\rho(k')|^2) \right]. \quad (3.13)$$

Let us note a few remarks on the resulting transmission function: First of all,  $\tau(k)$  is manifestly time-independent as it should because it does not depend on the dynamical variables  $\arg \rho(k)$  and  $\mu_n$ . Second, for real  $k$ , the distributional identity

$$\frac{1}{k' - k - i0} = \frac{1}{k' - k} + i\pi\delta(k' - k) \quad (3.14)$$

determines the magnitude of  $\tau(k)$  as

$$|\tau(k)| = \sqrt{1 - |\rho(k)|^2}. \quad (3.15)$$

The resulting relation  $|\tau|^2 + |\rho|^2 = 1$  together with the reality relations  $\tau(k)^* = \tau(-k)$  and  $\rho(k)^* = \rho(-k)$  is in agreement with unitarity of  $S$  in (3.10) with regard to the indefinite hermitian form  $\text{diag}(+1, -1)$ .<sup>7</sup> Third, the argument of  $\tau(k)$  interpolates between  $\tau(0) = \pi N$  at  $k = 0$  and  $\tau(+\infty) = 0$  at  $k = +\infty$ .

---

<sup>7</sup>Note that there exist two different notions of scattering matrices in two dimensions with two different notions of unitarity. See App. B for a (slightly off-topic) discussion.



### 3.2 Continuum Cuts

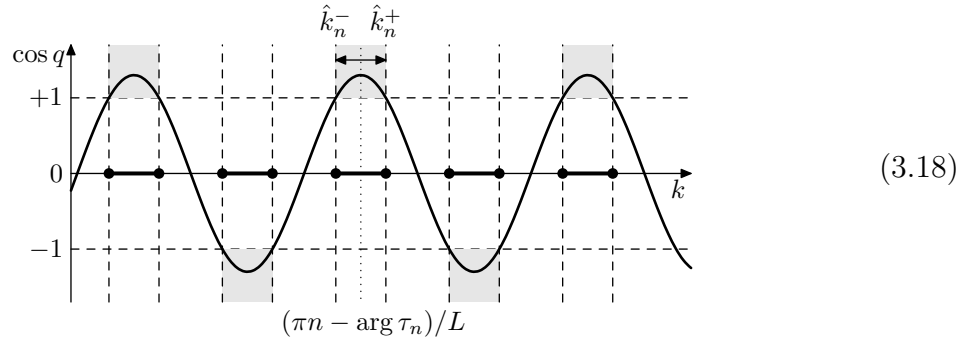
First, we would like to reconstruct the cuts of the spectral curve for real  $k$  (without loss of generality, we restrict to positive  $k$ ). For real momenta  $k$ , the scattering coefficients obey:

$$\tau(-k) = \tau(k)^*, \quad \rho(-k) = \rho(k)^*, \quad |\tau(k)|^2 + |\rho(k)|^2 = 1. \quad (3.16)$$

Choosing a radial form for the transmission coefficient  $\tau = |\tau| \exp(i \arg \tau)$ , we obtain the following approximation for the quasi-momentum

$$\cos q(k) \approx \frac{1}{|\tau(k)|} \cos(kL + \arg \tau(k)). \quad (3.17)$$

As noted above, the branch cuts of the spectral curve are the forbidden zones where  $|\cos q|$  exceeds 1:



In order to find the solutions to  $\cos q(k) = \pm 1$ , we note that for large length  $L$ , the term on the right-hand side of the equation represents a fast uniform oscillation in  $k$  which is modulated in amplitude and phase by the relatively slow function  $\tau(k)$ . For our purposes we can assume  $\tau(k) \approx \tau(k_n) =: \tau_n$  to be approximately constant in a neighbourhood of size  $\mathcal{O}(1/L)$  around the point  $k_n := \pi n/L$ . It is then straight-forward to approximate the branch points of the  $n$ -th cut where  $\text{Re } q = \pi n$ <sup>8</sup> as

$$\hat{k}_n^\pm \approx \frac{\pi n - \arg \tau_n \pm \arccos|\tau_n|}{L}. \quad (3.19)$$

We observe that the widths of the branch cuts are determined by the magnitude of the reflection coefficient:

$$\hat{k}_n^+ - \hat{k}_n^- \approx \frac{2}{L} \arccos|\tau_n| = \frac{2}{L} \arcsin|\rho_n| \leq \frac{\pi}{L}. \quad (3.20)$$

As  $\rho_n$  increases from 0 to 1, the length of a cut increases from 0 to  $\pi/L$ . Note that the linear relationship between the length of the branch cuts and the Fourier coefficients at small amplitudes was already observed in [16]. Furthermore, the branch cuts are arranged

<sup>8</sup>For these purposes, the phase  $\arg \tau(k)$  of the transmission coefficient should be understood as a continuous function interpolating between  $\arg \tau(0) = \pi N$  and  $\arg \tau(+\infty) = 0$  rather than as an angle bounded between  $-\pi$  and  $+\pi$ . We will see later that the first  $N$  cuts will be used to represent the  $N$  solitons, and  $n$  will consistently start at  $N + 1$  for branch cuts at real  $k$ .

on a lattice  $(\pi/L)\mathbb{Z}$  from which their centres are shifted by  $-\arg \tau_n/L$ :<sup>9</sup>

$$\frac{1}{2}(k_n^+ + k_n^-) \approx \frac{\pi n - \arg \tau_n}{L} = k_n - \frac{\arg \tau_n}{L}. \quad (3.21)$$

### 3.3 Continuum Divisor

Next, we would like to reconstruct the dynamical divisor which should correspond to the phase of the reflection coefficient  $\rho(k)$ . As discussed above, the divisor describes the poles  $\mathring{u} = u(\mathring{k})$  of the logarithmic derivative  $\varpi$  of the function  $\psi(x)$ . In the original basis for the Lax connection in (2.7), these are represented by the points where the eigenvector  $(\psi, \psi')$  aligns with the direction  $(0, 1)$ . For consideration of the auxiliary scattering problem we have transformed the basis for the Lax connection using the matrix  $M$  in (3.5) such that the transformed reference direction for the divisor is  $M(0, 1) = (1, 1)$ . The divisor therefore consists of the points  $\mathring{k}$  where the eigenvector of the monodromy  $W(x + L, x)$  points in the direction  $(1, 1)$ .<sup>10</sup>

Using our approximation for the monodromy, we find the relation

$$\frac{e^{-i\mathring{k}L}}{\tau(\mathring{k})} + \frac{e^{-i\mathring{k}(L+2x)}\rho(\mathring{k})}{\tau(\mathring{k})} - \frac{e^{i\mathring{k}(L+2x)}\rho(-\mathring{k})}{\tau(-\mathring{k})} - \frac{e^{i\mathring{k}L}}{\tau(-\mathring{k})} \approx 0. \quad (3.22)$$

Recalling that the contribution  $\mathring{k}L$  to the exponents has a significantly faster dependence on  $\mathring{k}$  than all others, we can treat the latter as constants.<sup>11</sup> Furthermore, using the radial representation of the scattering data for real  $k$ , we can express this equation near  $k_n = \pi n/L$  as

$$\sin(\mathring{k}L + \arg \tau_n) \approx -|\rho_n| \sin(\mathring{k}L + \arg \tau_n + 2\pi n x/L - \arg \rho_n). \quad (3.23)$$

Clearly, there is no solution away from the branch cuts because the magnitude of the left-hand side is larger than  $|\rho_n|$ . However, on a branch cut  $\mathring{k}_n^- < \mathring{k} < \mathring{k}_n^+$ , the left-hand side sweeps the entire range between  $-|\rho_n|$  and  $+|\rho_n|$  while the right-hand side only covers a part of the interval. Due to continuity, there is a solution on each branch cut, and one can convince oneself that it is unique,  $\mathring{k} =: \mathring{k}_n$ .

<sup>9</sup>It deserves mention that the notion of leading and sub-leading terms in the following expression depends on the situation: Superficially, the term  $k_n$  is of order 1 while the contribution from  $\arg \tau$  is of order  $1/L$ . However, when the overall expression is multiplied by  $L$ , the contribution  $k_n L = \pi n$  is an integer multiple of  $\pi$ , and as an angle it merely specifies a discrete parity rather than a continuous quantity. In that case, the second term becomes the leading continuous contribution, and this feature is what allowed us to determine it from the leading scattering data. Nevertheless, we will have to be careful because in other places there may be additional contributions whose order competes with the contribution from  $\arg \tau$ .

<sup>10</sup>Here, we assume the periodicity interval for the approximation to the monodromy to range from  $-L < x < 0$  through  $0 < x + L < L$  so as to capture the range of interest. Unfortunately, this turns out to be a slight contradiction in itself: We are mainly interested in the region  $|x| \ll L$  for the monodromy eigenvector. Modulo  $L$  this region corresponds to either  $x \approx -L$  for negative  $x$  or  $x \approx 0$  for positive  $x$ . For both of these regions,  $W(x + L, x)$  misses an essential part of the region of interest, and cannot be considered a good approximation for the monodromy. This seemingly leads to self-contradictory approximations which we may not be able to fully resolve. Nevertheless, we shall arrive at conclusions which turn out self-consistent and physically reasonable.

<sup>11</sup>The contributions  $2x\mathring{k}$  deserve special consideration since next to the region  $x \approx 0$  we are also interested in the region  $x \approx -L$ . In the latter case,  $2x\mathring{k}$  is approximated by  $-2\pi n$  which can be discarded from the exponent.

Let us briefly discuss the dependence of the point  $\mathring{k}_n$  on the variables. Here it makes sense to introduce an effective phase for the  $n$ -th cut as

$$\sigma_n := \frac{2\pi nx}{L} - \arg \rho_n. \quad (3.24)$$

Note that this phase is in agreement with results of [17]. As  $\sigma_n$  shifts by  $2\pi$ , the point  $\mathring{k}_n$  moves back and forth along the branch cut once.<sup>12</sup> Consequently, the same holds for the phase  $\arg \rho_n$  of the reflection coefficient. Furthermore, as the position  $x$  shifts by one entire period  $L$ , the point  $\mathring{k}_n$  of the  $n$ -th cut oscillates precisely  $n$  times.<sup>13</sup> This feature associates the  $n$ -th cut with the  $n$ -th periodic mode of the system. Finally, as  $n$  increases by one unit, the effective phase shifts by the leading amount  $2\pi x/L$ . Altogether, the distribution of the divisor poles on the array of cuts can be sketched as follows:



$$\quad (3.25)$$

### 3.4 Soliton Intervals

We now proceed to the case of cuts along the negative  $u$ -axis which will encode the solitons. Here, the momentum variable is positive imaginary  $k \in i\mathbb{R}^+$ , and the dispersion relation fixes the upper left component  $1/\tau(k)$  of the scattering matrix. The latter is a holomorphic function and its zeros or likewise the poles of  $\tau(k)$  reside at the soliton positions  $\check{k}_n \in i\mathbb{R}^+$ . We assume that there are  $N$  solitons, and we will order their positions such that their magnitude  $\text{Im } \check{k}_n$  decreases with  $n$ . Unfortunately, the other three components of the scattering matrix are not universally determined. There are several related indications and reasons why this is so, let us briefly discuss them before we continue.

First and foremost, the auxiliary linear problem fixes the scattering matrix based on asymptotic plane wave-like behaviour. This works well for real momenta, but introduces exponential amplification or attenuation for complex momenta. In this case, only the solutions with the most dominant asymptotic attenuation can be universally defined. The other solution has lower attenuation, and it can be supplemented with the solution of dominant attenuation violating its prescribed asymptotic behaviour. Such a change of basis can be introduced with arbitrary momentum-dependent coefficient in order to adjust the reflection coefficients  $\rho(k)$  and  $\rho(-k)$  to any desired function of  $k$  including even non-analytic ones. In this sense, the reflection coefficient  $\rho(k)$  away from the real  $k$ -axis bears no significant information. Eventually, the opposite transmission coefficient  $\tau(-k)$  is determined by the unimodularity relation  $\tau(k)\tau(-k) + \rho(k)\rho(-k) = 1$ , which shows clearly that it is also ambiguously defined. Fortunately, the upper left component  $1/\tau(k)$  of the scattering matrix is well-defined and even holomorphic on the upper half plane. Therefore, the latter is the only component of the scattering matrix that is at our disposal for the reconstruction of a suitable Lax monodromy.

A different approach to obtain the scattering matrix is to solve the parallel transport operator of the auxiliary linear problem. The result is defined uniquely for all values of  $k$ , but only when the supporting interval is finite. Here, the resulting matrix needs to be regularised properly according to the expected asymptotic behaviour of its components.

<sup>12</sup>The non-linearity of the equation results in different slopes for the forward and backward motion especially for large amplitudes  $|\rho| \rightarrow 1$  and depending on the position  $x$ .

<sup>13</sup>This property must hold by construction of the spectral curve because the corresponding state is exactly periodic.

In the infinite-length limit, the upper left component of the scattering matrix converges uniformly ensuring the benign properties of  $\tau(k)$ . The other components may or may not even converge depending on the value of  $k$ , e.g. for  $\text{Im } k$  exceeding the lowest soliton momentum. To ensure convergence for all  $k$  requires a non-trivial regularisation, but this also introduces dependency of the resulting components on higher-order corrections in the regularisation scheme. Effectively, these considerations imply that all but the upper left component of the scattering matrix are not universally defined.

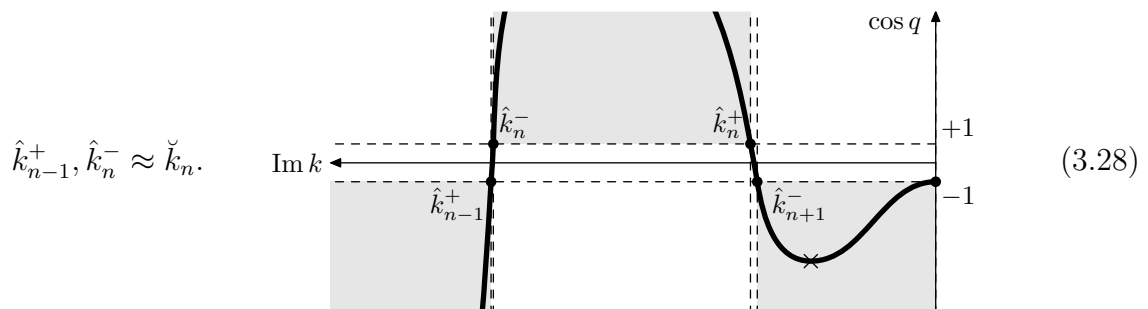
Nevertheless, we need to find the approximate monodromy for a periodic system in order to extract its branch points at finite  $L$ . We make the following proposal for the vicinity of a soliton position  $\check{k}_n$ ,

$$W(x+L, x) \approx \begin{pmatrix} e^{-ikL}/\tau(k) & B(k) \\ C(k) & e^{ikL}D(k) \end{pmatrix} \quad (3.26)$$

with some analytical functions  $B, C, D$  of  $k$  which may additionally depend on  $x$ . The dependency of the diagonal components on the length  $L$  follows from the regularisation of asymptotic states. We can thus take the trace and obtain

$$\cos q = \frac{1}{2} \text{tr } W(x+L, x) \approx \frac{e^{-ikL}}{2\tau(k)}. \quad (3.27)$$

The branch points of the quasi-momentum are where  $\cos q = \pm 1$ . As the function  $e^{-ikL}/\tau(k)$  has an exponentially steep slope at its zero, there must be two branch points nearby:



Their separation is determined by the slope and it is thus exponentially small:

$$\text{Im } \hat{k}_{n-1}^+ - \text{Im } \hat{k}_n^- \approx 4 \text{Im } \text{res } \tau(\check{k}_n) \exp(i\check{k}_n L). \quad (3.29)$$

This separation agrees with the above analysis of the elliptic solution for  $m \rightarrow 1$  where  $\text{res } \tau(\check{k}) = 2i\alpha = 2k$ .

### 3.5 Soliton Divisor

The dynamical divisor corresponding to the solitons is the most difficult element of the family of spectral curves to recover from our method. Effectively, the difficulty is due to the soliton positions dropping out completely from the regularised monodromy in the infinite-length limit. The corresponding variables  $\mu_n$  of the inverse scattering method at  $L = \infty$  are thus not actually encoded into the scattering matrix, but they can only be determined directly from correlators of the wave functions. Nonetheless, the information on the soliton positions is of course encoded into the dynamical divisor at finite length  $L$ . We would thus like to understand at least their qualitative representation in the

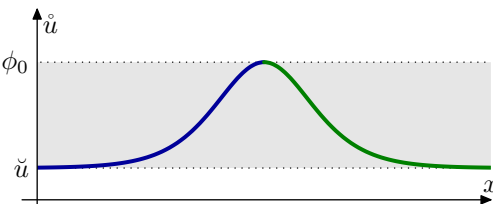
monodromy eigenvectors. In particular, it is not self-evident whether and how the overall requirements for the divisor of spectral curves (on each cut there is one pole and the one on the  $n$ -th cut encircles the latter  $n$  times) are compatible with the shape of a multi-soliton solution ( $N$  bumps of different widths which almost do not interfere).

We assume that the limiting infinite-length state has  $N$  solitons. Each branch cut carries precisely one associated pole of the eigenvector function  $\varpi_L$  with one overall pole permanently fixed to the point  $k = \infty$ . The above discussion showed that there are  $N + 1$  cuts on the imaginary  $k$ -axis. The pole for the cut stretching to  $k = \infty$  is fixed, consequently, there are  $N$  remaining poles  $\check{k}_n$  on the imaginary axis. Each one of these moves on one of the cuts whose branch points  $\hat{k}_n^\pm$  approach two consecutive soliton momenta  $(\check{k}_{n-1}, \check{k}_n)$  in the infinite-length limit. It therefore makes sense to assume that the  $N$  dynamical positions of the poles encode the  $N$  position variables  $\mu_n$  in some way, however, not necessarily one-to-one. In the following, let us gain some intuition how the poles of the eigenvector function  $\varpi_L$  are related to the soliton positions.

For elliptic solutions, we observed that the eigenvector function  $\varpi_L$  has a smooth infinite-length limit  $\varpi$  where the limit of the pole  $\check{k}_L$  actually describes the pole  $\check{k}$  for the asymptotic state. We suppose that the same holds for the spectral curve approximations of a generic asymptotic state. Concretely, we suggest that the poles at finite length  $L$  all have a proper infinite-length limit, and that this limit coincides with the poles of the asymptotic eigenvector function  $\varpi$ .

For a better understanding of the situation, it makes sense to inspect the poles of the asymptotic eigenvector function of pure soliton states. We will do so in terms of the spectral parameter  $u = k^2 + \phi_0$  where the resulting dependence of  $\check{u}(x)$  on  $x$  will be very illuminating.

For a single soliton, we find an  $x$ -dependence as described previously as

$$\check{u}(x) = \phi_0 - \alpha^2 \tanh(\alpha(x - \check{x}))^2. \quad (3.30)$$


Note that the divisor pole starts and ends asymptotically at the soliton point  $\check{u} = \phi_0 + \check{k}^2$ , and it switches to the other side of the branch cut when it reaches the peak at  $\phi_0$ .

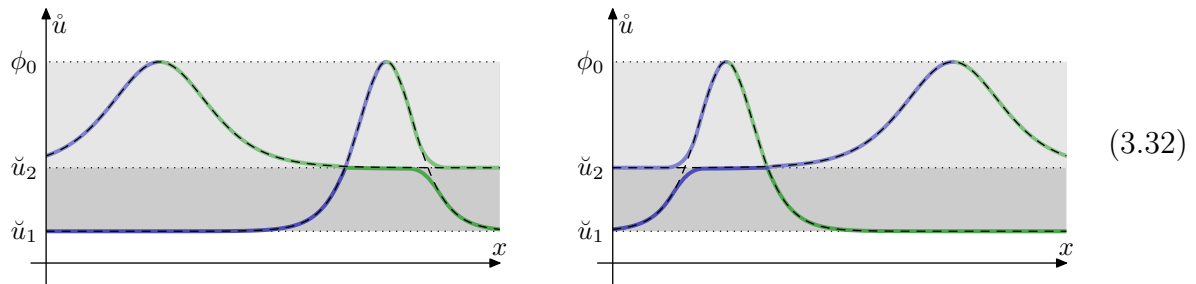
For a two-soliton state, the divisor poles  $\check{u}(x)$  are given by the solutions to a quadratic equation (formulated in terms of  $k$ ):

$$\check{k}_1(\check{k}^2 - \check{k}_2^2) \coth(-i\check{k}_1(x - \check{x}_1)) - \check{k}_2(\check{k}^2 - \check{k}_1^2) \tanh(-i\check{k}_2(x - \check{x}_2)) - \check{k}(\check{k}_1^2 - \check{k}_2^2) = 0. \quad (3.31)$$

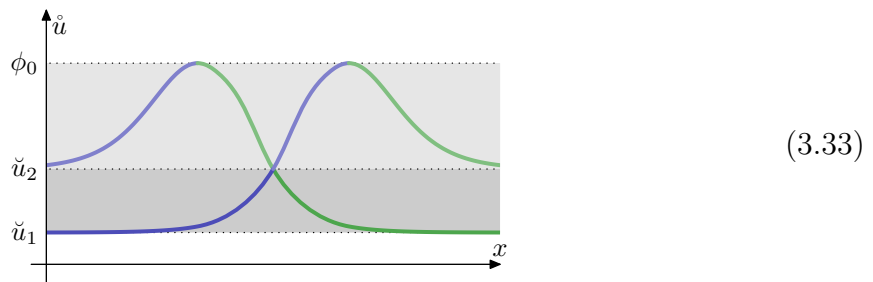
Here,  $\check{x}_{1,2}$  describe the positions of the two soliton centres.<sup>14</sup> The qualitative dependence of  $\check{u}$  on the position  $x$  depends largely on the distribution of the soliton centres. When the two solitons are well-separated, one finds that the resulting pair of functions is approximated

<sup>14</sup>The asymmetric dependency on the soliton parameters originates from an asymmetric yet convenient definition of the soliton centres  $\check{x}_{1,2}$  using the assumption  $\text{Im } \check{k}_1 > \text{Im } \check{k}_2$ .

by the superposition of the functions for two individual solitons:



We note that there are two distinct cases based on whether the slower and broader soliton is to the left or to the right of the faster and more focussed soliton. Conversely, when both solitons overlap significantly, one finds an  $x$ -dependency which is less evidently associated to the underlying state and its two contributing solitons:



Let us discuss the  $x$ -dependence of the divisor on the imaginary  $k$ -axis and point out relevant features supposing that the above picture generalises to arbitrary  $N$ .

Whenever the soliton centres are well-separated, the composition of the divisor as the union of the divisors of the individual solitons is well-expected because every soliton has an exponentially weak residual influence at the relevant regions for the other solitons. The cases where some solitons overlap significantly deforms smoothly to the cases where all solitons are well-separated

For all separations of soliton centres, every interval between two consecutive soliton momenta  $\check{u}_n$  and  $\check{u}_{n+1}$  is populated by exactly one pole  $\hat{u}_n$  of the divisor for all positions  $x$ .

The pattern of crossings of the divisor poles as a function of the position  $x$  is noteworthy: There are  $N(N - 1)/2$  actual pairwise crossings where the two poles  $\hat{u}_n$  and  $\hat{u}_{n+1}$  move in opposite directions and reside on opposite sides of the branch cuts. Moreover, these crossings must occur exactly at the soliton momentum  $\check{u}_{n+1}$  that separates the intervals of the divisor poles. The crossing can only occur at the prescribed point for the reason that every interval must be populated by one divisor pole for all  $x$ . This behaviour is compatible with spectral curves where the divisor poles must remain on the same branch cut for all  $x$ . The crossing at infinite length can thus be interpreted as an exchange of roles of two consecutive divisor poles.

Furthermore, one observes one avoided crossing for all pairs of well-separated solitons. Here, two consecutive poles come close while moving in the same direction, i.e. while they are on the same side of the cuts. Here, the crossing is avoided because such divisor poles repel each other.

It is interesting to observe that the divisor poles become exponentially slow at the soliton points  $\check{u}_n$ . This feature reflects the asymptotic behaviour of solitons.<sup>15</sup> However,

<sup>15</sup>In fact, this is how the position-dependence of the regularised monodromy gets suppressed in the

either by means of an actual or an avoided crossing, a pole can continue or pause and restart its journey around its branch cut. At such a crossing, the divisor poles exchange their roles in representing two different solitons.

Importantly, this pattern of crossings leads to the desired periodicity of the  $n$ -th divisor pole  $\check{u}_n$  encircling the  $n$ -th cut exactly  $n$  times as  $x$  advances by one period or, in the case of infinite length, along the whole real line.

In terms of physics, the position of the highest soliton divisor pole  $\check{u}_N$  is most immediately relevant: whenever it moves around the branch point  $\check{u}_{N+1} = \phi_0$ , the wave function displays a distinguished bump. This happens  $N$  times when all values of  $x$  are traversed, and these represent precisely the individual solitons. The other  $N - 1$  divisor poles merely act auxiliary variables that keep track of the positions of the other solitons. In the case of well-separated solitons, the other divisor poles are near their rest positions without significant influence on the shape of the wave function. However, when some solitons overlap, the subsequent divisor pole takes on a non-trivial position which contributes to an effective joining of the two soliton bumps into a single entity.

The most important conclusion to be drawn from the above discussion for our purposes is that all allowable configurations of divisor poles are actually realised by some configuration of the soliton centres relative to  $x$ . Therefore, the only requirement for a proper infinite-length limit is that the divisor poles associated to the cuts along the imaginary  $k$ -axis possess a proper limit, whereas the limiting divisor can be in an arbitrary configuration.

### 3.6 Local Charges

We have discussed a family of spectral curves that approximate a state on the infinite line. The branch cuts of these spectral curves must behave in a specific way, which also depends on the particular representation of the spectral curve, e.g. using a particular spectral parameter. Alternatively, the relevant moduli of spectral curves can be expressed in terms of action variables which express the sizes of cuts in a more universal scheme. Furthermore, action variables are the elementary phase space degrees of freedom to express integrable systems in. For instance, they obey useful relations with the local conserved charges and their corresponding wave numbers, see e.g. (2.28). Let us therefore investigate the infinite-length limit of action variables and local charges based on the discussion above.

From the family of spectral curves, we can read off the action variables as particular period integrals around the cuts. For the small cuts due to the continuum, we can locally assume as discussed in (3.17) that  $\cos q(k)$  oscillates with period  $2\pi/L$  and amplitude  $1/|\tau_n|$ . The action variable is determined by a period integral over the forbidden zone of the wave at position  $k_n$ . We find

$$\begin{aligned} I_n &= \frac{1}{i\pi} \oint_{\mathcal{A}_n} u \, dq \approx \frac{4k_n}{\pi L} \int_{-\arccos|\tau_n|}^{+\arccos|\tau_n|} \frac{z \sin(z) \, dz}{\sqrt{\cos(z)^2 - |\tau_n|^2}} \\ &= -\frac{4k_n}{L} \log|\tau_n| = -\frac{2\pi n}{L^2} \log(1 - |\rho_n|^2). \end{aligned} \quad (3.34)$$

---

infinite-length limit: for  $x \rightarrow \pm\infty$ , all soliton divisor poles  $\check{u}_n$  are exponentially close to their starting and ending positions at a soliton momentum  $\check{u}_n$ . Even though the full information on the soliton centres exists in the monodromy at finite but large  $L$  in the form of exponentially small contributions, it is impossible to extract it from the scattering matrix and difficult to reimplement manually into an approximation for the monodromy. Likewise, it is difficult to reconstruct the divisor at a position  $x$  within the region of interest because the soliton divisor poles are very different from their asymptotic values.

We can convert the discrete action variable  $I_n$  to an action density function  $I(k)$  which remains finite in the infinite-length limit:

$$I_n dn \approx I(k) dk, \quad I(k) := -\frac{2k}{\pi} \log(1 - |\rho(k)|^2). \quad (3.35)$$

Concerning the remaining branch cuts, we have to bear in mind that solitons are associated to the interval between two branch cuts rather than to a single branch cut. Consequently, every branch cut connects two consecutive soliton singularities. The action variable for the branch cut thus depends on the data for two solitons. We can disentangle the two contributions by composing the cycle around the  $n$ -th branch cut as the difference of two large cycles around all branch cuts from  $n$  through  $N$  and from  $n+1$  through  $N$ . For large  $L$ , the contributions from the other branch cuts on the period integral are suppressed and we can reuse the result obtained from the elliptic curve. We find

$$I_n \approx \frac{4L}{3\pi} \left( (\text{Im } \check{k}_n)^3 - (\text{Im } \check{k}_{n+1})^3 \right), \quad (3.36)$$

where we formally define  $\check{k}_{N+1} = 0$ . Note that here the action variable diverges linearly in the infinite-length limit.

Next, we would like to relate the action variables to the local charges expressed through the scattering data for states on the infinite line. These can be computed from the expansion of the quasi-momentum  $q(u)$  at  $u \rightarrow \infty$  and thus at  $k \rightarrow \infty$ . Using that  $\rho(k)$  should be exponentially small at  $k \rightarrow \infty$ , we have the relation  $q \approx kL + \arg \tau$ . Furthermore, using the relation  $u = k^2 + \phi_0$ , the expansion of  $q(u)$  at  $u \rightarrow \infty$  translates to an expansion of  $\arg \tau(k)$  in terms of the Galilei-invariant charges:

$$\arg \tau(k) = -\frac{Q - \frac{1}{2}\phi_0 L}{k} - \frac{\tilde{P}}{4k^3} - \frac{\tilde{E}}{16k^5} - \dots \quad (3.37)$$

We have seen that the transmission coefficient  $\tau(k)$  is determined by a convolution integral of the other scattering data. The expansion of  $\arg \tau(k)$  at  $k \rightarrow \infty$  yields

$$\arg \tau(k) = \sum_{j=0}^{\infty} \frac{1}{k^{2j+1}} \left( \sum_{n=1}^N \frac{2(-1)^j}{2j+1} (\text{Im } \check{k}_n)^{2j+1} + \int_0^{\infty} \frac{dk'}{\pi} k'^{2j} \log(1 - |\rho(k')|^2) \right), \quad (3.38)$$

where we have used the reality condition  $\rho(-k) = \rho(k)^*$ . We can now directly read off the Galilei-invariant conserved charges as

$$\begin{aligned} Q &\approx \frac{1}{2}\phi_0 L - \sum_n 2 \text{Im } \check{k}_n - \int_0^{\infty} \frac{dk}{\pi} \log(1 - |\rho(k)|^2), \\ \tilde{P} &\approx + \sum_n \frac{8}{3} (\text{Im } \check{k}_n)^3 - \int_0^{\infty} \frac{2k dk}{\pi} 2k \log(1 - |\rho(k)|^2), \\ \tilde{E} &\approx - \sum_n \frac{32}{5} (\text{Im } \check{k}_n)^5 - \int_0^{\infty} \frac{2k dk}{\pi} 8k^3 \log(1 - |\rho(k)|^2). \end{aligned} \quad (3.39)$$

We point out that for a non-zero asymptotic field value  $\phi_0$ , the charge  $Q$  (and thus the original charges  $P, E$ ) contain contributions with a non-trivial asymptotic charge density.

The differentials of these conserved charges can be expanded in the basis of differentials of action variables. We find the generic form for a conserved charge  $J = Q, \tilde{P}, \tilde{E}$  (up to



the contribution of  $d\phi_0$  to  $Q$ ) as

$$\begin{aligned} dJ &\approx \sum_{n=1}^N \left( \sum_{j=1}^n \frac{\pi f_J(\check{k}_j)}{\check{k}_j L} \right) dI_n - \int_0^\infty \frac{2k dk}{\pi} f_J(k) d \log(1 - |\rho(k)|^2) \\ &= - \sum_{n=1}^N 4 \operatorname{Im} f_J(\check{k}_n) d(\check{k}_n^2) + \int_0^\infty dk f_J(k) dI(k), \end{aligned} \quad (3.40)$$

where the  $f_J(k)$  are some applicable profile functions for which we find

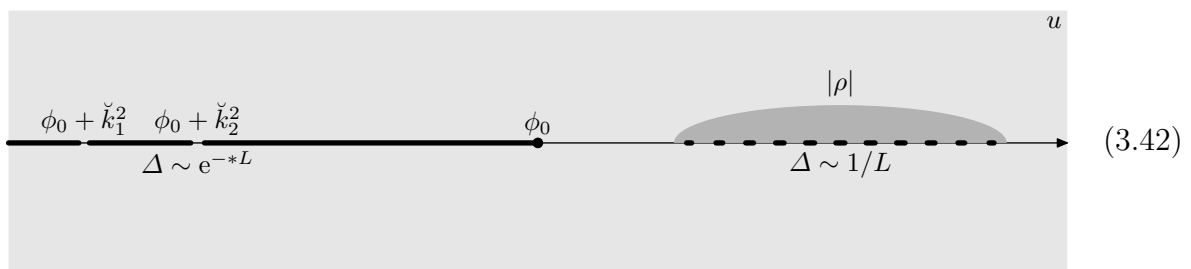
$$f_Q(k) \approx \frac{1}{2k}, \quad f_{\tilde{P}}(k) = 2k, \quad f_{\tilde{E}}(k) \approx 8k^3. \quad (3.41)$$

A fundamental relation of integrable systems is that angle variables shift linearly under transformations generated by conserved charges. Therefore, the coefficients  $f_J(k)$  represent periodicities for the corresponding angle variables. We can thus verify that the above action variables yield a consistent set of relations with the conserved charges and angle variables. First, we note that the slopes corresponding to translations in  $x$ , namely  $f_{\tilde{P}}(k_n) = 2\pi n/L$  and the coefficient  $2\pi n/L$  of  $dI_n$  in  $d\tilde{P}$ , take on the required discrete values  $(2\pi/L)\mathbb{Z}$  to ensure that the angle variables shift by integer multiples of  $2\pi$  over one period. At the level of spectral curves, this exact relation is ensured by the Riemann bilinear identity. Furthermore, the slope  $f_{\tilde{E}} \approx 8k^3$  is precisely the coefficient for time evolution of the argument of the reflection function  $\rho$ . Finally, all soliton slopes scale as  $1/L$  indicating that the wave trains for solitons lose their periodic behaviour in the infinite-length limit.

### 3.7 Asymptotic Limit

We have investigated how different structures of the inverse scattering method are represented in spectral curves in the infinite-length limit. We will now summarise the resulting asymptotic behaviour for spectral curves. This describes the conditions for the existence of the infinite-length limit at the level of spectral curves and it provides expressions for the limiting scattering data. We will also convert the expressions from the momentum variable  $k$  to the spectral parameter  $u = \phi_0 + k^2$  using (3.5) which is a more natural parameter for the spectral curve and all branch cuts reside on the real axis in this picture.

The distribution of the branch cuts for the spectral curve at large  $L$  takes the following form:



Let us sketch the expected distribution of branch cuts along the real line for a family of spectral curves with an appropriate asymptotic limit: The family of curves must consist of two distinct sets of branch cuts. There must be a fixed number of  $N + 1$  branch cuts on the left. All branch points must have a well-defined large- $L$  limit such that the intervals

between the cuts decrease exponentially with  $L$ . Note that the first branch point is fixed to  $-\infty$  while the last one limits to  $\phi_0$  that represents the asymptotic value of the KdV field. The second set consists of an asymptotically increasing number of branch cuts to the right of  $\phi_0$ .<sup>16</sup> These are arranged in a regular pattern such that their lengths shrink to zero as  $1/L$  while the relative filling along the real axis approaches a well-defined density in the large- $L$  limit.

The first set of  $N+1$  branch cuts (labelled by  $n = 0, \dots, N$ ) describes the configuration of solitons: a pair of consecutive branch points must have a common limit

$$\hat{u}_n^-, \hat{u}_{n-1}^+ \rightarrow \check{u}_n = \phi_0 + \check{k}_n^2, \quad \check{k}_n = i\sqrt{\phi_0 - \check{u}_n}, \quad (3.43)$$

and which describes the soliton pole  $\check{k}_n$ . The remaining cuts (labelled by  $n = N+1, \dots$ ) are delimited by the branch points (3.21) which for  $n \sim L$  must arrange in a regular pattern

$$\hat{u}_n^\pm \sim \phi_0 + \frac{\pi^2 n^2}{L^2} \pm \frac{2\pi n}{L^2} \arcsin|\rho(\pi n/L)| + \dots, \quad (3.44)$$

which describes the magnitude of the reflection function  $\rho(k)$ . This constitutes the complete set of conserved data for the asymptotic state in the inverse scattering method.

These data determine the transmission function  $\tau(k)$  according to the dispersion relation (3.13) which constrains the asymptotic behaviour of the spectral curve data further: The separation of the branch points corresponding to solitons shrinks exponentially according to the relation (3.29):

$$\hat{u}_n^- - \hat{u}_{n-1}^+ \approx 8 \operatorname{Im}(\check{k}_n) \operatorname{Im} \operatorname{res} \tau(\check{k}_n) \exp(i\check{k}_n L). \quad (3.45)$$

The remaining branch points corresponding to the continuum must take the limiting behaviour

$$\hat{u}_n^\pm \sim \phi_0 + \left[ \frac{\pi n - \arg \tau(\pi n/L) \pm \arccos|\tau(\pi n/L)|}{L} \right]^2. \quad (3.46)$$

In effect, this limiting relation describes the magnitude and phase of the transmission function  $\tau(k)$  in terms of the modulation pattern of the branch cuts which must behave as follows: As the length  $L$  increases, the individual branch cuts move towards  $\phi_0$  while they also shrink accordingly. However, the relative filling of the cuts remains fixed in place along the real axis according to the function  $\tau(\pi n/L)$ . Note that a finite point  $u$  resides near the  $n$ -th branch cut with  $n \approx Lu/\pi$ , therefore the number of branch cuts must asymptotically grow. Note further the shift by  $\arg \tau(\pi n/L)$  has a relatively large effect on the first few cuts with  $n = N+1, \dots$  where  $\arg \tau(0) \approx \pi N$  so that the first few cuts are positioned near the central point  $\phi_0$ .

To avoid some of the above complications in fixing detailed relations for the branch point positions, the spectral curve configuration can be described in terms of action variables, see (3.36) and (3.34). The relevant insight is that the action variables of the cuts on the left all scale as  $L$ . The soliton poles  $\check{k}_n$  on the imaginary axis are expressed in terms of the limiting behaviour of the action variables as

$$\sum_{m=n}^N I_m \sim \frac{4L}{3\pi} (\operatorname{Im} \check{k}_n)^3. \quad (3.47)$$

---

<sup>16</sup>Importantly, the lengths of cuts must follow a certain limiting pattern. This requirement yields some flexibility in assigning the individual cuts so that their number will typically increase linearly with  $L$ , but may actually fluctuate with  $L$  or be infinite altogether.

As discussed in Sec. 3.5, the divisor poles for these cuts must all have proper limiting points which can be in an arbitrary configuration. The action variables corresponding to continuum cuts were determined in (3.34),

$$I_n \sim -\frac{2\pi n}{L^2} \log(1 - |\rho(\pi n/L)|^2) = -\frac{4\pi n}{L^2} \log|\tau(\pi n/L)|. \quad (3.48)$$

Note that their limiting behaviour directly specifies the magnitude of the reflection and transmission functions.

The limiting behaviour of the divisor is more intricate, and it has been discussed in detail in Sec. 3.3 and Sec. 3.5. Most noteworthy, the analysis for the continuum cuts showed that the effective phases  $\sigma_n$  for the position of a divisor pole on its respective cut must be aligned properly for a coherent state to form in the infinite-length limit. These phases must shift rapidly by an angle of  $2\pi/L$  from one cut to the next according to (3.24). The effective phase then determines the argument of the reflection function  $\rho$

$$\frac{2\pi n x}{L} - \sigma_n \rightarrow \arg \rho(\pi n/L). \quad (3.49)$$

In this section, we have thus characterised how a family of spectral curves describing periodic KdV states degenerates to the scattering data describing a KdV state on an infinite line with proper asymptotic boundary conditions. We conclude that this family of spectral curves necessarily displays two sectors of branch cuts which behave very differently in the infinite-length limit and which describe the two distinct structures of the spectral data, namely the solitons and the continuum.

## 4 Continuous Heisenberg Magnet

After having laid down the procedure for finite-length extrapolation of a generic infinite-length KdV state in the previous section, we will now apply it to the continuous Heisenberg magnet (CHM). This further prototypical integrable model displays inverse scattering and spectral curve data with somewhat different features, which thus makes it an interesting case to discuss and compare. Its equation of motion is a version of the Landau–Lifshitz equation [22] and it is equivalent to the nonlinear Schrödinger (NLS) equation.

The CHM model consists of a spin vector field  $\vec{S} \in S^2 \subset \mathbb{R}^3$  in one spatial dimension. The equation of motion is the isotropic Landau–Lifshitz equation

$$\dot{\vec{S}} = \vec{S} \times \vec{S}'' . \quad (4.1)$$

We will express the spin vector in terms of the complex stereographic projection  $\zeta \in \bar{\mathbb{C}}$

$$\vec{S} = \frac{1}{1 + \zeta \bar{\zeta}} \begin{pmatrix} \zeta + \bar{\zeta} \\ -i\zeta + i\bar{\zeta} \\ 1 - \zeta \bar{\zeta} \end{pmatrix} . \quad (4.2)$$

The equation of motion for  $\zeta$  then takes the equivalent form

$$\dot{\zeta} = i\zeta'' - \frac{2i\bar{\zeta}\zeta'^2}{1 + \zeta \bar{\zeta}} . \quad (4.3)$$

The integrable structure of the model can be expressed in terms of the auxiliary linear problem

$$\Psi' = A\Psi, \quad A(u) = \frac{i}{u} \vec{\sigma} \cdot \vec{S} \quad (4.4)$$

with the components

$$A(u) = \frac{i}{u} \frac{1}{1 + \zeta \bar{\zeta}} \begin{pmatrix} 1 - \zeta \bar{\zeta} & 2\bar{\zeta} \\ 2\zeta & \zeta \bar{\zeta} - 1 \end{pmatrix}, \quad \Psi = \begin{pmatrix} \Psi_1 \\ \Psi_2 \end{pmatrix}. \quad (4.5)$$

Let us start by introducing the inverse scattering method for infinite-length states and the spectral curve method for finite-length periodic states along with their sets of data. We will then discuss some simple states and adjust our method for obtaining the infinite-length limit of periodic states. This allows us to extract the limiting structures that give rise to the continuum and solitons. Finally we summarise.

## 4.1 Scattering Data

The inverse scattering method for the CHM model has been discussed in [5, 6, 23, 24]. For the infinite line, we assume the asymptotic conditions

$$\lim_{x \rightarrow \pm\infty} \vec{S} = \begin{pmatrix} 0 \\ 0 \\ 1 \end{pmatrix} \iff \lim_{x \rightarrow \pm\infty} \zeta = 0. \quad (4.6)$$

As usual, the solutions of the auxiliary problem can be characterised by their asymptotic properties in the far left or in the far right where the Lax connection simplifies to the diagonal form

$$\lim_{x \rightarrow \pm\infty} A(u) = \begin{pmatrix} -ik & 0 \\ 0 & ik \end{pmatrix} \quad \text{with} \quad k := -\frac{1}{u}. \quad (4.7)$$

Consequently, the states are characterised by the spin direction (up or down) in combination with their momentum  $\pm k$ . The two states with prescribed asymptotics on the left and the two corresponding ones for the right are related by a linear relation which is expressed through the scattering matrix

$$S(k) = \lim_{x_{\mp} \rightarrow \mp\infty} \begin{pmatrix} e^{ikx_+} & 0 \\ 0 & e^{-ikx_+} \end{pmatrix} W(u; x_+, x_-) \begin{pmatrix} e^{-ikx_-} & 0 \\ 0 & e^{ikx_-} \end{pmatrix}. \quad (4.8)$$

The underlying Lax parallel transport  $W(u; x_+, x_-)$  from  $x_-$  to  $x_+$  takes the same general form as before in (3.8). We parametrise the auxiliary scattering matrix as

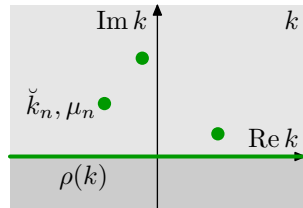
$$S(k) = \begin{pmatrix} 1/\tau(k) & -\rho(k)/\tau(k) \\ \rho(k^*)^*/\tau(k^*)^* & 1/\tau(k^*)^* \end{pmatrix} \quad (4.9)$$

in terms of the complex transmission and reflection functions  $\tau(k)$  and  $\rho(k)$ , respectively. The scattering matrix is unimodular by construction,  $\det S = 1$ , which implies the following relation between the scattering functions

$$1 + \rho(k)\rho(k^*)^* = \tau(k)\tau(k^*)^*. \quad (4.10)$$

Furthermore, the scattering matrix obeys the relation  $S(k)^\dagger = S(k^*)^{-1}$  which reduces to plain unitarity for real momenta  $k$ .

The scattering data for the CHM model consists of the reflection function  $\rho(k)$  on the real axis  $k \in \mathbb{R}$  together with  $N$  soliton momenta  $\check{k}_n \in \bar{\mathbb{C}}^+$  in the upper half complex plane and corresponding dynamical coefficients  $\mu_n \in \mathbb{C}$ :


(4.11)

The transmission function  $\tau(k)$  on the upper half of the complex plane including the real axis,  $\text{Im } k \geq 0$ , should be fixed by a dispersion relation. In analogy to the formula (3.13) for the KdV scattering problem, we expect it to take the form:

$$\tau(k) = \left[ \prod_j \frac{\check{k}_j}{\check{k}_j^*} \frac{k - \check{k}_j^*}{k - \check{k}_j} \right] \exp \left[ \frac{1}{2\pi i} \int dk' \left( \frac{1}{k' - k - i0} - \frac{1}{k'} \right) \log(1 + |\rho(k')|^2) \right]. \quad (4.12)$$

By construction, this function features the following analytic behaviour: It is meromorphic for  $\text{Im } k > 0$  with poles at the prescribed positions  $\check{k}_j$ . For  $\rho(k) = 0$ , it agrees with expectations for purely solitonic states, see also [23]. For small  $\rho(k)$  we have confirmed that it agrees with the leading-order result from the inverse scattering method. Furthermore, the magnitude of  $\tau(k)$  for real  $k$  is determined by the distributional identity in (3.14) as

$$|\tau(k)| = \sqrt{1 + |\rho(k)|^2}. \quad (4.13)$$

This implies the relation  $|\tau|^2 = 1 + |\rho|^2$  which follows from hermiticity of the CHM model auxiliary linear problem on the real  $k$ -axis. Finally, at  $k = 0$  and thus  $u = \infty$ , the Lax connection becomes trivial implying  $\tau = 1$ .

Let us now collect the key differences to the scattering data for the KdV model. First, the reflection and transmission functions are genuinely complex functions for the CHM model whereas in the KdV model they obey the reality conditions  $\tau(k)^* = \tau(-k)$  and  $\rho(k)^* = \rho(-k)$ . Second, the reflection function  $\rho(k)$  is unconstrained for  $k \in \mathbb{R}$ , its magnitude is not bounded by 1 as for the KdV model while the magnitude of the transmission function  $\tau(k)$  is bounded from below by 1 rather than from above. The soliton momenta  $\check{k}_j$  can reside anywhere on the upper complex half plane rather than being restricted to the positive imaginary axis, and the dynamical coefficients  $\mu_n$  are complex rather than real. Finally, the soliton momenta do not need to be distinct for the CHM model, there can be any number of coincident soliton momenta (supposing the corresponding dynamical coefficients  $\mu_n$  are adjusted appropriately to this situation).

Finally, it makes sense to express some essential conserved charges in terms of the scattering data. The momentum  $P$  and energy  $E$  can be expressed in terms of the expansion of  $\tau(k)$  around the point  $k = 0$  as

$$\arg \tau(k) = \frac{P}{2} + \frac{E}{4k} + \dots \quad (4.14)$$

Likewise, the angular momentum is expressed by the expansion around the point  $k = \infty$ :

$$\arg \tau(k) = \Delta J k + \dots \quad (4.15)$$

Here,  $\Delta J$  denotes the difference of the angular momentum to the angular momentum of the ground state which has a constant angular momentum density 1 and thus carries an

infinite amount of angular momentum on the infinite line. The resulting charges for an asymptotic state specified through its scattering data thus read

$$\begin{aligned}
P &= 4 \sum_j \arg \check{k}_j + \frac{1}{\pi} \int \frac{dk}{k} \log(1 + |\rho(k)|^2), \\
E &= 8 \sum_j \text{Im} \check{k}_j + \frac{2}{\pi} \int dk \log(1 + |\rho(k)|^2), \\
\Delta J &= -2 \sum_j \frac{\text{Im} \check{k}_j}{|\check{k}_j|^2} - \frac{1}{2\pi} \int \frac{dk}{k^2} \log(1 + |\rho(k)|^2).
\end{aligned} \tag{4.16}$$

The derivative of a charge  $Q = P, E, \Delta J$  can be expressed universally as

$$dQ = \sum_j 2 \text{Im} \left[ f_Q(\check{k}_j) d \left( -\frac{1}{\check{k}_j} \right) \right] + \int f_Q(k) \frac{dk}{2\pi k^2} d \log(1 + |\rho(k)|^2), \tag{4.17}$$

with the profile functions

$$f_P(k) = 2k, \quad f_E(k) = 4k^2, \quad f_{\Delta J}(k) = -1. \tag{4.18}$$

## 4.2 Spectral Curve and Divisor

We now turn to the states for a finite interval with periodic boundary conditions

$$\vec{S}(x + L) = \vec{S}(x). \tag{4.19}$$

States with these boundary conditions are described by spectral curves which are likewise based on the above auxiliary linear problem, see [12]. Here, the monodromy  $T(u)$  is defined as the parallel transport of the Lax connection  $A(u; x)$  over one period

$$T(u; x) = W(u; x + L, x). \tag{4.20}$$

The data of the underlying state are encoded by the eigensystem of the monodromy  $T$  as follows.

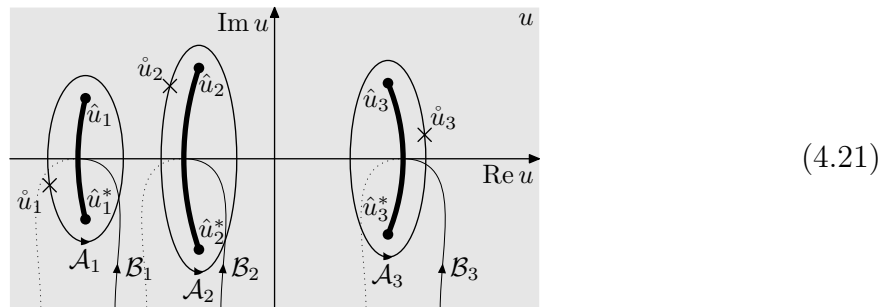
The two eigenvalues are independent of the reference point  $x$  and they are conserved in time. As  $\det T = 1$  is fixed, it suffices to denote the eigenvalue functions as  $\tau(u)$  and  $1/\tau(u)$ . The diagonalisation of  $T(u)$  introduces  $2K$  square-root branch points  $\hat{u}_j$  for the eigenvalue function  $\tau(u)$  on the complex  $u$ -plane. These are the points where the monodromy becomes non-diagonalisable implying that both eigenvalues coincide, thus  $\tau(\hat{u}_j) = \pm 1$ . Due to reality of the physical system, the branch points  $\hat{u}_j$  are distributed symmetrically around the real axis. Furthermore, the branch points cannot reside on the real axis because the monodromy is unitary and thus diagonalisable for real  $u$ . Therefore, it makes sense to pair up branch points as complex conjugates  $\hat{u}_{K+j} = \hat{u}_j^*$  such that a branch cut extends vertically between them in the complex plane.<sup>17</sup>

---

<sup>17</sup>The position of branch cuts is not universally defined: The simplest choice is to let all branch cuts extend purely vertically. A more physically meaningful choice is to require the action density to be real along the branch cut; then the branch cuts curl slightly away from the origin of the  $u$ -plane [25]. Unfortunately, the resulting configuration of branch cuts can be rather intricate even leaving some discrete freedom.

Next to the branch points  $\hat{u}_j$ , there are two distinguished values  $u = \infty$  and  $u = 0$ . For the former, the Lax connection trivialises such that  $T(\infty) = 1$ . For the latter, the singularity of the Lax connection yields an exponential singularity in  $\tau(u)$  at  $u = 0$ . To better control it, we introduce the quasi-momentum  $q(u)$  defined as the logarithm of the eigenvalue function,  $q(u) := -i \log \tau(u)$ . This function has a single pole at  $u = 0$  with residue  $L$ . As the logarithm introduces a  $2\pi$ -ambiguity in  $q$ , it makes sense to instead consider its derivative  $dq/du$ .

Altogether, the spectrum of the monodromy determines the spectral curve as the set of permissible pairs  $(u, \pm dq/du)$ . With the above properties of  $\tau(u)$ , the spectral curve is a Riemann surface of genus  $K - 1$  with punctures at the two points  $u = 0$ . The branch cuts split the spectral curve into two sheets corresponding to the two eigenvalues. The distribution of branch cuts of can be depicted as follows:



The configuration of branch points encodes the conserved charges of the state through integrals on the spectral curve: We define  $\mathcal{A}_j$  as a closed contour encircling the complex conjugate pairs of branch points  $\hat{u}_j, \hat{u}_j^*$  and  $\mathcal{B}_j$  as an open contour connecting the two points with  $u = \infty$  passing between  $\hat{u}_j$  and  $\hat{u}_j^*$ .<sup>18</sup> The A-periods of  $dq$  are all zero while its B-periods<sup>19</sup> evaluate to integer multiples of  $2\pi$ . The remaining continuous data on conserved charges is expressed by A-periods of  $u dq$ . Altogether we have the relations

$$\oint_{\mathcal{A}_j} dq = 0, \quad \frac{1}{2\pi} \int_{\mathcal{B}_j} dq = n_j, \quad \frac{1}{2\pi i} \oint_{\mathcal{A}_j} u dq = I_j. \quad (4.22)$$

In physical terms, the data of the spectral curve describe a set of  $K$  excitations with action variables  $I_j \in \mathbb{R}$  and mode numbers  $n_j \in \mathbb{Z}$  corresponding to the spatial period. The mode numbers are equivalently obtained as the values of the quasi-momentum function at the branch points,  $q(\hat{u}_j) = q(\hat{u}_j^*) = \pi n_j$ . All of the  $I_j$  and  $n_j$  represent independent quantities. Furthermore, the expansions of the quasi-momentum at the special points  $u = \infty$  and  $u = 0$  yield the total angular momentum  $J$ , the momentum  $P$  and the energy  $E$  (as well as the higher conserved charges):

$$q(u) = \frac{J}{u} + \mathcal{O}(1/u^2), \quad q(u) = \frac{L}{u} - \frac{1}{2}P + \frac{1}{4}Eu + \mathcal{O}(u^2). \quad (4.23)$$

The conserved charges are related to the action variables by the vanishing of the net residue of  $u dq$ :

$$\sum_{j=1}^K I_j = L - J. \quad (4.24)$$

<sup>18</sup>This assignment is not universal, it depends on the choice of branch cut distribution. Our choice is clearest if the branch cuts are short and well separated, but there also exist situations where branch cuts collide, overlap or join. To address the latter, we take a continuous deformation to well-separated branch cuts to define a proper assignment.

<sup>19</sup>Strictly speaking, only differences of B-periods are period integrals for closed cycles. Here, it is convenient to incorporate the fixed values  $\tau(u) = +1$  at  $u = \infty$ .

Furthermore, a Riemann bilinear identity implies the following relation among the conserved charges

$$-2\pi \sum_{j=1}^K n_j I_j = LP. \quad (4.25)$$

This concludes the description of conserved data.

The time-dependent data of the underlying state are encoded by the eigenvectors of the monodromy  $T(u)$ . It suffices to consider the points  $u = \check{u}_j$ <sup>20</sup> where the monodromy eigenvector points in a given reference direction. There are precisely  $K$  such points, their set is called the dynamical divisor and they encode the dynamical data for the state.

The divisor points depend on the reference point  $x$  for the monodromy  $T(u; x)$ . Towards reconstruction of a state  $\vec{S}(x)$ , it makes sense to consider the entire dependence of the divisor on  $x$ . This dependency is well-prescribed by the Lax connection and it which can be sketched qualitatively as follows: Each divisor point  $u = \check{u}_j$  is associated to one branch cut. As  $x$  increases by one period, the divisor point moves  $n_j$  times around the associated branch cut (loosely speaking along  $\mathcal{A}_j$ ).<sup>21</sup>

To conclude, let us compare the spectral curve picture with the one for the KdV model, and point out relevant differences. The most immediate difference is that for the CHM model the branch cuts are oriented in a vertical direction rather than horizontally along the real axis as for the KdV model. There is no semi-infinite branch cut in the CHM model. Also the behaviour of the divisor points is substantially more intricate in the CHM model than in the KdV model. In the KdV model, each divisor point resides on a unique branch point as far as the reference direction for the monodromy eigenvectors is suitably chosen. In the CHM model, there is no such choice, and the divisor points merely move around a loosely associated branch cut.

### 4.3 Simple States

In this section, we will gather some experience on the infinite-length limit for the CHM model by considering three families of explicit states and how they are related. They all represent travelling wave solutions with an invariant shape [26, 5] travelling at a fixed velocity  $v$  and rotating about the  $z$ -axis with an angular frequency  $\omega$ . Using rotational symmetry, we always fix the overall angular momentum to be aligned with the  $z$ -axis.

The first family of states describes a single CHM soliton which in stereographic projection takes the form

$$\zeta(x) = \exp(2i \operatorname{Re}(\check{k})(x - y) + i\phi) \frac{i \sin(\arg \check{k})}{\cosh(2 \operatorname{Im}(\check{k})(x - y) - i \arg \check{k})}. \quad (4.26)$$

This state describes a localised travelling and rotating bump on the real line with asymptotics  $\zeta(x) \rightarrow 0$  as  $x \rightarrow \pm\infty$ . The complex parameter  $\check{k}$  with  $\operatorname{Im} \check{k} > 0$  describes the singularity of the scattering matrix in the inverse scattering method. It encodes the spatial velocity and angular frequency of the soliton wave function as

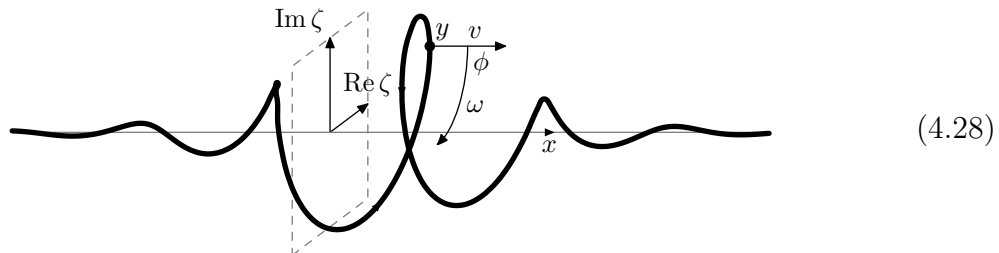
$$\check{k} = -\frac{1}{4}v + \frac{i}{4}\sqrt{4\omega - v^2} \quad \iff \quad v = -4 \operatorname{Re}(\check{k}), \quad \omega = 4|\check{k}|^2. \quad (4.27)$$

<sup>20</sup>More precisely, points on the spectral curve because these also specify uniquely the corresponding eigenvalue or eigenvector.

<sup>21</sup>Unfortunately, this is merely an oversimplified picture because the contours around the branch points may recombine when they are too large (depending on the choice of reference direction) or when branch cuts are too close or even unite. Nevertheless, the simplified picture can be used for bookkeeping purposes.



An interesting consequence of these relations is that for a given velocity  $v$  there is a lower bound  $\omega \geq \frac{1}{4}v^2$  on the angular frequency. The two dynamical variables  $y$  and  $\phi$  describe the spatial position of the bump and its angle about the  $z$ -axis. The shape of the soliton can be depicted as follows:



The conserved charges of the soliton read:

$$P = 4 \arg(\check{k}), \quad E = 8 \operatorname{Im}(\check{k}), \quad \Delta J = -2 \frac{\operatorname{Im}(\check{k})}{|\check{k}|^2}. \quad (4.29)$$

They are in perfect agreement with the general expressions (4.16) for the inverse scattering method.

The second family of states describes spin waves with constant amplitude

$$\zeta(x) = \tan(\frac{1}{2}\vartheta) \exp(-i\kappa x + i\phi), \quad \kappa := \frac{2\pi n}{L}. \quad (4.30)$$

In this state, the spin vector rotates at a constant latitude  $\vartheta$  around the  $z$ -axis. The state is periodic with wave length  $L > 0$  and it has the periodicity mode number  $n \in \mathbb{Z}$ . The wave number in the spatial direction is thus  $\kappa = 2\pi n/L$  so that the wave function actually repeats  $|n|$  times within the periodicity interval  $L$ .<sup>22</sup> The sign  $s = \operatorname{sign} n = \operatorname{sign} \kappa = \pm 1$  determines the direction of motion. As their amplitude is perfectly constant, the notion of initial position  $y$  is intertwined with the notion of initial angle  $\phi$ , and the state is already specified by either quantity. In terms of dynamics, the state travels along the spatial direction with velocity  $v = -\kappa \cos \vartheta$  and rotates about the  $z$ -axis with angular frequency  $\omega = -\kappa v = \kappa^2 \cos \vartheta$ . Again, the latter two processes are indistinguishable.

Let us briefly discuss the spectral curve data for this periodic class of states. The quasi-momentum function is given by

$$q = \pi n + \frac{\pi n}{u} \sqrt{u^2 - \frac{4u}{\kappa} \cos \vartheta + \frac{4}{\kappa^2}} = \pi n + \frac{\pi n}{u} \sqrt{u - \hat{u}} \sqrt{u - \hat{u}^*} \quad (4.31)$$

with the complex branch point

$$\hat{u} = \frac{L}{\pi n} \exp(is\vartheta) \quad \Longleftrightarrow \quad L = \pi |n\hat{u}|, \quad \vartheta = s \arg(s\hat{u}). \quad (4.32)$$

The spectral curve is of the rational kind

$$\frac{dq}{du} = \pi n \operatorname{Re}(\hat{u}) \frac{u - u_*}{u^2 \sqrt{u - \hat{u}} \sqrt{u - \hat{u}^*}}, \quad u_* = \frac{L}{\pi n \cos \vartheta} = \frac{|\hat{u}|^2}{\operatorname{Re}(\hat{u})}. \quad (4.33)$$

<sup>22</sup>One might effectively divide  $L$  by  $n$  and consider only states with mode number  $\pm 1$ . These have the same wave function, but they belong to different sectors of the mechanical model specified by the periodicity parameter  $L$ . In particular, general states can be viewed as (non-linear) superpositions of spin waves with different  $n$ .

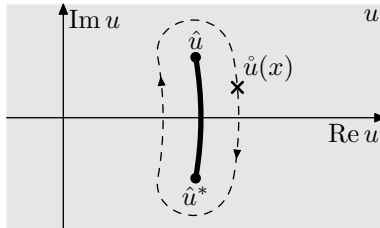
The conserved charges of the state read:

$$P = -2\pi n(1 - \cos \vartheta), \quad E = \frac{2\pi^2 n^2}{L} \sin^2 \vartheta, \quad J = L \cos \vartheta. \quad (4.34)$$

Furthermore, the action variable integral yields:

$$I = \frac{1}{2\pi i} \oint_{\mathcal{A}} u dq = L(1 - \cos \vartheta) = \pi |n\hat{u}| - \pi n \operatorname{Re}(\hat{u}). \quad (4.35)$$

We sketch a branch cut trivialisation of the spectral curve:


(4.36)

We point out that states with the opposite angle  $\vartheta' = \pi - \vartheta$  and the opposite mode number  $n' = -n$  are related by a rotation of the spin vector by  $\pi$ . Their spectral curves are therefore the same. However, some of the above quantities are not identical, in particular,  $P' = 4\pi n + P$  and  $J' = -J$  as well as  $I' = 2L - I$ . These differences arise from a different configuration of the branch cut: In one case, the branch cut directly connects the two branch points, whereas in the other, it also winds around the singular point at  $u = 0$ . The associated A,B-cycles differ in their direction and in additional contributions from winding around  $u = 0$ .

Let us finally discuss the dynamical divisor for the class of rational states. From the explicit solution for  $\Psi$  of the auxiliary linear problem (4.4), we obtain its direction function  $\varpi(u) := \Psi_2/\Psi_1$  as

$$\varpi(u) = \frac{2e^{i\kappa x - i\phi} \sin(\vartheta)}{2 \cos(\vartheta) - u\kappa - \kappa\sqrt{u^2 - 4u \cos(\vartheta)}/\kappa + 4/\kappa^2}. \quad (4.37)$$

This expression can be inverted to get the divisor location for a reference direction  $\varpi_0$  as

$$\hat{u} = \frac{2 \cos(\vartheta) + \sin(\vartheta) (e^{i\kappa x - i\phi} \varpi_0 - (e^{i\kappa x - i\phi} \varpi_0)^{-1})}{\kappa}. \quad (4.38)$$

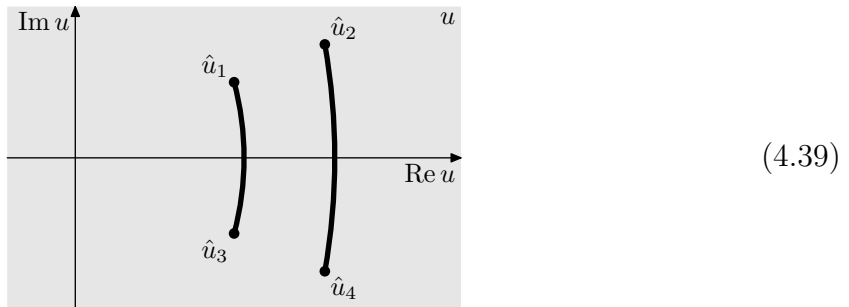
Effectively, the divisor as a function of  $x$  encircles the branch cut as sketched in the above figure. The initial angle  $\phi$  of the spin wave essentially corresponds to the phase of the around the branch cut.

The third family of states comprises wave functions of elliptic kind whose spectral curves therefore have genus  $g = 1$ . These states and corresponding curves are somewhat tractable in explicit form but nevertheless they lead to lengthy expressions which have not found much attention in the literature. For our purposes they illustrate the link between periodic and asymptotic states, and we work out the class of elliptic travelling wave solutions in App. A. Here we suffice ourselves by a qualitative discussion.

The travelling wave profile resembles the soliton profile in (4.28), but where the central part is periodically repeated (with properly smooth continuation). In other words, the amplitude  $|\zeta(x)|$  does not asymptote to zero at  $x \rightarrow \pm\infty$  as for the soliton, but rather

periodically oscillates between a maximum and minimum value. Next to the length of periodicity  $L$  and their overall orientation, travelling wave states are parametrised by two continuous static quantities  $v$  (velocity) and  $\omega$  (angular velocity), two discrete static quantities  $n_{1,2}$  (mode numbers for amplitude and angle) as well as two continuous dynamical quantities  $y$  (centre) and  $\phi$  (angle at centre).

In the spectral curve picture, the four static quantities relate to the four branch points  $\hat{u}_{1,2,3,4}$  which are distributed symmetrically in the complex plane around the real axis:



The dynamical divisor consists of two points  $\hat{u}_{1,2}$  which ultimately encode the two dynamical quantities of the state. As discussed in App. A.6, the functional shape of the divisor is intricate and it strongly depends on the parameters and additional choices that have to be made. For example, a divisor point may encircle one or both cuts one time, multiple times or not at all. We refrain from attempting to describe their shapes further.

We conclude this section by considering limiting cases of the above families of states: The soliton (4.26) degenerates into the ground state  $\zeta(x) = 0$  in the limit  $\text{Re}(\check{k}) \rightarrow 0$ . Similarly, the spin wave (4.30) degenerates into the ground state  $\zeta(x) = 0$  in the limit  $\vartheta \rightarrow 0$  (or equivalently to  $\zeta(x) = \infty$  at  $\vartheta \rightarrow \pi$ ). As the limit is approached, one can observe that the cut of the spectral curve closes and the action variable  $I$  vanishes. The states are plain trigonometric waves with small amplitude which in the KdV case correspondingly came to use for the finite-length approximation of the continuum in the inverse scattering method (see Sec. 2.7); we will see the same phenomenon in the infinite-length limit for the CHM model.

For the elliptic travelling waves, there are two qualitatively different limiting cases: We will discuss them in terms of the complex branch points  $\hat{u}_{1,2}$  of its spectral curve. When either of the branch points approaches the real axis,  $\text{Re}(\hat{u}_{1,2}) \rightarrow 0$ , the state degenerates into a spin wave (4.30) which is described by a spectral curve with the remaining non-trivial branch point  $\hat{u}_{2,1}$  and associated cut. When approaching the limit, the state is composed from the spin wave with a second small-amplitude spin wave superimposed on it. In the limit, the fluctuation disappears completely, and the parameter  $\hat{u}_{1,2}$  has no impact.

The elliptic travelling wave can also degenerate to the soliton (4.26) in the limit where the two branch cuts of the spectral curve are made to coincide, i.e. in the limit  $\hat{u}_2 \rightarrow \hat{u}_1$ . This degeneration results in a state of infinite length,  $L \rightarrow \infty$ , while keeping  $v$ ,  $\omega$  and  $n_{1,2}$  finite. The common limit of the two branch points serves as the parameter  $\check{k}$  for the soliton wave function (4.26) as  $\check{k} = -1/\check{u}$ . This is similar to how KdV elliptic states degenerate to solitons (see Sec. 2.6) with the main distinction that now branch points are off the real axis whereas in the KdV case they were restricted to it. Consequently, CHM solitons have one complex degree of freedom rather than a real one for KdV solitons. Similarly, it takes two branch cuts to coincide for the CHM spectral curve whereas merely the end of one branch cut degenerates with the beginning of the next in the KdV case.

## 4.4 Finite-Length Extrapolation

In the following, we will implement the finite-length extrapolation introduced in Sec. 3 for the CHM model.

We start by constructing a family of states  $\vec{S}_L(x)$  approximating some fixed infinite-length state  $\vec{S}(x)$  with asymptotic boundary conditions. We require the function  $\vec{S}_L(x)$  to periodically repeat a window of interest of  $\vec{S}(x)$  with the length  $L$ . These periodic states are thus defined by

$$\vec{S}_L(x + \mathbb{Z}L) := \vec{S}(x) \quad \text{with} \quad x_{-,L} < x < x_{+,L} = x_{-,L} + L. \quad (4.40)$$

In order to extract the Lax monodromy for  $\vec{S}_L$ , we again refer to the construction of the scattering matrix (4.8). To that end, the asymptotics of the Lax transport  $W(x_+, x_-)$  for small  $x_-$  and large  $x_+$  and for spectral parameter  $u = -1/k$  must be of the form

$$W(x_+, x_-) \sim \text{diag}(e^{-ikx_+}, e^{ikx_+}) S \text{diag}(e^{ikx_-}, e^{-ikx_-}). \quad (4.41)$$

Here we substitute the form of the scattering matrix (4.9) of the inverse scattering problem in terms of transmission and reflection functions, to find the approximation

$$W(x_+, x_-) \sim \begin{pmatrix} e^{-ik(x_+ - x_-)} / \tau(k) & -e^{-ik(x_+ + x_-)} \rho(k) / \tau(k) \\ e^{ik(x_+ + x_-)} \rho(k^*)^* / \tau(k^*)^* & e^{ik(x_+ - x_-)} / \tau(k^*)^* \end{pmatrix}. \quad (4.42)$$

The same qualifications as for the KdV model apply to this approximation. As discussed above, the transmission coefficient  $\tau$  can be reconstructed from the magnitude of the reflection coefficient  $|\rho|$  and the  $N$  soliton momenta  $\hat{k}_n$  using the dispersion relation.

To finally identify the branch points of the spectral curve, we consider the quasi-momentum function  $q$  via the monodromy trace:

$$\cos(q(k)) = \frac{1}{2} \text{tr} T(x) = \frac{1}{2} \text{tr} W(x + L, x) \approx \frac{e^{-ikL}}{2\tau(k)} + \frac{e^{ikL}}{2\tau(k^*)^*}. \quad (4.43)$$

The branch points are located where  $q(k) \in \pi\mathbb{Z}$  or, equivalently,  $\cos q(k) = \pm 1$ .

## 4.5 Continuum Cuts

First, we want to find the branch cuts associated to the continuum due to the reflection function  $\rho(k)$ . These ought to be short branch cuts near the real axis, so we can assume  $k \in \mathbb{R}$  such that the quasi-momentum can be expressed as

$$\cos(q(k)) \approx \frac{1}{|\tau(k)|} \cos(kL + \arg \tau(k)). \quad (4.44)$$

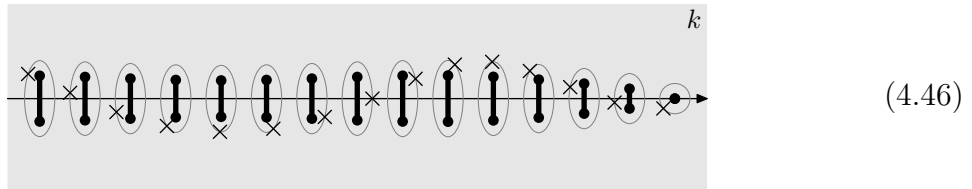
Recall that unitarity of the scattering problem for  $k \in \mathbb{R}$  implies that  $|\tau(k)| \geq 1$ , which means  $|\cos q(k)| \leq 1$ . The function  $\cos q(k)$  thus oscillates with an amplitude less than 1 and the values  $\pm 1$  could be attained only exceptionally.<sup>23</sup> This observation is in line with our earlier observation that there are no branch cuts on the real axis for the CHM model. However, if the argument to  $\cos$  acquires an imaginary part, also larger values absolute values are attained. We assume the quasi-momentum  $q(k)$  to be analytic near the real axis, and extrapolate  $\cos q(k)$  to the complex plane. The solutions  $\hat{k}$  to  $\cos q(k) = \pm 1$

<sup>23</sup>This can happen only where  $\rho = 0$ , and the resulting points are in fact no square-root branch points.

turn out to have only a small imaginary part which is attenuated by the factor of  $L$  in the argument of  $\cos$ . We can approximate the solutions as

$$\hat{k}_n^\pm \approx \frac{\pi n - \arg \tau_n \pm i \operatorname{arccosh} |\tau_n|}{L}, \quad (4.45)$$

leading to a distribution of branch cuts which we illustrate as follows:



This result is similar to the expression (3.19) for the KdV model, merely the trigonometric functions have been traded in for hyperbolic functions and the cuts are distributed vertically on the complex plane.

The distribution can be described as a deformed lattice of short cuts: Each short cut represents a small fluctuation of the ground state. The fluctuation with mode  $n$  is naturally located at momentum  $k_n := \pi n/L$ . The non-zero density of cuts along the real axis leads to a distortion of the horizontal lattice positions  $(\pi/L)\mathbb{Z}$  by the phase of the transmission function  $-\arg(\tau_n)/L$ :<sup>24</sup>

$$\frac{1}{2}(k_n^+ + k_n^-) \approx \frac{\pi n - \arg \tau_n}{L} = k_n - \frac{\arg \tau_n}{L}. \quad (4.47)$$

The lengths of the branch cuts are determined by the magnitude of the reflection function

$$\hat{k}_n^+ - \hat{k}_n^- \approx \frac{2i}{L} \operatorname{arccosh} |\tau_n| = \frac{2i}{L} \operatorname{arsinh} |\rho_n|. \quad (4.48)$$

For the second equality we have used the unitarity relation  $|\tau|^2 = 1 + |\rho|^2$ . Therefore, the length of the cuts is proportional to  $|\rho|$  for a small reflection coefficient  $\rho$ , and it scales as  $1/L$  for large periodicity length.

Let us also discuss the action variables associated to the continuum cuts. These relations will be useful in specifying the spectral curve in terms of such abstract but universally defined data. The action variable is given as a contour integral on the spectral curve. According to (4.44) the function  $\cos q(k)$  oscillates with amplitude  $1/|\tau_n|$  and periodicity  $2\pi/L$ . We then find

$$\begin{aligned} I_n &= \frac{1}{2\pi i} \oint_{\mathcal{A}_n} u \, dq \approx \frac{1}{\pi L k_n^2} \int_{-\operatorname{arccosh} |\tau_n|}^{+\operatorname{arccosh} |\tau_n|} \frac{z \sinh(z) \, dz}{\sqrt{|\tau_n|^2 - \cosh(z)^2}} \\ &= \frac{1}{L k_n^2} \log |\tau_n| = \frac{1}{2L k_n^2} \log(1 + |\rho_n|^2), \end{aligned} \quad (4.49)$$

which implies the following density function for the infinite-length limit

$$I(k) = \frac{1}{2\pi k^2} \log(1 + |\rho(k)|^2). \quad (4.50)$$

<sup>24</sup>Note that the phase of the transmission function should be understood as a continuous function on the real axis with the asymptotics  $\arg \tau(k) \rightarrow 0$  as  $k \rightarrow \infty$ .

The expression  $I_n$  agrees with the action variable for a rational state at leading order in small  $\rho_n$ , see (4.35) and the form  $I(k)$  matches with the integral kernel in (4.17).

The configuration of the dynamical divisor for asymptotic CHM states is much harder to discuss analytically for various reasons. For instance, the monodromy eigenvectors will change rapidly around the branch cuts which become dense in the infinite-length limit. Picking out a dedicated direction therefore is delicate given that we have access to the reflection function only for real  $u$ . Furthermore, see the comments on the divisor shape in App. A.6. Qualitatively, we expect a distribution of divisor points which move around their associated branch cut in a coherent fashion determined by the reflection function, see (4.46), and in analogy to the KdV case discussed in Sec. 3.3.

## 4.6 Soliton Cuts

To retrieve the branch points corresponding to solitons, we approximate the quasi-momentum for  $k$  in the upper half plane in analogy to (3.27) as

$$\cos q \approx \frac{e^{-ikL}}{2\tau(k)}. \quad (4.51)$$

Branch points are determined by the condition  $\cos q = \pm 1$ . Note that the exponent in  $\cos q$  becomes very large in the upper half plane, so branch points must be exponentially close to the poles of the transmission function  $\tau$  so that the denominator can balance the numerator. These points precisely describe the momenta of solitons and their generalisations. Let us assume that there are  $m$  coincident soliton momenta at  $k = \check{k}$ . The transmission function then expands as

$$\tau(k) = \alpha(k - \check{k})^{-m} + \dots \quad (4.52)$$

We thus find  $2m$  solutions  $\hat{k}_j$ ,  $j = 1, \dots, 2m$ , to the equation  $\cos q(k) = \pm 1$  given by<sup>25</sup>

$$\hat{k}_j = \check{k} + (2\alpha)^{1/m} \exp\left(\frac{i\check{k}L + i\pi j}{m}\right) + \dots \quad (4.53)$$

These branch points are symmetrically situated on a circle around the soliton momentum  $\check{k}$ .<sup>26</sup> As for the KdV model, the soliton branch points are separated by an exponentially small distance  $\sim \exp(-L \operatorname{Im} \check{k}/m)$  at large length  $L$ . In addition, the soliton branch points for CHM spiral towards the soliton momentum  $\check{k}$  with the angle increasing as  $\sim L \operatorname{Re} \check{k}/m$ , and thus the spiral is tilted with an angle of  $\arg(-i\check{k})$ .

Let us first discuss the elementary configuration for a simple soliton,  $m = 1$ , which consists of  $2m = 2$  branch cuts. This is different from the representation of solitons in the KdV model where a soliton is encoded by the gap between two branch cuts and thus requires only half as many branch cuts in total. This is also related to the fact that the motion of a soliton in KdV has merely a single real degree of freedom (speed), whereas here we need two real degrees of freedom (speed and frequency) or one complex degree of freedom ( $\check{k}$ ) to describe the motion of CHM solitons.

<sup>25</sup>There is always an even number of solutions, and the sign of  $\cos q(\hat{k}_j)$  alternates with  $j$ .

<sup>26</sup>This feature provides a compelling reason why configurations with  $m > 1$  coincident soliton momenta cannot exist in the KdV model: In the spectral curve, configurations with  $m > 1$  would clearly imply branch points away from  $u \in \mathbb{R}$ . Only for  $m = 1$ , the symmetric distribution yields (two) branch points aligned on a straight line.

The resulting structures for  $m = 1$  can be inferred from the detailed discussion of the family of elliptic states in App. A, in particular from the discussion of the infinite-length limit in App. A.8. The configuration is described by two mode numbers  $n_{1,2}$  and two action variables  $I_{1,2}$ . The mode numbers are consecutive integers  $n_2 = n_1 + 1$ .<sup>27</sup> The action variables have the leading-order behaviour

$$I_{1,2} = \pm \frac{2L}{\pi} \arg \check{k} + \dots, \quad (4.54)$$

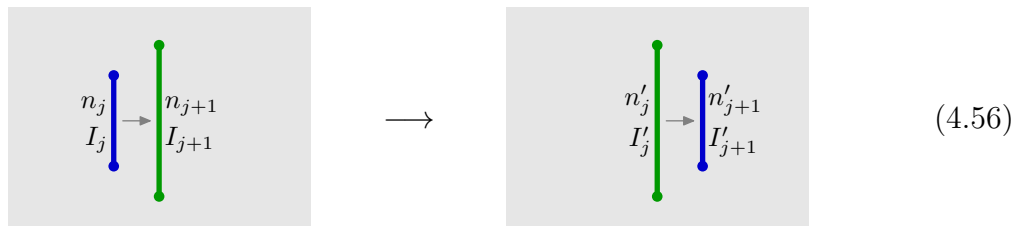
which is determined by the complex angle of  $\check{k}$  alone. The magnitude of the variable  $\check{k}$  appears only at the next-to-leading order

$$I_1 + I_2 = \frac{2 \sin(\arg \check{k})}{|\check{k}|} + \dots = \frac{2 \operatorname{Im} \check{k}}{|\check{k}|^2} + \dots \quad (4.55)$$

Curiously, the action variable  $I_2$  is negative: This is related to the fact, that the soliton is in fact a large excitation of the opposite vacuum state  $\zeta = \infty$ . The action variable that describes the excitation above the opposite vacuum is given by  $\tilde{I}_2 = I_2 + 2J$  and it is positive. Nevertheless, it is easier to work with action variables corresponding to the  $\zeta = 0$  vacuum which can consequently attain negative values.

An important observation concerning the configurations branch points and cuts was made in [27]: As the continuous parameters of the family of elliptic states are varied, the branch cuts move in the complex plane. This can happen in such a way that the branch points circle around their centre, and this is precisely what happens as the length  $L$  increases, see App. A.8: Consider two branch cuts with adjacent mode numbers  $n$  and  $n + 1$ . The branch cuts start out short and are then expanded in such a way that the branch points remain close. One finds that at first the two cuts are separate (case  $I_{n,n+1}$ , see [27]). At some point the growing cuts meet at their centres (case  $D_{n,n+1}$ ) and join by a condensate of two straight cuts (case  $II_{n,n+1}$ ). The branch points then circle around each other until the one with mode number  $n$  meets the condensate cut (case  $C_{n+1}$ ). By crossing the condensate cut the mode number of the branch cut changes from  $n$  to  $n + 2$  (case  $II_{n+1,n+2}$ ). The circling of branch cut can continue indefinitely as the mode numbers increase one step for each half rotation.

A relevant operation in this sequence is to move branch points or singularities through a branch cut which implies a reshuffling the A,B-cycles and thus of the mode numbers  $n_j$  and action variables  $I_j$ . For instance when branch cut  $j$  including its branch points moves through branch cut  $j + 1$ ,



$$(4.56)$$

these numbers transform as follows:

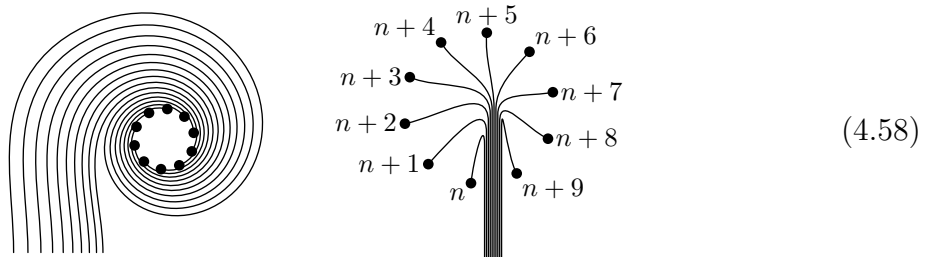
$$n'_j = n_{j+1}, \quad n'_{j+1} = 2n_{j+1} - n_j, \quad I'_j = 2I_j + I_{j+1}, \quad I'_{j+1} = -I_j. \quad (4.57)$$

<sup>27</sup>In fact, the labelling of cuts and mode numbers is opposite in App. A, but it can be adjusted by switching labels or signs.

As the branch cuts exchange their relative position, we also exchange the labels accordingly. If we have two consecutive mode numbers,  $n_{j+1} = n_j + 1$ , the transformation effectively shifts both mode numbers by one unit,  $(n'_j, n'_{j+1}) = (n_j + 1, n_{j+1} + 1)$ . This explains the transition from case  $I_{n,n+1}$  to case  $I_{n+1,n+2}$ . Conversely, the large-length assignments (4.54,4.55) effectively remain unchanged.

It remains to generalise the above limiting behaviour to the case of coincident solitons with poles of higher degree  $m > 1$ , but there are several difficulties in doing so: We do not have explicit expressions to investigate the general case concretely. For  $2m$  branch cuts, we need to assign  $2m$  mode numbers  $n_j$  and  $2m$  action variables  $I_j$ . These are more values to be assigned than the two degrees of freedom (speed and frequency), hence there have to be some constraints or ambiguities among the values. Even worse, the  $2m$  branch cuts can be distributed in various entangled ways to connect the branch points  $\hat{k}_j$  to their respective complex conjugates  $\hat{k}_j^*$ . Even though such different configurations are equivalent to each other, they lead to different assignments of values for the mode numbers and action variables. Nevertheless, let us explore how the above picture may generalise to a larger number of branch points.

We first consider some suitable (topological) configurations of branch cuts. We highlight two useful choices for the configuration of branch cuts and discuss their implications:



The configurations essentially differ in that the cuts all extend either outwards from the circle or inwards into it.

In the first configuration, the branch cuts extend on a spiralling path along the large-length trajectories of the branch points described above. One can obtain it starting with very short branch cuts and letting the branch points circle around each other. In doing so, we deform the branch cuts to avoid crossings with any of the branch points. The cuts thus follow a spiralling path towards the branch points in the upper half of the complex plane. Here, the configuration of mode numbers

$$n_j = n + \frac{1}{2} + \frac{1}{2}(-1)^j, \quad (4.59)$$

should alternate between two adjacent integers  $n$  and  $n + 1$ . A basic argument in favour of this pattern is as follows: The quasi-momentum function  $q$  is continuous on the disc centred at  $\check{k}$  and it is approximated through (4.52) there. By construction the quasi-momentum alternates between even and odd integers on the perimeter. If these were not adjacent integers, the quasi-momentum would attain further integer values near  $\check{k}$  which would correspond to further, undesirable branch points.

In the second configuration, all  $2m$  branch cuts meet near  $k$  before extending towards  $k^*$  as a bundle and splitting up again. Here, one naturally obtains a pattern of mode numbers

$$n_j = n + j - 1, \quad (4.60)$$

which increases linearly along the circle from  $n$  to  $n + 2m - 1$ . The bundled branch cuts serve as the boundary which starts and ends the sequence. Here, the branch cuts within



the disk invalidate the argument which constrained the mode number to be adjacent integers in the former configuration. Note that the beginning and end of the sequence can be altered by moving the first or last branch cut through all others. The corresponding transformation (4.57) shifts all mode number effectively by  $+1$  or  $-1$ , respectively, but the overall increasing sequence remains intact.

The two configurations of branch cuts can be transformed into each other: Here one has to revert the order of all branch cuts which effectively flips the ends of branch cuts inside out. It turns out that the corresponding sequence of transformations (4.57) maps between the alternating pattern  $n_j = n + \frac{1}{2} + \frac{1}{2}(-1)^j$  for the first configuration and the linearly increasing pattern  $n_j = n + j - 1$  for the second configuration. Note that the base mode number  $n$  does not appear to play a role in the infinite-length limit as the position  $\check{k}$  is fully determined by the action variables in (4.54) and (4.55).

Based on the explicit results (4.54,4.55) for the elementary soliton with  $m = 1$ , we conjecture that the action variables have the following large-length behaviour

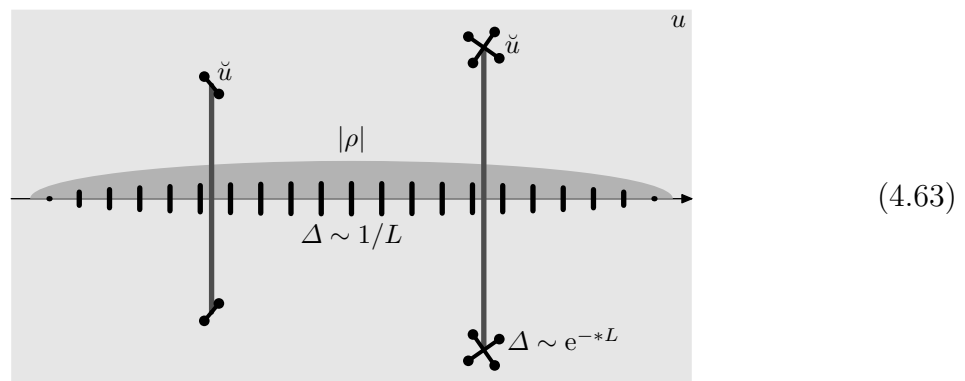
$$I_j = (-1)^{j+1} \frac{2L}{\pi m} \arg \check{k} + \dots, \quad \sum_{j=1}^{2m} I_j = \frac{2 \operatorname{Im} \check{k}}{|\check{k}|^2} + \dots \quad (4.61)$$

The second relation simply reflects the soliton contribution to  $\Delta J = J - L$  in (4.16) to the identity (4.24)  $\sum_j I_j = L - J = -\Delta J$ . The pattern of leading-order contributions to the action variables merely alters between negative and positive sign. This pattern is distinguished by being stable under the transformation (4.57) for any pair of adjacent branch cuts, and in particular for the cyclic shift that shifts the mode numbers by one unit in the second configuration for the branch cuts. The magnitude of the leading-order contributions to the action variables  $I_j$  can then be inferred from the identity (4.25) such that

$$-2\pi \sum_{j=1}^{2m} n_j I_j = 4L \arg \check{k} + \dots = LP. \quad (4.62)$$

## 4.7 Asymptotic Limit

Now we summarise the resulting asymptotic behaviour for a family of spectral curves in parallel to Sec. 3.7 in the  $u$ -plane. We recall from the previous sections that the branch cuts have two different types of limiting behaviour for large length. The distribution of the branch cuts for the spectral curve at large  $L$  can be sketched as follows:



We point out that some of the features of the infinite-length asymptotics of spectral curve data have been described in [18], albeit for the case of the sine-Gordon model whose

spectral curves share several aspects with those of the CHM model. In particular, one can recognise the lattice of short cuts which is described as a sequence of spines protruding from the real axis.

The first admissible configuration is a bundle of long branch cuts which is identified with (multiple coincident) solitons: A general soliton configuration consists of  $N$  pole singularities  $\check{k}_j$  of degree  $m_j$  in the upper half of the complex plane (with their conjugates in the lower half). For each singularity of degree  $m$ , there are  $2m$  corresponding branch points  $\hat{u}_j$ ,  $j = 1, \dots, 2m$  (as well as their complex conjugates), which approach a common value

$$\hat{u}_j \rightarrow \check{u} = -\frac{1}{\check{k}}. \quad (4.64)$$

This limiting behaviour determines the momentum  $\check{k}$  and multiplicity  $m$  of the associated soliton.

The second set of short branch cuts located symmetrically around the real  $u$ -axis are identified with the continuum. They are delimited by pairs of complex conjugate branch points which for  $n \sim L$  are approximated by

$$\hat{u}_n, \hat{u}_n^* = -\frac{L}{\pi n} \pm \frac{L}{\pi^2 n^2} i \operatorname{arsinh} |\rho(\pi n/L)| + \dots \quad (4.65)$$

Here, the length determines the magnitude of the reflection function for the continuum. We thus recover all invariant data required for the inverse scattering method.

The transmission function  $\tau(k)$  is then fixed by the dispersion relation (4.12). As for the KdV model, it constrains the limiting behaviour further. In particular, the  $2m$  branch points  $\hat{u}_j$  corresponding to an  $m$ -fold soliton must be located symmetrically around  $\check{u}$ . As  $L \rightarrow \infty$ , their distance shrinks exponentially and they spin around the centre according to the relation (4.53):

$$\hat{u}_j \approx \check{u} + (2\alpha)^{1/m} \check{u}^2 \exp\left(-\frac{L}{m} \frac{\operatorname{Im} \check{u}}{|\check{u}|^2}\right) \exp\left(-i \frac{L}{m} \frac{\operatorname{Re} \check{u}}{|\check{u}|^2} + \frac{i\pi j}{m}\right). \quad (4.66)$$

Here,  $\alpha$  is the coefficient of the  $m$ -fold pole in the transmission function  $\tau(k)$  at  $k = \check{k}$  defined by the expansion

$$\tau(k) = \frac{\alpha}{(k - \check{k})^m} + \dots \quad (4.67)$$

The branch points corresponding to the continuum must obey the limiting behaviour

$$\hat{u}_n = -\frac{L}{\pi n} + \frac{L}{\pi^2 n^2} \left[ -\arg \tau(\pi n/L) + i \operatorname{arcosh} |\tau(\pi n/L)| \right] + \dots \quad (4.68)$$

Note that the mode number  $n$  is assumed to be of the order of  $L$  such that the above relation consists of a leading-order term  $-L/\pi n$  and a sub-leading correction. This limiting relation describes the magnitude and phase of the transmission function  $\tau(k)$  in terms of the modulation pattern of the branch cuts which must behave as follows: As the length  $L$  increases, the individual branch cuts grow but also move towards  $\infty$  in a linear fashion. However, the relative filling of the cuts remains fixed in place along the real axis according to the function  $\tau(\pi n/L)$ . Since a finite point  $u$  resides near the  $n$ -th branch cut with  $n \approx Lu/\pi$ , the number of branch cuts must asymptotically grow and only those modes contribute whose  $n$  grows with the same rate as  $L$ .

## 5 Conclusions and Outlook

In this paper we have explored the infinite-length limit of states of the spectral curve method in detail. For two prototypical integrable models of one-dimensional fields, the Korteweg-de Vries equation and the Continuous Heisenberg Magnet, we have investigated the features of families of states that provide them with a proper infinite-length limit which is consequently described by the inverse scattering method. In brief our results can be summarised as follows:

There are two distinct classes of branch cut configurations for spectral curves with proper infinite-length limits. One class consists of a collection of a growing number of branch cuts whose size and separation shrinks correspondingly. This configuration gives rise to continuum states in the inverse scattering method such that the density of branch cuts relates to the magnitude of the reflection and transmission functions. The other class consists of a fixed number of branch cuts whose ends approach each other exponentially fast. Such a configuration gives rise to soliton states where the limit of branch points describes the soliton momenta. The qualitative features of the branch cut configurations depend somewhat on the underlying model. In particular there is a major distinction between a positive and negative signature of excitations which is related to the compactness of the fields, signature of unitarity and orientation of branch cuts in the complex plane which also has an impact on the statistics for soliton excitations.

Next to the conserved data for states, we have also addressed the time-dependent data which is embodied by the dynamical divisor for spectral curves as well as by phase information for the inverse scattering method. The configuration of dynamical divisors turn out to be rather complex and they depend strongly on the situation and on various implementation details. Therefore we have merely discussed them at a qualitative level. Roughly the divisor points orbit around the branch cuts and the phases of the orbits must be correlated strongly for a proper infinite-length limit. The phases of the orbits describe the complex phases of the infinite scattering method data.

The scheme for the infinite-length limit of integrability methods has several generalisation and applications that may be explored further:

As emphasised above, our understanding of the time-dependent data is incomplete and could be described in more detail. This would require a better understanding of the dynamical divisor which likely requires a mapping to the Jacobian of the spectral curve by means of the Abel map and theta-functions. This may come close to a formal functional treatment of the spectral curve solutions, see the earlier work [14–18]. Moreover, we have only addressed the limit of the data. It would be interesting to derive the relevant inverse scattering equations, in particular the Gel'fand–Levitan–Marchenko integral equation, from the equations of the spectral curve method.

The scheme ought to be applicable to wider classes of integrable one-dimensional models. These could be deformations of the above models with twisted closed boundary conditions such that their infinite-length limit can result in different boundary conditions in the left and right asymptotic region. These could as well be different kinds of models, such as the sine-Gordon model, where it will be interesting to understand and interpret the the relevant adjustments. Furthermore, the methods of integrability extend to one-dimensional integrable lattice models with minor adjustments due to discreteness. We expect that the scheme extends to chain models with minor adjustments due to discreteness.

Finally, in terms of applications, one might use states of the inverse scattering method

as a first approximation to states of the spectral curve method. Such states can be used as a suitable starting point in an approximation method for reasonably long states, which avoids having to deal with elaborate functional analysis for higher-genus Riemann surfaces.

## Acknowledgements

We thank Jacqueline Angersbach, Patrick Dorey, Egor Im, Alexander Its, Fedor Smirnov, Charles Thull and Anders Wallberg for discussions related to the project and previous work on the subject. The work of NB is partially supported by the Swiss National Science Foundation through the NCCR SwissMAP. The work of KG is supported by the Inlaks Shivdasani Foundation Scholarship, Knut and Alice Wallenberg Foundation Grant KAW 2021.0170, and by the Olle Engkvists Stiftelse Grant 2180108.

## A Elliptic Solution in CHM

In this appendix we derive the class of elliptic solutions to the continuous Heisenberg model. We extend the early work [26] by analysing and discussing some of the relevant properties of these solutions in detail.

We will proceed in analogy with the derivation of the KdV elliptic solution in Sec. 2 by assuming a travelling wave with a constant shape. This will turn out to produce a general elliptic solution which is quasi-periodic in space and which can be specialised to properly periodic or asymptotic solutions by suitable choices of parameters.

### A.1 Equation of Motion

The continuous Heisenberg model is based on a field  $\vec{S}(x, t) \in \mathbb{R}^3$  which is restricted to the unit sphere  $S^2$  by the constraint  $\|\vec{S}\| = 1$ . The equation of motion with normalised parameters takes the form

$$\dot{\vec{S}} = \vec{S} \times \vec{S}'' . \quad (\text{A.1})$$

We parametrise points  $\vec{S} \in S^2$  in terms of a complex variable  $\zeta \in \mathbb{C}$  by means of the stereographic projection

$$\vec{S} = \frac{1}{1 + \zeta\bar{\zeta}} \begin{pmatrix} \zeta + \bar{\zeta} \\ -i\zeta + i\bar{\zeta} \\ 1 - \zeta\bar{\zeta} \end{pmatrix} . \quad (\text{A.2})$$

The equations of motion in these variables take the form

$$\dot{\zeta} = i\zeta'' - \frac{2i\bar{\zeta}\zeta'^2}{1 + \zeta\bar{\zeta}}, \quad \dot{\bar{\zeta}} = -i\bar{\zeta}'' + \frac{2i\zeta\bar{\zeta}'^2}{1 + \zeta\bar{\zeta}} . \quad (\text{A.3})$$

Here, it will be convenient to assume  $\bar{\zeta} \in \mathbb{C}$  to be another complex variable independent of  $\zeta$ , and only eventually identify it with the complex conjugate  $\zeta^*$  by means of the reality condition  $\bar{\zeta} = \zeta^*$ . With that assumption, the first equation is linear in  $\bar{\zeta}$  and can be solved exactly in this variable:

$$\bar{\zeta} = - \frac{i\dot{\zeta} + \zeta''}{i\dot{\zeta}\zeta + \zeta''\zeta - 2\zeta'^2} . \quad (\text{A.4})$$

By substituting this solution back into the second equation yields a second-order differential equation for  $\zeta$ :

$$\frac{\ddot{\zeta}}{\zeta'} - \frac{4\dot{\zeta}\dot{\zeta}'}{\zeta'^2} + \frac{3\dot{\zeta}^2\zeta''}{\zeta'^3} + \frac{3\zeta''^3}{\zeta'^3} - \frac{4\zeta''\zeta'''}{\zeta'^2} + \frac{\zeta''''}{\zeta'} = 0. \quad (\text{A.5})$$

As an aside, we note that this equation can be integrated once to a conservation equation:

$$\frac{\partial}{\partial t} \frac{\dot{\zeta}}{\zeta'} + \frac{\partial}{\partial x} \left[ -\frac{3\dot{\zeta}^2}{2\zeta'^2} + \frac{\zeta'''}{\zeta'} - \frac{3\zeta''^2}{2\zeta'^2} \right] = 0. \quad (\text{A.6})$$

Here, we observe the Schwarzian derivative in the latter two terms: The model has an  $\text{SO}(3)$  rotational symmetry which amounts to a Möbius transformation for  $\zeta$ . The Schwarzian derivative is invariant under this transformation and also the terms involving time derivatives happen to be invariant.

## A.2 Travelling Wave Ansatz

We now make an ansatz of a wave function with constant shape analogously to the ansatz for the KdV equation that led to the class of elliptic solutions. Such an ansatz links the spatial translation symmetry with time translation symmetry such that the wave function takes on a constant velocity  $v$ . In addition, here we can make use of rotational symmetry and link it to time translations as well such that the wave function still preserves shape but rotates with a constant angular velocity  $\omega$ . Out of the  $\text{SO}(3)$  symmetries, without loss of generality, we choose rotations about the  $z$ -axis. The travelling wave ansatz reads

$$\zeta(x, t) = \exp(i\omega t) \zeta(x - x_0 - vt). \quad (\text{A.7})$$

The equation of motion translates into a fourth-order differential equation for  $\zeta(x)$  which also ensures that the equation of motion for  $\zeta(x, t)$  holds for all  $x$  and all  $t$  using the above symmetry considerations. Taking into account that the residual 2D rotational symmetry acts by multiplication on  $\zeta(x)$ , it makes sense to formulate the wave equation in terms of the logarithmic derivative  $G(x)$ :

$$G(x) := -i \frac{\zeta'(x)}{\zeta(x)}, \quad \frac{G'''}{G} - \frac{4G'G''}{G^2} + \frac{3G'^3}{G^3} + GG' - \frac{2\omega v G'}{G^2} + \frac{3\omega G'}{G^3} = 0. \quad (\text{A.8})$$

It is straight-forward to integrate this differential equation once:

$$\frac{G''}{G} - \frac{3G'^2}{2G^2} + \frac{1}{2}G^2 + \frac{2\omega v}{G} - \frac{3\omega^2}{2G^2} + \kappa = 0. \quad (\text{A.9})$$

However, we may as well divide the original equation by  $G$  and integrate to obtain an alternate second-order differential equation:

$$\frac{G''}{G^2} - \frac{G'^2}{G^3} + G + \frac{\omega v}{G^2} - \frac{\omega^2}{G^3} + \chi = 0. \quad (\text{A.10})$$

By combining the two equations, we eliminate the second-order term  $G''$  to obtain a first-order differential equation:

$$G'^2 = -P(G), \quad P(g) := g^4 + 2\chi g^3 - 2\kappa g^2 - 2\omega v g + \omega^2. \quad (\text{A.11})$$

The polynomial  $P(g)$  on the right-hand side is quartic with coefficients freely adjustable by choosing the parameters  $v$  and  $\omega$  as well as the integration constants  $\kappa$  and  $\chi$ . We can cast the polynomial in factorised form:

$$P(g) = (g - \hat{g}_1)(g - \hat{g}_2)(g - \hat{g}_3)(g - \hat{g}_4), \quad (\text{A.12})$$

where the roots  $\hat{g}_k$  are related to the parameters as follows:<sup>28</sup>

$$\begin{aligned} \omega &= \sqrt{\hat{g}_1 \hat{g}_2 \hat{g}_3 \hat{g}_4}, \\ v &= \frac{1}{2} \sqrt{\hat{g}_1 \hat{g}_2 \hat{g}_3 \hat{g}_4} (\hat{g}_1^{-1} + \hat{g}_2^{-1} + \hat{g}_3^{-1} + \hat{g}_4^{-1}), \\ \kappa &= -\frac{1}{2} (\hat{g}_1 \hat{g}_2 + \hat{g}_1 \hat{g}_3 + \hat{g}_1 \hat{g}_4 + \hat{g}_2 \hat{g}_3 + \hat{g}_2 \hat{g}_4 + \hat{g}_3 \hat{g}_4), \\ \chi &= -\frac{1}{2} (\hat{g}_1 + \hat{g}_2 + \hat{g}_3 + \hat{g}_4). \end{aligned} \quad (\text{A.13})$$

The differential equation is solved by the elliptic function

$$G(x) = \frac{(\hat{g}_4 - \hat{g}_1)\hat{g}_3 - (\hat{g}_3 - \hat{g}_1)\hat{g}_4 \operatorname{sn}(\alpha x + b, m)^2}{(\hat{g}_4 - \hat{g}_1) - (\hat{g}_3 - \hat{g}_1) \operatorname{sn}(\alpha x + b, m)^2}, \quad (\text{A.14})$$

where the elliptic modulus  $m$  and the scaling parameter  $\alpha$  are given by

$$m = \frac{(\hat{g}_3 - \hat{g}_1)(\hat{g}_4 - \hat{g}_2)}{(\hat{g}_3 - \hat{g}_2)(\hat{g}_4 - \hat{g}_1)}, \quad \alpha = \frac{1}{2} \sqrt{(\hat{g}_3 - \hat{g}_2)(\hat{g}_1 - \hat{g}_4)}, \quad (\text{A.15})$$

and where  $b$  is an integration constant incorporating the offset  $x_0$ .

In order to integrate the logarithmic derivative function  $G(x)$ , let us discuss its analytic structure: It is a meromorphic function with poles at  $\alpha x + b = \pm c$  with residues

$$G((-b \pm c)/\alpha + \epsilon) = \mp \frac{i}{\epsilon} + \mathcal{O}(\epsilon), \quad (\text{A.16})$$

where the constant  $c$  is defined by the inverse elliptic relations<sup>29</sup>

$$\operatorname{sn}(c)^2 = \frac{\hat{g}_1 - \hat{g}_3}{\hat{g}_3 - \hat{g}_1}, \quad \frac{\operatorname{sn}(c) \operatorname{cn}(c)}{\operatorname{dn}(c)} = \frac{2i\alpha}{\hat{g}_3 - \hat{g}_1}. \quad (\text{A.17})$$

The above poles imply zeros and poles at the respective positions. With this information, we can integrate  $G(x)$  and exponentiate to ultimately obtain the wave function  $\zeta(x)$  in terms of the Neville elliptic theta function  $\vartheta_s(z, m)$ :

$$\zeta(x) = \eta \exp(i\lambda(\alpha x + b)/2K) \frac{\vartheta_s(\alpha x + b - c)}{\vartheta_s(\alpha x + b + c)}. \quad (\text{A.18})$$

The constant  $\lambda$  of the exponent is defined in terms of the elliptic zeta function  $\operatorname{zn}(z, m)$ :

$$\lambda := \left[ \frac{\hat{g}_4}{\alpha} - 2i \operatorname{zn}(c) \right] 2K. \quad (\text{A.19})$$

<sup>28</sup>For any given  $P(g)$ , there are two choices for the sign of  $\omega$ . These correspond to two distinct solutions  $\zeta(x)$  and  $1/\zeta(-x)$ .

<sup>29</sup>Note that it takes two independent evaluations of elliptic functions to uniquely specify a point on the elliptic curve (up to shifts by the periods  $2K$  and  $2iK'$ ).

### A.3 Conjugate Field

We should now address the conjugate field  $\bar{\zeta}(x, t)$ . We first introduce a corresponding travelling wave ansatz and define the conjugate logarithmic derivative  $\bar{G}$ :

$$\bar{\zeta}(x, t) = \exp(-i\omega t) \bar{\zeta}(x - x_0 - vt), \quad \bar{G}(x) := i \frac{\bar{\zeta}'(x)}{\bar{\zeta}(x)}. \quad (\text{A.20})$$

As before, this reduces the equation of motion to a wave equation for  $\bar{G}$ , which is precisely the same as for  $G$ .<sup>30</sup> Note that the wave equation is homogeneous, therefore the solution for  $\bar{G}$  can differ from the one for  $G$  by a shift in the argument; in anticipation of the reality conditions, we choose the shift to be  $\bar{b} + K$  rather than  $b$  with some parameter  $\bar{b}$  so that

$$\bar{G}(x) = G(x - (b - \bar{b} - K)/\alpha). \quad (\text{A.21})$$

The integrated wave function  $\bar{\zeta}$  then takes the form

$$\bar{\zeta}(x) = \bar{\eta} \exp(-i\lambda(\alpha x + \bar{b})/2K) \frac{\vartheta_s(\alpha x + \bar{b} - c + K)}{\vartheta_s(\alpha x + \bar{b} + c - K)}. \quad (\text{A.22})$$

As such,  $\bar{\zeta}(x)$  merely describes a solution to the conjugate wave equation. We still need to satisfy the compatibility relation (A.4) between  $\bar{\zeta}(x)$  and  $\zeta(x)$ :

$$\bar{\zeta} = -\frac{1}{\zeta} \frac{\omega - vG - iG' + G^2}{\omega - vG - iG' - G^2}. \quad (\text{A.23})$$

Here, it is sufficient to consider selected points  $x$  to determine how the parameters of the two solutions are related. We find a relation between  $b$  and  $\bar{b}$  as well as between  $\eta$  and  $\bar{\eta}$ :

$$b - \bar{b} = 2d + K, \quad \eta\bar{\eta} = \exp(-i\lambda(2d + K)/2K) \frac{\vartheta_n(d + c)^2}{\vartheta_n(d - c)^2}, \quad (\text{A.24})$$

where the parameter  $d$  is defined by

$$\text{sn}(d)^2 = \frac{\hat{g}_1(\hat{g}_2 - \hat{g}_2)}{\hat{g}_3(\hat{g}_4 - \hat{g}_2)}, \quad \frac{\text{sn}(d) \text{cn}(d)}{\text{dn}(d)} = \frac{-2i\alpha\hat{g}_4\hat{g}_2}{\omega(\hat{g}_4 - \hat{g}_2)}. \quad (\text{A.25})$$

We have now satisfied all of the defining complexified equations.

In order to further restrict to physical solutions with  $\bar{\zeta}(x) = \zeta(x)^*$ , it makes sense to consider the combination  $\zeta\bar{\zeta}$  given by (A.23). Evidently, this function represents an absolute value squared and it needs to be positive real for all real values of  $x$ . As a consequence it turns out that the set of points  $\{\hat{g}_k\}$  must be self-conjugate. Without loss of generality and for concreteness, we make the assignments

$$\hat{g}_3 = \hat{g}_1^*, \quad \hat{g}_4 = \hat{g}_2^*, \quad (\text{Im } \hat{g}_3)(\text{Im } \hat{g}_4) \geq 0. \quad (\text{A.26})$$

Furthermore, the dynamical parameters  $b$  and  $\eta$  need to be chosen suitably. For that, we consider the extrema of the function  $\zeta\bar{\zeta}$  which are located at  $\alpha x + b = d$  and  $\alpha x + b = d + K$ . As the function  $\zeta\bar{\zeta}$  is real for real  $x$ , the extrema need to reside on the real axis thus requiring  $\text{Im } b = \text{Im } d$ . Together with the relation (A.24) we can solve for  $b$  and  $\bar{b}$ :

$$b = d + \beta, \quad \bar{b} = -K - d + \beta, \quad (\text{A.27})$$

---

<sup>30</sup>Note that the polynomial  $P(g)$  is real and hence it equally applies to  $G$  as for its complex conjugate  $\bar{G}$ .

where the remaining real constant  $\beta$  incorporates the spatial offset  $x_0$ . The relation between the pre-factors is resolved by

$$\eta = \exp(-i\lambda d/2K + i\phi) \frac{\vartheta_n(d+c)}{\vartheta_n(d-c)}, \quad \bar{\eta} = \exp(-i\lambda(d+K)/2K - i\phi) \frac{\vartheta_n(d+c)}{\vartheta_n(d-c)}, \quad (\text{A.28})$$

where  $\phi$  describes the initial angle around the  $z$ -axis.

This completes the derivation of the physical solution; let us summarise: The wave function takes the form<sup>31</sup>

$$\zeta(x) = \exp(i\lambda(\alpha x + \beta)/2K + i\phi) \frac{\vartheta_n(d+c)}{\vartheta_n(d-c)} \frac{\vartheta_s(\alpha x + \beta + d - c)}{\vartheta_s(\alpha x + \beta + d + c)}. \quad (\text{A.29})$$

Furthermore, the combination  $\zeta\bar{\zeta}$  can be written as the elliptic function

$$\zeta\bar{\zeta} = -\frac{\text{sn}(c-d)^2 - \text{sn}(\alpha x + \beta)^2}{\text{sn}(c+d)^2 - \text{sn}(\alpha x + \beta)^2}. \quad (\text{A.30})$$

The various contributing constants take the following reality conditions

$$v, \omega, \alpha, \beta, \lambda, \phi, m \in \mathbb{R}, \quad c, d \in (\frac{1}{2} + \mathbb{Z})K + i\mathbb{R}, \quad (\text{A.31})$$

as well as

$$\hat{g}_3 = \hat{g}_1^*, \quad \hat{g}_4 = \hat{g}_2^*, \quad (\text{Im } \hat{g}_3)(\text{Im } \hat{g}_4) \geq 0, \quad \bar{b} = b^*, \quad \bar{\eta} = \eta^*. \quad (\text{A.32})$$

This choice implies that the elliptic modulus is in the principal interval:

$$0 \leq m \leq 1. \quad (\text{A.33})$$

Qualitatively, the wave function  $\zeta(x)$  takes on a maximum magnitude at  $\alpha x + \beta = 0$  and a minimum magnitude at  $\alpha x + \beta = K$ . The magnitude further oscillates periodically between these two values, while the complex phase develops linearly with some superimposed oscillation of the same periodicity.

For the further discussion, it makes sense to express the various constants in terms of the independent parameters  $\alpha, m, d, c$ . We find<sup>32</sup>

$$\begin{aligned} \hat{g}_1 &= i\alpha \text{dc}(d) \text{dc}(c) (\text{sn}(d-c) - \text{sn}(d+c)), \\ \hat{g}_2 &= i\alpha m \text{cd}(d) \text{cd}(c) (\text{sn}(d-c) - \text{sn}(d+c)), \\ \hat{g}_3 &= i\alpha \text{ns}(d) \text{ns}(c) (\text{sn}(d-c) + \text{sn}(d+c)), \\ \hat{g}_4 &= i\alpha m \text{sn}(d) \text{sn}(c) (\text{sn}(d-c) + \text{sn}(d+c)), \\ \omega &= \alpha^2 m (\text{sn}(d-c)^2 - \text{sn}(d+c)^2), \\ v &= 2i\alpha \frac{\text{sn}(d-c) \text{cn}(d-c) \text{dn}(d-c) - \text{sn}(d+c) \text{cn}(d+c) \text{dn}(d+c)}{\text{sn}(d-c)^2 - \text{sn}(d+c)^2}, \\ \lambda &= 2i(\text{zn}(d-c) - \text{zn}(d+c))K. \end{aligned} \quad (\text{A.34})$$

The parameters  $\alpha, m, d, c$  take the following qualitative roles for the points  $\{\hat{g}_k\}$ : The shape of the configuration of  $\{\hat{g}_k\}$  is determined by  $c$  and  $m$ , while changing  $d$  and  $\alpha$  merely shifts and scales all  $\{\hat{g}_k\}$ , respectively.

<sup>31</sup>In this form, the function is invariant under shifts of the parameters  $c$  and  $d$  by  $2K$  and  $2iK'$ . Note that the shift of  $c$  by  $2iK'$  also induces a shift of  $\lambda$  by  $-4\pi$ .

<sup>32</sup>For what it is worth, the following derivative relations hold:  $\partial\lambda/\partial d = -i\omega L/\alpha$  and  $\partial\omega/\partial d = -i\omega v/\alpha$ .



## A.4 Auxiliary Linear Problem

Let us now construct the solution to the auxiliary linear problem for the CHM elliptic state:

$$\Psi' = A\Psi, \quad A = \frac{i}{u} \vec{\sigma} \cdot \vec{S} = \frac{i}{u} \frac{1}{1 + \zeta\bar{\zeta}} \begin{pmatrix} 1 - \zeta\bar{\zeta} & 2\bar{\zeta} \\ 2\zeta & \zeta\bar{\zeta} - 1 \end{pmatrix}, \quad \Psi = \begin{pmatrix} \Psi_1 \\ \Psi_2 \end{pmatrix}. \quad (\text{A.35})$$

As above, we can algebraically solve for the second component of the vector  $\Psi$  in terms of the first:

$$\Psi_2 = -\frac{i(1 + \zeta\bar{\zeta})u}{2\bar{\zeta}} \Psi_1' - \frac{(1 - \zeta\bar{\zeta})}{2\bar{\zeta}} \Psi_1. \quad (\text{A.36})$$

Upon substitution of  $\Psi_2$  into the second component of the auxiliary linear problem we obtain a second-order differential equation for  $\Psi_1$

$$\Psi_1'' + \left[ i \frac{\bar{G} + G\zeta\bar{\zeta}}{1 + \zeta\bar{\zeta}} \right] \Psi_1' + \left[ \frac{\bar{G} - G\zeta\bar{\zeta}}{1 + \zeta\bar{\zeta}} \frac{1}{u} + \frac{1}{u^2} \right] \Psi_1 = 0. \quad (\text{A.37})$$

By careful analysis of the coefficient function properties and singularities, the form of the solution can be deduced:

$$\begin{aligned} \Psi_1(x) &= \exp[iq(z)(\alpha x + \beta)/2K] \frac{\vartheta_n(\alpha x + \beta + c - z)}{\vartheta_n(\alpha x + \beta) \vartheta_s(z - c)}, \\ \Psi_2(x) &= \exp[i(q(z) + \lambda)(\alpha x + \beta)/2K + i\phi] \frac{\vartheta_n(\alpha x + \beta - c - z)}{\vartheta_n(\alpha x + \beta) \vartheta_s(z + c)}. \end{aligned} \quad (\text{A.38})$$

The spectral parameter  $u = u(z)$  in the above differential equation is expressed in terms of the uniformised parameter  $z$  by the function

$$u(z) = \frac{i}{\alpha m} \frac{1 - m \operatorname{sn}(d)^2 \operatorname{sn}(c)^2}{\operatorname{sn}(d) \operatorname{cn}(d) \operatorname{dn}(d)} \frac{1 - m \operatorname{sn}(d)^2 \operatorname{sn}(z)^2}{\operatorname{sn}(c)^2 - \operatorname{sn}(z)^2}. \quad (\text{A.39})$$

The function  $q(z)$  takes the form<sup>33</sup>

$$q(z) = i(\operatorname{zn}(d - z) - \operatorname{zn}(d - c) - \operatorname{zn}(d + z) + \operatorname{zn}(d + c))K. \quad (\text{A.40})$$

Note that the quasi-momentum function and spectral curve for the elliptic state of CHM have been discussed in detail in [27] in the case of periodic boundary conditions.

Let us discuss some properties of the above quantities: First of all, we note that the above differential equation is of second order and therefore has a basis of two solutions. Correspondingly, the map  $z \mapsto u$  has two pre-images  $\pm z$  for every  $u$  (on the fundamental domain of the elliptic curve), and each one corresponds to one of the two elements of the basis. Flipping the sign of  $z$  acts on the above functions  $u(z)$  and  $q(z)$  as follows:

$$u(-z) = u(z), \quad q(-z) = -\lambda - q(z). \quad (\text{A.41})$$

Second, we note that the functions  $u(z)$  and  $G(x)$  are closely related:

$$u(\alpha x + \beta + d) = -\frac{2}{\omega} G(x). \quad (\text{A.42})$$

---

<sup>33</sup>The elliptic zeta functions can be combined into  $-2 \operatorname{zn}(z - c)$  plus an elliptic function by means of addition theorems. However, doing so may not be convenient.

Furthermore, the function  $q(z)$  serves as the quasi-momentum defining the spectral curve:

$$\left[\frac{dq}{du}\right]^2 = \left[\frac{q'(z)}{u'(z)}\right]^2 = \frac{4K^2\hat{u}_1\hat{u}_2\hat{u}_3\hat{u}_4}{\alpha^2} \frac{(1 + \frac{1}{2}vu + \frac{1}{2}(\omega^2\hat{u}_1\hat{u}_2 + \omega^2\hat{u}_3\hat{u}_4 - \alpha^2E/K)u^2)^2}{u^4(u - \hat{u}_1)(u - \hat{u}_2)(u - \hat{u}_3)(u - \hat{u}_4)}. \quad (\text{A.43})$$

Here, the branch points  $\hat{u}_k$  coincide with the distinguished points  $\hat{g}_k$  up to a common factor:

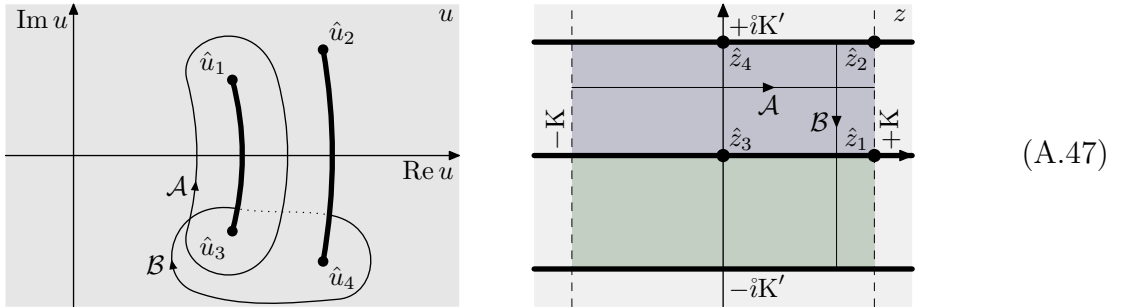
$$\hat{u}_k = -\frac{2}{\omega}\hat{g}_k. \quad (\text{A.44})$$

Hence, they take the form

$$\begin{aligned} \hat{u}_1 &= -\frac{2i}{\alpha m} \frac{dc(d)dc(c)}{\text{sn}(d-c) + \text{sn}(d+c)}, & \hat{u}_2 &= -\frac{2i}{\alpha} \frac{cd(d)cd(c)}{\text{sn}(d-c) + \text{sn}(d+c)}, \\ \hat{u}_3 &= -\frac{2i}{\alpha m} \frac{ns(d)ns(c)}{\text{sn}(d-c) - \text{sn}(d+c)}, & \hat{u}_4 &= -\frac{2i}{\alpha} \frac{\text{sn}(d)\text{sn}(c)}{\text{sn}(d-c) - \text{sn}(d+c)}. \end{aligned} \quad (\text{A.45})$$

In fact, these branch points are given by the following points on the spectral curve:

$$\begin{aligned} z = \hat{z}_1 = K, & & u(z) = \hat{u}_1, & & q(z) = -\frac{1}{2}\lambda, \\ z = \hat{z}_2 = K + iK', & & u(z) = \hat{u}_2, & & q(z) = -\pi - \frac{1}{2}\lambda. \\ z = \hat{z}_3 = 0, & & u(z) = \hat{u}_3, & & q(z) = -\frac{1}{2}\lambda, \\ z = \hat{z}_4 = iK', & & u(z) = \hat{u}_4, & & q(z) = -\pi - \frac{1}{2}\lambda. \end{aligned} \quad (\text{A.46})$$



Note that the branch points are located where the periodicity factor  $\exp(iq)$  coincides with the periodicity factor  $\exp(-iq - i\lambda)$  for the second solution of the auxiliary linear problem with the same value of  $u$ . Finally, we state the representation of the points  $u = \infty$  and  $u = 0$  which are related to rotational symmetries and local quantities, respectively:

$$\begin{aligned} z = +c, & & u(z) = \infty, & & q(z) = 0, \\ z = -c, & & u(z) = \infty, & & q(z) = -\lambda, \\ z = +d - iK', & & u(z) = 0, & & q(z) = \infty, \\ z = -d + iK', & & u(z) = 0, & & q(z) = \infty. \end{aligned} \quad (\text{A.48})$$

## A.5 Periodicity and Moduli

Let us now consider the periodicities of the travelling wave state. The logarithmic derivative  $G(x)$  is given by an elliptic function, and as such it has two periods in the complex plane. These are given by the lengths

$$L = \frac{2K}{\alpha}, \quad L' = \frac{2iK'}{\alpha}. \quad (\text{A.49})$$

The actual state function  $\zeta(x)$  is quasi-periodic as follows:

$$\zeta(x + L) = \exp(i\lambda)\zeta(x), \quad \zeta(x + L') = \exp\left(\frac{2\pi ic - K'\lambda}{K}\right)\zeta(x), \quad (\text{A.50})$$

Quasi-periodicity means that upon a shift of  $x$  by  $L$  the wave function  $\vec{S}(x)$  returns to its original shape but rotated by an angle of  $\lambda$  about the  $z$ -axis. We will thus call  $\lambda$  the angle of quasi-periodicity. In particular, the solution is perfectly periodic if and only if  $\lambda \in 2\pi\mathbb{Z}$ . The imaginary period  $L'$  leads to a complex factor, but it bears no physical significance because it shifts off the physical real  $x$ -axis.

The quasi-periodicity is linked to the mode numbers of the two elementary modes contributing to the elliptic state. According to (A.46) with  $\pi n = q(\hat{z}) - q(c)$  these mode numbers are  $n_1 = -\lambda/2\pi$  and  $n_2 = -(\lambda + 2\pi)/2\pi$ . As such, the mode numbers of this state are always separated by one unit. A more general state with two arbitrary integer mode numbers  $n_1, n_2$  is obtained by regarding  $n_1 - n_2$  copies of the elementary interval  $L$  as the effective periodicity  $L_{\text{eff}} = (n_1 - n_2)L$ . The quasi-periodicity for the elementary interval then takes a rational value  $\lambda = -2\pi n_1/(n_1 - n_2)$ .

There are different ways to deal with the quasi-periodicity of the state. On the one hand, the periodicity of the field is determined by the boundary conditions. Closed boundaries can be specified as  $\zeta(x + L) = \zeta(x)$  or as  $\zeta(x + L) = \exp(i\lambda)\zeta(x)$ , both are equally valid, however, they define distinct physical models a priori. For instance, the twist parameter  $\exp(i\lambda)$  does not belong to phase space (otherwise it would have to be accompanied by a canonically conjugate variable). On the other hand, the function and equation of motion could be transformed by the local rotation  $\tilde{\zeta}(x) = \exp(-i\lambda x/L)\zeta(x)$ . In this case, the equation of motion as well as the Lax connection will receive few additional local terms from the relationship  $\tilde{\zeta}' = \exp(-i\lambda x/L)(\zeta' - i\lambda\zeta/L)$ . Here, we will mostly disregard the implications of quasi-periodicity on the mechanical system by allowing an arbitrary quasi-periodicity angle  $\lambda$ . Where needed, we may fix  $\lambda \in 2\pi\mathbb{Z}$  for perfect periodicity of the state  $\zeta(x)$ .

The solution  $\Psi(x)$  to the auxiliary linear problem obeys the following quasi-periodicity relations:

$$\Psi_j(x + L) = \exp(iq_j)\Psi_j(x), \quad \Psi_j(x + L') = \exp(i\tilde{q}_j)\Psi_j(x) \quad (\text{A.51})$$

with

$$q_1 = q, \quad q_2 = q + \lambda, \quad \tilde{q}_1 = \frac{iK'q + \pi(z - c)}{K}, \quad \tilde{q}_2 = \frac{iK'(q + \lambda) + \pi(z + c)}{K}. \quad (\text{A.52})$$

The solution  $\Psi_1(x)$  to the auxiliary linear problem is quasi-periodic by construction. Interestingly, the corresponding second component  $\Psi_2(x)$  to the auxiliary linear problem is quasi-periodic as well, yet with a different phase. Essentially, the additional phase  $\lambda$  is needed to compensate for the quasi-periodicity of the state  $\zeta(x)$ . The two different quasi-periodicity phases applicable to the components  $\Psi_1(x)$  and  $\Psi_2(x)$  render the combined vector a twisted eigenvector of the Lax parallel transport by  $L$ . Note further, that the second solution to the auxiliary linear problem has the eigenvalues  $\exp(-iq - i\lambda)$  and  $\exp(-iq)$ , so that again the quasi-periodicity of  $\zeta(x)$  is respected.

The following periodicity relations hold for the uniformised spectral parameter  $z$ : The original spectral parameter  $u(z)$  is properly periodic. The solutions to the auxiliary linear problem display some anti-periodicity:

$$\Psi_{1,2}(z + 2K) = -\Psi_{1,2}(z), \quad \Psi_{1,2}(z + 2iK') = +\Psi_{1,2}(z). \quad (\text{A.53})$$

The quasi-momentum shifts by a constant:

$$q(z + 2K) = q(z), \quad q(z + 2iK') = q(z) - 2\pi. \quad (\text{A.54})$$

In fact, the shifts represent the integrals of  $dq$  around the two cycles of the elliptic curve:

$$\oint_{\mathcal{A}} dq = 0, \quad \oint_{\mathcal{B}} dq = -2\pi. \quad (\text{A.55})$$

As these are shifts by multiples of  $2\pi$ , they leave the relevant exponent  $\exp(iq)$  invariant.

Next, it makes sense to consider transformations of the parameters  $c$  and  $d$ : All functions and quantities are properly periodic under shifts of  $c$  and  $d$  by  $2K$  and  $2iK'$ . The only exception is the quasi-periodicity angle  $\lambda$  which shifts as  $\lambda \rightarrow \lambda - 4\pi$  upon the periodicity  $c \rightarrow c + 2iK'$ . Furthermore, it is possible to simultaneously shift  $c$  and  $d$  by  $\pm K$  or by  $\pm iK'$ . These generate inessential permutations of the branch points as follows:

$$\begin{aligned} d \rightarrow d + K, \quad c \rightarrow c + K : \quad \hat{u}_{3,4} \leftrightarrow \hat{u}_{1,2}, \quad \phi \rightarrow \phi + \pi; \\ d \rightarrow d \pm iK', \quad c \rightarrow c + iK' : \quad \hat{u}_{1,3} \leftrightarrow \hat{u}_{2,4}, \quad \lambda \rightarrow \lambda - 2\pi. \end{aligned} \quad (\text{A.56})$$

Apart from these, there are a couple of discrete transformations. The following transformation effectively generates a parity operation:

$$(c, d, \beta) \rightarrow -(c, d, \beta) : \quad \zeta(x) \rightarrow \zeta(-x), \quad (v, \lambda, q, u, z) \rightarrow -(v, \lambda, q, u, z). \quad (\text{A.57})$$

Here, we note that the elliptic state has the following self-conjugation property:

$$\bar{\zeta}(x) = -\exp(-2i\phi) \zeta(-x - 2\beta/\alpha). \quad (\text{A.58})$$

Finally, there is a transformation which effectively rotates the spin field by  $\pi$  around the  $y$ -axis:

$$c \rightarrow -c, \quad \phi \rightarrow -\phi : \quad \zeta(x) \rightarrow 1/\zeta(x), \quad (\omega, \lambda, z, q) \rightarrow -(\omega, \lambda, z, q). \quad (\text{A.59})$$

Curiously, this transformation preserves all the branch points. Moreover, it flips the sign of  $\omega$  which cannot be achieved by a continuous transformation of the parameters. In fact, the sign of  $\omega$  is linked to the real parts of  $c$  and  $d$  as follows:

$$\begin{aligned} \text{Re}(d + c) \equiv 0, \quad \text{Re}(d - c) \equiv K : \quad \omega > 0; \\ \text{Re}(d + c) \equiv K, \quad \text{Re}(d - c) \equiv 0 : \quad \omega < 0. \end{aligned} \quad (\text{A.60})$$

Furthermore, the former case includes the vacuum state  $\zeta(x) = \infty$  with  $J = -L$  while the latter case includes the opposite vacuum  $\zeta(x) = 0$  with  $J = +L$ .

## A.6 Dynamical Divisor

The dynamical divisor for the state consists of the points  $z = \hat{z}(x)$  where the solution  $\Psi(x)$  to the auxiliary linear problem aligns with a particular reference direction. To that end, we consider the directional function  $\varpi(x) \in \bar{\mathbb{C}}$  for the solution  $\Psi(x)$ :

$$\varpi(x) := \frac{\Psi_2(x)}{\Psi_1(x)} = \exp[i\lambda(\alpha x + \beta)/2K + i\phi] \frac{\vartheta_s(z - c) \vartheta_n(\alpha x + \beta - c - z)}{\vartheta_s(z + c) \vartheta_n(\alpha x + \beta + c - z)}. \quad (\text{A.61})$$

This is a perfectly periodic function in  $z$ , but by construction it is quasi-periodic in  $x$  as  $\varpi(x+L) = \exp(i\lambda)\varpi(x)$ . In particular, this function directly reproduces the corresponding state at the point  $u = 0$  as

$$\begin{aligned} z = -d + iK' &: & \varpi(x) &= \zeta(x), \\ z = +d - iK' &: & \varpi(x) &= -1/\bar{\zeta}(x). \end{aligned} \tag{A.62}$$

For a given reference direction  $\varpi_0$ , we define the dynamical divisor  $\{\mathring{z}(x)\}$  as the set of solutions to the equation

$$\varpi(x) = \varpi_0 \quad \text{for} \quad z = \mathring{z}(x). \tag{A.63}$$

We note that since  $\varpi(x)$  is an elliptic function in  $z$  of lowest degree, it can be solved in terms of inverse elliptic functions which yields two solutions  $\mathring{z}_{1,2}(x)$ .

The choice of reference direction  $\varpi_0$  strongly influences the qualitative  $x$ -dependency of the divisor points  $\mathring{z}_{1,2}(x)$ . Two special reference directions are given by  $\varpi_0 = 0$  or  $\varpi_0 = \infty$ . Here, one of the two divisor points is evidently fixed to  $\mathring{z}_1 = \pm c$ , respectively, while the other moves along a linear trajectory  $\mathring{z}_2(x) = \alpha x + \beta \mp c + iK'$  as  $x$  increases. In terms of  $u$ , one divisor points is fixed to  $\mathring{u}_1 = \infty$ , the other one  $\mathring{u}_2$  moves around one of the two branch cuts as  $x$  increases. In particular, this is a perfectly closed path winding once around the cut for one period in  $x$ . Unfortunately, this divisor does not capture the information on the angle  $\phi$ .

Two further distinguished reference directions are given by

$$\varpi_0 = \pm \exp(i\phi). \tag{A.64}$$

Here, the divisor points meet two of the branch points at the maximum  $\alpha x + \beta = 0$ ,

$$\{\mathring{u}(-\beta/\alpha)\} = \{\hat{u}_3, \hat{u}_4\} \quad \text{or} \quad \{\mathring{u}(-\beta/\alpha)\} = \{\hat{u}_1, \hat{u}_2\}. \tag{A.65}$$

As  $x$  increases by one period, the divisor points  $\mathring{u}_{1,2}(x)$  qualitatively oscillate along and transversely to the branch cut. There will be  $\lambda/2\pi$  and  $(\lambda+2\pi)/2\pi$  oscillations along the cuts for one period. Note that for generic values of the quasi-periodicity angle  $\lambda$ , the path of the divisor poles does not close. The paths are closed only if  $\lambda \in 2\pi\mathbb{Z}$ . In the special case  $\lambda \in \pi + 2\pi\mathbb{Z}$ , the path connects both ends of the branch cuts during one period.

For intermediate values of the magnitude  $|\varpi_0|$ , one finds that the divisor points  $\mathring{u}_{1,2}(x)$  take a highly complex path in the complex plane. Their path can be understood as some interpolation between the trivial fixed and circular behaviour at  $\varpi_0 = 0, \infty$  and the mostly longitudinal oscillations at  $|\varpi_0| = 1$ . The qualitative description of the paths is complicated by the observation that tuning  $\varpi_0$  continuously may change the topology of the paths including their winding around the branch points (such changes are necessary to connect the two topologically distinct situations at both ends). We observe two effects: First, a path is strongly deflected by nearby branch points. For discrete values of  $\varpi_0$  a path will directly hit a branch point. Here, the winding of the path around this branch point can change. Second, the two paths  $\mathring{u}_{1,2}(x)$  of the divisor points may come arbitrarily close. For discrete values of  $\varpi_0$  they perfectly align and can recombine.

A further obstacle in describing the divisor paths is their quasi-periodicity. Only for  $\lambda \in 2\pi\mathbb{Z}$  the paths close after one period in  $x$ . For  $\lambda \notin 2\pi\mathbb{Z}$ , we have two alternatives for our consideration: We can either accept that the paths are merely quasi-periodic. There is nothing wrong with this point of view, especially since the state itself is merely quasi-periodic in these cases. However, topology will provide a less clear description of the open

paths. Otherwise, we may generalise the divisor condition by picking an  $x$ -dependent reference direction  $\varpi_0(x)$ . A simple but particularly useful choice is

$$\varpi_0(x) \sim \exp(-i\lambda x/L). \quad (\text{A.66})$$

Here, the divisor condition becomes perfectly periodic such that the paths of the divisor points  $\dot{z}(x)$  close. We might also consider more elaborate choices for  $\varpi_0(x)$ , and certainly, the qualitative behaviour of the paths will depend on them. Nevertheless, even for  $\lambda \notin 2\pi\mathbb{Z}$ , we can achieve close paths.

Finally, we point out that even for a perfectly periodic divisor, there are two qualitatively distinct cases: The divisor consists of two points which are perfectly equivalent, and therefore the divisor takes the role of an unordered set rather than an ordered pair. Hence, a periodic divisor merely implies that the set agrees for  $x$  and  $x + L$ . For the paths of the individual points  $\dot{z}_{1,2}(x)$  we can have one of the two periodicity situations

$$\dot{z}_{1,2}(x + L) = \dot{z}_{1,2}(x) \quad \text{or} \quad \dot{z}_{1,2}(x + L) = \dot{z}_{2,1}(x). \quad (\text{A.67})$$

Both cases do arise, but it is hard to predict for which values of the reference direction  $\varpi_0$  one obtains which case.

## A.7 Charges

We can read off conserved charges from the expansion of the quasi-momentum at  $u = 0$ ,  $z = d - iK$  and  $u = \infty$ ,  $z = c$  as

$$q = \frac{L}{u} - \frac{1}{2}P + \frac{1}{4}Eu + \mathcal{O}(u^2), \quad q = \frac{J}{u} + \mathcal{O}(u^{-2}). \quad (\text{A.68})$$

These are the momentum  $P$ , energy  $E$  and total angular momentum  $J$ .<sup>34</sup>

$$\begin{aligned} P &= \int \frac{i\zeta\bar{\zeta}' - i\zeta'\bar{\zeta}}{1 + \zeta\bar{\zeta}} dx = L(-v - 2i\alpha \operatorname{zn}(d + c)) + 2\pi, \\ E &= \int dx \frac{1}{2} \vec{S}^2 = \int dx \frac{2\zeta'\bar{\zeta}'}{(1 + \zeta\bar{\zeta})^2} = \frac{L\alpha^2}{8} \left[ 4 \frac{E}{K} + \left( \frac{\operatorname{cn}(d)}{\operatorname{sn}(d) \operatorname{dn}(d)} - \frac{\operatorname{sn}(d) \operatorname{dn}(d)}{\operatorname{cn}(d)} \right)^2 \right], \\ J &= \int dx S_z = \int dx \frac{1 - \zeta\bar{\zeta}}{1 + \zeta\bar{\zeta}} = \frac{L\alpha^2}{\omega} \left( -2 \frac{E}{K} + \operatorname{dn}(d + c)^2 + \operatorname{dn}(d - c)^2 \right). \end{aligned} \quad (\text{A.69})$$

The spectral curve also defines appropriate action variables via the contour integral

$$I = \frac{1}{2\pi i} \oint_{\mathcal{A}} u dq. \quad (\text{A.70})$$

The indefinite integral yields

$$\begin{aligned} \frac{1}{2\pi i} \int u dq &= \frac{z}{4\pi K} (L(P - 2\pi - \lambda) + \lambda J) \\ &\quad + \frac{J}{2\pi i} \log \left[ -\frac{\vartheta_s(z - c)}{\vartheta_s(z + c)} \right] + \frac{L}{2\pi i} \log \left[ \frac{\vartheta_n(z - d)}{\vartheta_n(z + d)} \right]. \end{aligned} \quad (\text{A.71})$$

<sup>34</sup>Incidentally,  $\partial\lambda/\partial c = -i\omega J/\alpha$ , as well as  $\partial P/\partial c = i\omega(L - J)/\alpha$  and  $\partial P/\partial d + \partial P/\partial c = 2iE/\alpha$ .

The elliptic curve has two branch cuts, and the contour integrals can be evaluated as

$$I_1 = \frac{-LP + (L - J)(\lambda + 2\pi)}{2\pi}, \quad I_2 = \frac{LP - (L - J)\lambda}{2\pi}. \quad (\text{A.72})$$

Here, the cycles around the two cuts can be deformed into each other while crossing pole singularities at  $u = 0$  and  $u = \infty$  whose residues are  $J$  and  $L$ , respectively. Altogether this implies a relationship with the total angular momentum  $J$ :

$$I_1 + I_2 = L - J. \quad (\text{A.73})$$

Furthermore, the Riemann bilinear identity implies a second exact relationship with the momentum  $P$ :

$$\lambda I_1 + (\lambda + 2\pi)I_2 = LP. \quad (\text{A.74})$$

Let us consider the action variables for small branch cuts of the spectral curve. Suppose a small branch cut of length  $\Delta\hat{u}$  is located near the point  $\hat{u}$  on the real axis. Then the action variable can be approximated as

$$I \approx \frac{L}{8} \frac{(\text{Im } \Delta\hat{u})^2}{\hat{u}^2}. \quad (\text{A.75})$$

We have to point out that the above discussion fits well the one half of phase space with  $\omega < 0$  (for  $\text{Re } d \equiv +\text{Re } c$ ) while the charges are not ideally represented on the other half with  $\omega > 0$  (for  $\text{Re } d \equiv -\text{Re } c$ ). The contours defining the action variables  $I_{1,2}$  have been chosen such that the contour integrals are zero,  $I_1 = I_2 = 0$ , at the vacuum state

$$\zeta(x) = 0 : \quad m = 0, \quad d = c = \frac{1}{2}K + \frac{i}{2}K'. \quad (\text{A.76})$$

The situation for the opposite vacuum is not as fortunate:

$$\zeta(x) = \infty : \quad m = 0, \quad d = -c = \frac{1}{2}K + \frac{i}{2}K'. \quad (\text{A.77})$$

For instance, the definition of the total momentum  $P$  as an integral of a local density is singular at  $\zeta = \infty$  and thus ill-defined. Instead, we can evaluate relevant changes via expansion of the quasi-momentum. Here, the momentum  $P = 2\lambda$  and action variables  $I_1 = -2J$  and  $I_2 = 0$  take peculiar non-trivial values. It thus makes sense to redefine these quantities as follows

$$\tilde{P} = P - 2\lambda, \quad \tilde{I}_1 = I_1 + 2J, \quad \tilde{I}_2 = I_2. \quad (\text{A.78})$$

The alternative action variable can be achieved by picking a different contour. The alternative total momentum  $\tilde{P}$  is obtained from expansion of the quasi-momentum at the alternate point  $z = -d + iK$  corresponding to  $u = 0$

$$q = -\frac{L}{u} + \frac{1}{2}\tilde{P} - \frac{1}{4}Eu + \mathcal{O}(u^2). \quad (\text{A.79})$$

The alternative momentum also has as an expression as an integral of a local density

$$\tilde{P} = P - 2\lambda = \int \frac{i\zeta'/\zeta - i\bar{\zeta}'/\bar{\zeta}}{1 + \zeta\bar{\zeta}} dx = L(-v - 2i\alpha \text{zn}(d - c)) + 2\pi, \quad (\text{A.80})$$

where the quasi-periodicity angle  $\lambda$  can be defined via the integrals

$$\lambda = -i \int dx \frac{\zeta'}{\zeta} = i \int dx \frac{\bar{\zeta}'}{\bar{\zeta}}. \quad (\text{A.81})$$

In fact, the alternative total momentum properly vanishes for the vacuum  $\zeta(x) = \infty$ , but it is ill-defined for  $\zeta(x) = 0$ . The alternative action variables satisfy the relations

$$\tilde{I}_1 + \tilde{I}_2 = L + J, \quad -\lambda \tilde{I}_1 + (-\lambda + 2\pi) \tilde{I}_2 = L\tilde{P}. \quad (\text{A.82})$$

The action variables display an interesting behaviour under shifts of the variables  $c, d$ . For the combined discrete shift introduced above, we find

$$d \rightarrow d \pm iK', \quad c \rightarrow c + iK' : \quad I_1 \rightarrow I_1 + (J \pm L), \quad I_2 \rightarrow I_2 - (J \pm L). \quad (\text{A.83})$$

Note that here the variable  $d$  fails to be strictly periodic under a shift by  $2iK'$  even though all other quantities remain invariant. This potentially puzzling behaviour can be understood as follows: Shifting the imaginary parts of  $d$  and  $c$  by equal or opposite continuous amounts, effectively makes the branch points circle around each other. For every shift of  $K'$ , the two branch points are exchanged while a shift of  $2K'$  brings the branch points back to their original positions. The resulting situation appears to be the same as before. However, this is not so because the action variables  $I_{1,2}$  are constructed as contour integrals around the branch cuts. If the branch cuts or their surrounding contours are continuously deformed in such a way that no other branch cuts or structures on the elliptic curve are crossed, they will have to twist around the pair of encircling branch points before they can reach them. Each half-turn will lead to a different situation, and therefore it is justified that  $I_{1,2}$  are merely quasi-periodic. In fact, the curling of branch cuts can be unwound via the remainder of the elliptic curve. By doing so, they necessarily cross the poles at  $u = 0$  and  $u = \infty$  from which they pick up the respective contributions. In fact, the above discussion is reminiscent and related to the detailed discussion of branch cuts in [27]. There, it was observed that branch points may move through other branch cuts resulting in modified mode numbers. This phenomenon occurs especially in the case of two adjacent mode numbers, which is equivalent to the present case where  $\lambda/2\pi$  and  $(\lambda + 2\pi)/2\pi$  serve as the mode numbers.

We further point out that the moduli space is subdivided by singular configurations of the branch points at the locations  $d \pm c \equiv iK'$ . For continuous deformations of the moduli, the parameters should remain within the strips defined by these boundaries. To this end, we note that the vacuum states with  $I_1 = I_2 = 0$  or with  $\tilde{I}_1 = \tilde{I}_2 = 0$  reside within the following fundamental intervals:

$$\text{Re}(d) \equiv \pm \text{Re}(c) : \quad -K' < \text{Im}(d \mp c) < +K'. \quad (\text{A.84})$$

## A.8 Soliton Limit

In the following, we will derive the CHM soliton as a limit of the elliptic state. We will proceed analogously to the KdV elliptic solution where we saw that two branch points degenerate in the limit  $m \rightarrow 1$ . Here, the branch points are organised in complex conjugate pairs, hence, the limit will consist in degenerating two pairs of branch points. As the branch points can move freely on the complex plane, the approach now takes place in two dimensions and thus with additional degrees of freedom.



We choose the two branch points  $\hat{u}_{2,4}$  to approach a common point  $\check{u}$  while their distance shrinks exponentially with the length  $L$ . In addition, in this two-dimensional setting we can assume a linear rotation of the separation vector. The target point  $\check{u}$  will describe the momentum  $\check{k}$  of the bound state pole corresponding to the soliton according to the map

$$\check{k} = -\frac{1}{\check{u}}. \quad (\text{A.85})$$

Altogether this results in a spiralling motion ansatz for the branch points

$$\hat{u}_{2,4} = \check{u} \mp 4 \operatorname{Im}(\check{u}) \exp\left(-\frac{1}{2}(1 + i\delta)\alpha L - \frac{i}{2}\pi - i\gamma\right) + \dots \quad (\text{A.86})$$

The coefficients  $\gamma$  and  $\delta$  describe the angle and angular velocity of the separation. Their values specify certain aspects of the limit, and we shall tune them to achieve specific desirable effects. The limit described by the above branch points corresponds to the following parameters of the elliptic curve

$$\begin{aligned} m &= 1 - 16 \exp(-\alpha L) + \dots, \\ \alpha &= \frac{2 \operatorname{Im} \check{u}}{|\check{u}|^2} = 2 \operatorname{Im} \check{k}, \\ d &= -\frac{1}{2}\mathbf{K} + i\left(\frac{1}{4}\delta\alpha L + \frac{1}{2}\gamma + \frac{1}{2}\pi - \arg \check{k}\right) + \dots, \\ c &= +\frac{1}{2}\mathbf{K} - i\left(\frac{1}{4}\delta\alpha L + \frac{1}{2}\gamma\right) + \dots \end{aligned} \quad (\text{A.87})$$

Note that these parameters correspond to a state based on the vacuum  $\zeta(x) = \infty$ . However, for large  $L$  the state will be highly excited so that most parts reside at  $\zeta(x) \approx 0$ .

By careful analysis we find the large-length limit of the wave function

$$\zeta(x) = \exp(i \cot(\arg \check{k})(\alpha x + \beta) + i\phi) \frac{i \sin(\arg \check{k})}{\cosh(\alpha x + \beta - i \arg \check{k})} + \dots, \quad (\text{A.88})$$

as well as of the various characteristic quantities of the state

$$\begin{aligned} v &= -4 \operatorname{Re}(\check{k}) + \dots, & \omega &= 4|\check{k}|^2 + \dots, \\ \lambda &= 2L(\delta \operatorname{Im}(\check{k}) + \operatorname{Re}(\check{k})) + 2\gamma + \dots, & P &= 4 \arg \check{k} + \dots, \\ J &= L - 2 \frac{\operatorname{Im}(\check{k})}{|\check{k}|^2} + \dots, & E &= 8 \operatorname{Im}(\check{k}) + \dots, \\ \tilde{I}_1 &= \frac{2L(\pi - \arg \check{k})}{\pi} + \frac{(\lambda - 2\pi) \operatorname{Im}(\check{k})}{\pi|\check{k}|^2} + \dots, & \tilde{I}_2 &= \frac{2L \arg \check{k}}{\pi} - \frac{\lambda \operatorname{Im}(\check{k})}{\pi|\check{k}|^2} + \dots \end{aligned} \quad (\text{A.89})$$

The wave function and associated quantities agree, where applicable, with the CHM soliton. We note that this soliton approaches the vacuum  $\zeta(x) = 0$  when  $|\alpha x + \beta|$  is large. However, it also has  $\omega > 0$ , so it belongs to the family of solutions which are connected to the other vacuum  $\zeta(x) = \infty$ . In that sense, all of the soliton wave function can be considered highly excited.

In the limit, the spectral curve splits into two disconnected components near  $z = \pm c$  corresponding to the two independent solutions of the auxiliary linear problem for common spectral parameter  $u$ . In the first case, we set  $z = c + z_\infty$ . The limit of the uniformisation of the spectral parameter reads

$$u = |\check{u}| \frac{\sinh(z_\infty + i \arg \check{u})}{\sinh(z_\infty)}, \quad k := -\frac{1}{u} = \frac{|\check{k}| \sinh(z_\infty)}{\sinh(z_\infty - i \arg \check{k})}, \quad (\text{A.90})$$

which has the following inverse relation

$$z_\infty = \frac{1}{2} \log \frac{\check{k}(k - \check{k}^*)}{\check{k}^*(k - \check{k})} = \frac{1}{2} \log \frac{u - \check{u}^*}{u - \check{u}}. \quad (\text{A.91})$$

The solution to the auxiliary linear problem has the following limit

$$\begin{aligned} \Psi_1(x) &= \exp \left[ \frac{-i \sinh(z_\infty)(\alpha x + \beta)}{2 \sin(\arg \check{k}) \sinh(z_\infty - i \arg \check{k})} \right] \frac{\cosh(\alpha x + \beta - z_\infty)}{\sinh(z_\infty) \cosh(\alpha x + \beta)} + \dots, \\ \Psi_2(x) &= \exp \left[ \frac{i \sinh(z_\infty - 2i \arg \check{k})(\alpha x + \beta)}{2 \sin(\arg \check{k}) \sinh(z_\infty - i \arg \check{k})} + i\phi \right] \frac{1}{\cosh(\alpha x + \beta)} + \dots, \end{aligned} \quad (\text{A.92})$$

and the corresponding quasi-momentum expands as

$$q = -Lk + i \log \left[ \frac{\check{k}}{\check{k}^*} \frac{k - \check{k}^*}{k - \check{k}} \right] + \dots = \frac{L}{u} + i \log \frac{u - \check{u}^*}{u - \check{u}} + \dots \quad (\text{A.93})$$

These functions and dependencies describe the integrable structure for the CHM soliton. In particular, the regularised quasi-momentum  $q + Lk$  describes the transfer coefficient of the auxiliary scattering matrix. In the second case, we set  $z = -c - z_\infty$  in order to obtain obtain agreement with the above uniformisation relations. The limit then takes the form

$$\begin{aligned} \Psi_1(x) &= - \exp \left[ \frac{-i \sinh(z_\infty - 2i \arg \check{k})(\alpha x + \beta)}{2 \sin(\arg \check{k}) \sinh(z_\infty - i \arg \check{k})} \right] \frac{1}{\cosh(\alpha x + \beta)} + \dots, \\ \Psi_2(x) &= - \exp \left[ \frac{i \sinh(z_\infty)(\alpha x + \beta)}{2 \sin(\arg \check{k}) \sinh(z_\infty - i \arg \check{k})} + i\phi \right] \frac{\cosh(\alpha x + \beta + z_\infty)}{\sinh(z_\infty) \cosh(\alpha x + \beta)} + \dots, \\ q &= -\lambda + Lk - i \log \left[ \frac{\check{k}}{\check{k}^*} \frac{k - \check{k}^*}{k - \check{k}} \right] + \dots = -\lambda - \frac{L}{u} - i \log \frac{u - \check{u}^*}{u - \check{u}} + \dots \end{aligned} \quad (\text{A.94})$$

This describes the other solution to the auxiliary linear problem and the other transfer coefficient.

We note that in order to perform the limit  $m \rightarrow 1$  it was necessary to carefully expand the elliptic theta and zeta functions with arguments of order  $K \sim \log(1-m)$ . For instance, for an argument  $z$  with a large imaginary part, we have to use the non-standard relations

$$\begin{aligned} \vartheta_n(z) &= \exp(-z^2/2K) \cosh(z) + \dots, \\ \text{zn}(z) &= \tanh(z) - z/K + \dots \end{aligned} \quad (\text{A.95})$$

In particular, these relations are consistent with the exact imaginary periodicity relation for these elliptic functions.

Let us now discuss the significance and effect of the parameters  $\gamma, \delta$  which relate to the orientation and rotation of the branch point configuration. First, we observe that the resulting expressions are largely independent of them. Merely the quasi-periodicity angle  $\lambda$  and the action variables depend on them, but these are necessarily finite-length concepts.

There are several useful options to adjust  $\gamma, \delta$ : We can aim to fix the quasi-periodicity angle  $\lambda$  for all lengths  $L$ . This is achieved by the assignment

$$\delta = \frac{\text{Re}(\check{u})}{\text{Im}(\check{u})} = - \frac{\text{Re}(\check{k})}{\text{Im}(\check{k})} = - \cot(\arg \check{k}), \quad \gamma = -\frac{1}{2}\lambda. \quad (\text{A.96})$$

In this case, the branch points perform a spiralling exponential motion towards their limiting position

$$\hat{u}_{2,4} = \check{u} \mp 4 \operatorname{Im}(\check{u}) \exp\left(-iL/\check{u} - \frac{i}{2}\pi + \frac{i}{2}\lambda\right) + \dots \quad (\text{A.97})$$

In particular, the driving term  $-iL/\check{u} = i\check{k}L$  of the twirling motion takes a very natural form here. With this choice of parameters, we can adjust the length  $L$  continuously while preserving the desired quasi-periodicity angle  $\lambda$  which can be considered an essential parameter of the underlying mechanical model.

Another viable option is to fix the orientation of the branch points as  $L$  increases by setting  $\delta = 0$ . In this case, the quasi-periodicity angle has a linear asymptotic dependency on the length

$$\lambda(L) = 2L \operatorname{Re}(\check{k}) + 2\gamma + \dots \quad (\text{A.98})$$

We might also choose  $\delta$  differently or, even more generally, assume  $\gamma$  to be some more elaborate function of  $L$ . In all of these cases,  $\lambda$  will depend non-trivially on  $L$ . We can then either accept a continuously changing  $\lambda$ . A freely adjustable parameter  $\lambda$  can be dealt with well at the level of the differential equations. However, it may represent a conflict with the role of  $\lambda$  as specifying the periodic boundary conditions within the model of Hamiltonian mechanics.

Alternatively, we can deal with a varying quasi-periodicity angle  $\lambda$  by making use of the fact that the angle is defined modulo  $2\pi$ : Supposing that the function  $\lambda(L)$  keeps crossing the fixed lattice  $2\pi\mathbb{Z} + \lambda_0$  as  $L \rightarrow \infty$ , we can focus on states at specific lengths  $L_k$  which are chosen such that

$$\lambda(L_k) \in 2\pi\mathbb{Z} + \lambda_0. \quad (\text{A.99})$$

We can thus reduce the family of states with continuous  $L$  to a sequence of states at specific lengths  $L_k$  which define the large- $L$  limit. Here, the value of  $\lambda(L)$  changes between the states of the sequence, but the quasi-periodicity angle  $\lambda(L)$  is equivalent to a fixed target value  $\lambda_0$ . While this approach appears to resolve the technical issue of a variable  $\lambda(L)$ , we point out that it is equivalent to assuming a fixed  $\lambda$ : To that end, we note that  $\lambda$  may only shift by a multiple of  $2\pi$  between elements of the sequence. Such a shift is equivalent to the rotation of the pair of branch points by a multiple of  $\pi$ . Such a rotation merely exchanges the branch points (as well as a deformation of the branch cuts on the spectral curve), and has no physical significance. In conclusion, we may either take  $\lambda$  to be fixed or to be continuously adjustable within an extended notion of boundary conditions.

Let us finally discuss how to abstractly describe the configuration of branch cuts that limit to a CHM soliton configuration. We shall assume  $\lambda$  to be fixed. Since  $|\lambda| \ll L$ , the two branch cuts that make up the soliton correspond to small and fixed mode numbers  $n_1 = -\lambda/2\pi$  and  $n_2 = -(\lambda + 2\pi)/2\pi$ . Furthermore, these two branch cuts are adjacent. As a consequence we have for the quasi-momentum at the branch points

$$\exp(iq(\hat{z}_1)) = -\exp(iq(\hat{z}_3)) = \exp\left(-\frac{i}{2}\lambda\right). \quad (\text{A.100})$$

In particular,  $\exp(iq(\hat{z}_{1,3}))$  have opposite signs. The position  $\check{k}$  of the corresponding bound state pole can be identified through the action variables  $I_{1,2}$  or their alternative versions  $\tilde{I}_{1,2}$ . The large- $L$  behaviour specifies the angle  $\arg \check{k}$

$$\frac{\tilde{I}_1}{L} = \frac{I_1 + 2J}{L} = \frac{2}{\pi} (\pi - \arg \check{k}) + \dots, \quad \frac{\tilde{I}_2}{L} = \frac{I_2}{L} = \frac{2}{\pi} \arg \check{k} + \dots \quad (\text{A.101})$$

Furthermore, the finite remainder in the sum  $I_1 + I_2$  determines the magnitude  $|\check{k}|$

$$I_1 + I_2 = \tilde{I}_1 + \tilde{I}_2 - 2J = \frac{2 \sin(\arg \check{k})}{|\check{k}|} + \dots \quad (\text{A.102})$$

## B Scattering Unitarity on the Double Space

In this appendix we consider how space-like and time-like scattering problems in two dimensions and their unitarity properties are related. Here, space-like scattering relates left and right asymptotic states (which is specific to two dimensions) while time-like scattering relates in (past) and out (future) asymptotic states. The curious observation is that unitarity of one scattering problem translates to unitarity of the other, albeit with regard to a different signature. Here we treat the transformation between the two pictures as an abstract problem of linear algebra.

Suppose we have a matrix which identifies vectors  $L, R$  from two equivalent spaces via

$$L = SR. \quad (\text{B.1})$$

Suppose further the matrix satisfies a unitarity relation

$$S^{-1} = HSH^{-1} \quad (\text{B.2})$$

with  $H$  some hermitian form we take to be a diagonal matrix with entries  $\pm 1$ .

One can now exchange a subset of directions between the two subspaces,<sup>35</sup>

$$\begin{aligned} I &= (L_1, \dots, L_k, R_{k+1}, \dots, R_n)^\top, \\ O &= (R_1, \dots, R_k, L_{k+1}, \dots, L_n)^\top, \end{aligned} \quad (\text{B.3})$$

and again solve one subspace in terms of the other. To that end, we have to invert the above relation for the subset of directions that is to be exchanged. The resulting relation takes the same form

$$I = \tilde{S}O \quad (\text{B.4})$$

with a new matrix  $\tilde{S}$ . The new matrix turns out to satisfy a unitarity relation as well

$$\tilde{S}^{-1} = \tilde{H}\tilde{S}\tilde{H}^{-1}. \quad (\text{B.5})$$

Curiously, the new hermitian form  $\tilde{H}$  is the same as the old one up to a change of signs for all the directions that were exchanged between the spaces

$$\tilde{H} = \text{diag}(H_{11}, \dots, H_{kk}, -H_{k+1,k+1}, \dots, -H_{n,n}). \quad (\text{B.6})$$

For two left/right or in/out states ( $n = 2, k = 1$ ), this implies that unitarity with signature  $++$  translates to unitarity with signature  $+-$  and vice versa.

Let us try to understand better how the unitarity relations are related by going to the double space. The original relation between the two spaces can be formulated on the double space which is the direct sum of the two spaces

$$(1 \quad -S) \begin{pmatrix} L \\ R \end{pmatrix} = 0. \quad (\text{B.7})$$

---

<sup>35</sup>In the scattering picture, the left and the right states with prescribed asymptotics  $e^{\pm ikx}$  typically split evenly into incoming and outgoing states with prescribed asymptotics  $e^{\pm i\omega t}$  such that  $k = n/2$ . Here we consider a more general permutation of elements between two abstract spaces.

Here  $1$  denotes the unit matrix. The solution to the relation takes the form of a kernel of a rectangular matrix. The alternative relation can be formulated on the same space by introducing a permutation matrix  $P$  which interchanges some rows between the subspaces

$$\begin{pmatrix} L \\ R \end{pmatrix} = P \begin{pmatrix} I \\ O \end{pmatrix}. \quad (\text{B.8})$$

Then we can transform the rectangular matrix by an appropriate matrix  $U$

$$(1 \quad -S) P = U (1 \quad -\tilde{S}), \quad (\text{B.9})$$

such that the left block returns to an identity matrix. This relation implicitly defines both  $\tilde{S}$  and  $U$ . With this we find the alternative relation right away

$$(1 \quad -\tilde{S}) \begin{pmatrix} I \\ O \end{pmatrix} = 0. \quad (\text{B.10})$$

Now let us also double the original relation by introducing a square matrix on the double space

$$W := \begin{pmatrix} 1 & -S \\ S^{-1} & -1 \end{pmatrix}, \quad V := \begin{pmatrix} L \\ R \end{pmatrix}, \quad WV = 0. \quad (\text{B.11})$$

This matrix is nilpotent and hermitian

$$W^2 = 0, \quad MW^\dagger M^{-1} = W, \quad M := \begin{pmatrix} H & 0 \\ 0 & -H \end{pmatrix}, \quad (\text{B.12})$$

where  $M$  is a hermitian form on the double space. It also has half rank such that the kernel of  $W$  equals the image of  $W$ . The nilpotent matrix for the alternative picture reads

$$\tilde{W} := \begin{pmatrix} 1 & -\tilde{S} \\ \tilde{S}^{-1} & -1 \end{pmatrix}, \quad \tilde{W}^2 = 0, \quad \tilde{V} := \begin{pmatrix} I \\ O \end{pmatrix}, \quad \tilde{W}\tilde{V} = 0. \quad (\text{B.13})$$

The unitarity relation for  $\tilde{S}$  is equivalent to hermiticity of  $\tilde{W}$

$$\tilde{M}\tilde{W}^\dagger\tilde{M}^{-1} = \tilde{W}, \quad \tilde{M} := \begin{pmatrix} \tilde{H} & 0 \\ 0 & -\tilde{H} \end{pmatrix}. \quad (\text{B.14})$$

It turns out that it  $\tilde{S}$  is unitary if and only if

$$P\tilde{M}P^\dagger = \tilde{M}. \quad (\text{B.15})$$

This would manifestly hold if  $P\tilde{W}P^{-1} = \tilde{W}$ , but the two nilpotent matrices are in fact more immediately related by the relation

$$\begin{pmatrix} U & 0 \\ 0 & S^{-1}U\tilde{S} \end{pmatrix} \tilde{W}P^{-1} = \tilde{W}. \quad (\text{B.16})$$

However, note that the two matrices are singular, hence the above form of the relation is not unique. In order to obtain a conclusive answer, we assume that  $H$  is diagonal and the permutation matrix takes the simple form

$$P = \begin{pmatrix} 1-X & X \\ X & 1-X \end{pmatrix} \quad (\text{B.17})$$

with  $X$  a diagonal matrix of elements 0 and 1. The relation between  $M$  and  $\tilde{M}$  then flips a sign between  $H$  and  $\tilde{H}$  precisely where  $X$  has a non-zero diagonal element which is achieved by permuting elements between the blocks  $H$  and  $-H$ .

## References

- [1] C. S. Gardner, J. M. Greene, M. D. Kruskal and R. M. Miura, “*Method for solving the Korteweg-de Vries equation*”, *Phys. Rev. Lett.* 19, 1095 (1967).
- [2] P. D. Lax, “*Integrals of Nonlinear Equations of Evolution and Solitary Waves*”, *Commun. Pure Appl. Math.* 21, 467 (1968).
- [3] R. M. Miura, C. S. Gardner and M. D. Kruskal, “*Korteweg-de Vries equation and generalizations II: Existence of conservation laws and constants of motion*”, *J. Math. Phys.* 9, 1204 (1968). • V. E. Zakharov and L. D. Faddeev, “*Korteweg-de Vries equation: A completely integrable Hamiltonian system*”, *Funct. Anal. Appl.* 5, 280 (1971). • C. S. Gardner, “*Korteweg-de Vries Equation and Generalizations. IV. The Korteweg-de Vries Equation as a Hamiltonian System*”, *J. Math. Phys.* 12, 1548–1551 (1971).
- [4] A. Shabat and V. Zakharov, “*Exact theory of two-dimensional self-focusing and one-dimensional self-modulation of waves in nonlinear media*”, *Sov. Phys. JETP* 34, 62 (1972).
- [5] L. A. Takhtajan, “*Integration of the Continuous Heisenberg Spin Chain Through the Inverse Scattering Method*”, *Phys. Lett. A* 64, 235 (1977). • H. C. Fogedby, “*Solitons and magnons in the classical Heisenberg chain*”, *J. Phys. A* 13, 1467 (1980).
- [6] I. M. Gel’fand and B. M. Levitan, “*On the determination of a differential equation from its spectral function*”, *Amer. Math. Soc. Transl. Ser. 2* 1, 253 (1955). • V. A. Marchenko, “*Some questions of the theory of one-dimensional linear differential operators of the second order. I*”, *Trudy Mosk. Mat. Obs.* 1, 327 (1952), <https://www.mathnet.ru/eng/mmo/v1/p327>.
- [7] S. P. Novikov, “*The periodic problem for the Korteweg-de Vries equation*”, *Funct. Anal. Appl.* 8, 236 (1974).
- [8] B. A. Dubrovin, “*Inverse problem of scattering theory for periodic finite-zone potentials*”, *Funct. Anal. Appl.* 9, 61 (1975). • A. R. Its and V. B. Matveev, “*Hill’s operator with finitely many gaps*”, *Funct. Anal. Appl.* 9, 65 (1975). • B. A. Dubrovin, “*Periodic problems for the Korteweg-de Vries equation in the class of finite band potentials*”, *Funct. Anal. Appl.* 9, 215 (1975).
- [9] P. D. Lax, “*Periodic solutions of the KdV equation*”, *Commun. Pure Appl. Math.* 28, 141 (1975). • V. A. Marchenko, “*A periodic Korteweg–de Vries problem*”, *Dokl. Akad. Nauk SSSR* 217, 276 (1974), <https://www.mathnet.ru/eng/dan/v217/i2/p276>.
- [10] N. I. Akhiezer, “*Continuous analogues of orthogonal polynomials on a system of intervals*”, *Dokl. Akad. Nauk SSSR* 141, 263 (1961), <https://www.mathnet.ru/eng/dan/v141/i2/p263>.
- [11] B. A. Dubrovin, V. B. Matveev and S. P. Novikov, “*Nonlinear equations of Korteweg-de Vries type, finite zoned linear operators, and Abelian varieties*”, *Russ. Math. Surveys* 31, 59 (1976).
- [12] V. P. Kotlyarov, “*Periodic problem for the Schrödinger nonlinear equation*”, *Voprosy matematicheskoi fiziki i funkcionalnogo analiza* 1, 121 (1976). • O. R. Its and V. P. Kotlyarov, “*Explicit formulas for the solutions of a nonlinear Schrödinger equation*”, *Dokl. Akad. Nauk Ukrainian SSR Ser. A* 1, 965 (1976).
- [13] M. Lakshmanan, “*Continuum spin system as an exactly solvable dynamical system*”, *Phys. Lett. A* 61, 53 (1977). • V. E. Zakharov and L. A. Takhtajan, “*Equivalence of the nonlinear Schrödinger equation and the equation of a Heisenberg ferromagnet*”, *Theor. Math. Phys.* 38, 17 (1979).

- [14] A. R. Its and V. B. Matveev, “*On a Class of Solutions of the Korteweg-de Vries Equation*”, *Problemy Mat. Fiz.* 8, 70 (1976).
- [15] A. R. Its, “*Connection between Soliton and Finite-Gap Solutions to the NS equations*”, *Problemy Mat. Fiz.* 10, 118 (1983). • E. D. Belokolos, A. I. Bobenko, V. Z. Enol’skii, A. R. Its and V. B. Matveev, “*Algebro-Geometric Approach to Nonlinear Integrable Equations*”, Springer (1994), Berlin, Germany.
- [16] A. R. Osborne and L. Bergamasco, “*The small-amplitude limit of the spectral transform for the periodic Korteweg-de Vries equation*”, *Nuovo Cim. B* 85, 229 (1985).
- [17] A. R. Osborne and L. Bergamasco, “*The solitons of Zabusky and Kruskal revisited: Perspective in terms of the periodic spectral transform*”, *Physica D* 18, 26 (1986).
- [18] M. G. Forest and D. W. McLaughlin, “*Spectral theory for the periodic sine-Gordon equation: A concrete viewpoint*”, *J. Math. Phys.* 23, 1248 (1982).
- [19] J. S. Russell, “*Report on Waves: Made to the Meetings of the British Association in 1842–43*”.
- [20] J. Boussinesq, “*Essai sur la théorie des eaux courantes*”, Académie des sciences de l’Institut de France, mémoires présentés par divers savants 23 (1877). • D. J. Korteweg and G. de Vries, “*On the change of form of long waves advancing in a rectangular channel, and a new type of long stationary wave*”, *Phil. Mag.* 39, 422 (1895).
- [21] L. D. Faddeev, “*Properties of the S-matrix of the one-dimensional Schrödinger equation*”, *Amer. Math. Soc. Transl. Ser. 2* 65, 4 (1967).
- [22] L. D. Landau and E. Lifshitz, “*On the theory of the dispersion of magnetic permeability in ferromagnetic bodies*”, *Phys. Z. Sowjet.* 8, 153 (1935).
- [23] F. Demontis, S. Lombardo, M. Sommacal, C. van der Mee and F. Vargiu, “*Effective generation of closed-form soliton solutions of the continuous classical Heisenberg ferromagnet equation*”, *Commun. Nonlinear Sci. Numer. Simul.* 64, 35 (2018).
- [24] F. Demontis, G. Ortenzi, M. Sommacal and C. van der Mee, “*The continuous classical Heisenberg ferromagnet equation with in-plane asymptotic conditions. I. Direct and inverse scattering theory*”, *Ricerche Mat.* 68, 145 (2019).
- [25] N. Beisert, J. A. Minahan, M. Staudacher and K. Zarembo, “*Stringing spins and spinning strings*”, *JHEP* 0309, 010 (2003), hep-th/0306139.
- [26] K. Nakamura and T. Sasada, “*Solitons and wave trains in ferromagnets*”, *Phys. Lett. A* 48, 321 (1974). • M. Lakshmanan, T. W. Ruijgrok and C. J. Thompson, “*On the dynamics of a continuum spin system*”, *Physica A* 84, 577 (1976). • J. Tjon and J. Wright, “*Solitons in the continuous Heisenberg spin chain*”, *Phys. Rev. B* 15, 3470 (1977).
- [27] T. Bargheer, N. Beisert and N. Gromov, “*Quantum Stability for the Heisenberg Ferromagnet*”, *New J. Phys.* 10, 103023 (2008), arxiv:0804.0324.